REPUBLIC OF TURKEY

YILDIZ TECHNICAL UNIVERSITY

GRADUATE SCHOOL OF NATURAL AND APPLIED SCIENCES

MODELING AND ANALYSIS OF A REVERSIBLE SOLID OXIDE CELL SYSTEM

Muiz Adekunle AGBAJE

MASTER OF SCIENCE THESIS

Department of Mechanical Engineering

Energy Program

Advisor

Assoc. Prof. Dr. Ali Volkan AKKAYA

July, 2021

REPUBLIC OF TURKEY
YILDIZ TECHNICAL UNIVERSITY
GRADUATE SCHOOL OF NATURAL AND APPLIED SCIENCES

MODELING AND ANALYSIS OF A REVERSIBLE SOLID OXIDE CELL SYSTEM

A thesis submitted by Muiz Adekunle AGBAJE in partial fulfillment of the requirements for the degree of MASTER OF SCIENCE is approved by the committee on 12.07.2021 in Department of Mechanical Engineering, Energy Program.

Assoc. Prof. Dr. Ali Volkan AKKAYA
Yıldız Technical University
Advisor

Approved By the Examining Committee

Assoc. Prof. Dr. Ali Volkan AKKAYA, Advisor
Yıldız Technical University

Assoc. Prof. Dr. Şaban PUSAT, Member
Yıldız Technical University

Assoc. Prof. Dr. Hasan KÖTEN, Member
Istanbul Medeniyet University

I hereby declare that I have obtained the required legal permissions during data collection and exploitation procedures, that I have made the in-text citations and cited the references properly, that I haven't falsified and/or fabricated research data and results of the study and that I have abided by the principles of the scientific research and ethics during my Thesis Study under the title of Modeling and Analysis of a Reversible Solid Oxide Cell System supervised by my supervisor, Assoc. Prof. Dr. Ali Volkan AKKAYA. In the case of a discovery of a false statement, I am to acknowledge any legal consequence.

Muiz Adekunle AGBAJE

This work was supported by the Research Fund of Yildiz Technical University (BAP). Project Number: FYL-2021-3884.

Dedicated to Almighty Allah

and my families

ACKNOWLEDGEMENTS

Profound gratitude goes to Almighty God for this opportunity to complete a postgraduate degree. I am grateful for the support of my supervisor and mentor, Dr. Ali Volkan AKKAYA who trained me in this path of knowledge without whom this thesis would not have been a success. The contribution of my course lecturers Dr. Nader Javani, Prof. Zehra Yumurtacı, Prof. Hasan Hüseyin Erdem, Prof. Surkay Akbarov, Prof. Ali Pinarbaşı, and Prof. Ahmet Selim Dalkılıç whose courses in one way or the other contributed to the success of my master's degree cannot go unmentioned. Also, I acknowledge the contributions of Dr. Christopher Wendel for his explanations of the modeling approach.

The support I receive from friends and family will not go unmentioned. I appreciate every bit of advice and help I have received from the international family I made during my time in Turkey. The family I left back home who look forward to the greatness I will return with deserves all the accolades for their patience towards and hope in me. To my cherished partner, thank you for being there with me all the way. You are truly a rare gem.

I thank the Turkish government's presidency for Turks abroad and related communities for Türkiye Bursları (Turkey Scholarships) who sponsored the education. The support of the university, graduate school of natural sciences, the department of mechanical engineering, and the research fund of Yildiz Technical University is also appreciated.

Muiz Adekunle AGBAJE

TABLE OF CONTENTS

LIST OF SYMBOLS

E_{act}	Activation Energy
OM_t	Annual operation and maintenance cost
A_t	Annual recurring expenditure
A	Area
Z	Capital cost
CRF	Capital recovery factor
$\Delta\hat{h}$	Change in specific enthalpy
$\Delta\hat{s}$	Change in specific entropy
$\Delta\hat{g}$	Change in specific Gibb's free energy
K	Chemical constant
σ_i	conductivity
j	Current density
T_0	Dead state temperature
D_i	Diffusivity
r	Discounted rate
D_i^{eff}	Effective Diffusivity
i	Electric current or discounted rate
R_i	Electric resistance
E_i	Electrical energy
ξ	Electrode porosity
δ_i	Electrode thickness
E	Electromotive force
e^-	Electron
$\Delta\mathrm{H}$	Enthalpy change
$H/\dot{H}_i$	Enthalpy/Enthalpy rate
S	Entropy
λ_{O_2}	Excess or stoichiometric air ratio
$j_{0,i}$	Exchange current density
ζ	Exergoeconomic factor
$\dot{C}_i$	Exergy cost rate
$Y_{D,k}$	Exergy destruction ratio
ε_i	Exergy efficiency
$\dot{E}x_i$	Exergy rate
F	Faraday's constant
U_f	Fuel utilization factor
v	Fuller's diffusion volume
G	Gibbs free energy
C_i	Heat capacity rate
$\in$	Heat exchanger effectiveness
Q	Heat flow
U	Heat transfer coefficient
L	Loss (exergy)
LHV_i	Lower heating value

$\dot{m}_\mathrm{i}$	Mass flow rate
$\dot{n}_i$	Molar flow rate
M_k	Molar mass
X_i	Molar ratio
n	Number of electrons transferred
φ	Operation and maintenance factor
η_i	Overpotential or energy efficiency
O^{2-}	Oxygen ion
p_i^j	Partial pressure
d_p	Pore diameter
$\dot{W}$	Power
pd	Power density
P	Pressure
$\dot{Q}/q$	Rate of heat flow
$\dot{Z}$	Rate of redox reaction or component capital cost rate
$\dot{Y}_r$	Rate of reformation reaction
$\dot{Y}_s$	Rate of water-gas shift reaction
U_r	Reactant production factor
$I_{re,t}$	Replacement capital cost
c_i	Specific cost
ex_i	Specific exergy
$c_{p,i}$	Specific heat capacity
es_i^{ch}	Standard chemical exergy
T	Temperature or Time in years
t	Time (seconds, hours, or years)
τ	Tortuosity
I_0	Total Investment cost
α	Transfer coefficient
R	Universal gas constant
V	Voltage
W	Work done

Subscripts and superscripts

0	Standard/dead state (parameter)
act	Activation (overpotential)
b	boundary
CH/ch	Chemical (Exergy)
cha	Channel
COM/comp	Compressor
conc	Concentration (overpotential)
d/D	Destruction (exergy)
EC	Electrolysis cell
ELE	Electrical/Electrolyte
FC	Fuel cell
FE	Fuel electrode

HEX	Heat Exchanger
HRC	Heat Recuperator
INV	inverter
kn	Knudsen diffusion
max	Maximum
min	Minimum
OE	Oxide electrode
ohm	Activation (overpotential)
op	Operating (parameter)
PH	Physical (Exergy)
ref	reference
RT	Roundtrip
sta	Stack
sys	System
TN	Thermoneutral
tot	total
TPB	Tripple phase boundary

LIST OF ABBREVIATIONS

0D	Zero-dimensional
3D	Three-dimensional
AC	Alternating Current
AFC	Alkaline fuel cell
Al-ion	Aluminum ion
ASR	Area-specific resistance
B2B	Buyer to Buyer
BOP	Balance of plant
CAES	Compressed air energy storage
CCUS	Carbon capture utilization and storage
CEPCI	Chemical engineers’ plant cost index
CFD	Computational fluid dynamics
C-H-O	Carbon-Hydrogen-Oxygen (Ternary diagram)
COM/comp	Compressor
CRF	Capital recovery factor
DC	Direct Current
DIR-SOC	Direct internal reforming solid oxide cell
DMFC	Direct methane fuel cell
EC	Electrolysis cell
EES	Engineering equation solver
EPC	Exergy performance coefficient
ER-SOC	External reforming solid oxide cell
FC	Fuel cell
HEX	Heat Exchanger
HRC	Heat Recuperator
HTMH	High-temperature metal hydride
HT-SOFC	High-temperature solid oxide fuel cell
IIR-SOC	Indirect internal reforming solid oxide cell
IT-SOFC	Intermediate temperature solid oxide fuel cell
LCOE	Levelized cost of electricity
LCOS	Levelized cost of storage
LHV	Lower heating value
Li-ion	Lithium-ion
LSCF	Lanthanum strontium cobalt ferrite
LSCF-GDC	Lanthanum strontium cobalt ferrite- Gadolinium doped ceria
LSCM	Lanthanum strontium cobalt manganite
LSGM	Lanthanum strontium gallium magnesium oxide
LTMH	Low-temperature metal hydride
LT-SOC	Low-temperature solid oxide fuel cell
MCFC	Molten carbonate fuel cell
NaS	Sodium Sulfide
Ni-metal	Nickel metal
Nm^3	Newton-meter cube

NOAA	National Oceanic and atmospheric administration
NTU	Number of transfer units
O&M	Operating and Maintenance
OCV	Open-circuit voltage
Pb Acid	Lead-acid
PEMFC	Polymer electrolyte membrane fuel cell
PhD	Doctor of Philosophy
PRV	Pressure Reduction Valve
PSB	Polysulphide/Bromine Flow Battery
ReSOC	Reversible solid oxide cell
SLT	Strontium lanthanum titanate
SOC	Solid oxide cell
SOEC	Solid oxide electrolysis cell
SOFC	Solid oxide fuel cell
SPECO	Specific exergy cost
TRR	Total Revenue Requirement
VRB	Vanadium redox flow battery
ZBB	Zinc/Bromine Flow Battery
ZEBRA	Zeolite Battery Research Africa

Units

$	United States' dollars
¢	cents
A	Amperes
bar	Barometers (pressure)
cm	Centimeters
g	Gram
h/hr	Hour
K	Kelvin
kJ/MJ/GJ	Kilo/Mega/Giga-joule
kPa	Kilopascal
kW/MW	Kilo/Mega-Watt
kWh/MWh/TWh	Kilo/Mega/Terra-Watt-hour
m	Meters
s	Seconds
Sm^3	Standard meter cube
TL	Turkish Lira
V	Voltage

LIST OF FIGURES

LIST OF TABLES

ABSTRACT

Modeling and Analysis of a Reversible Solid Oxide Cell System

Muiz Adekunle AGBAJE

Department of Mechanical Engineering

Master of Science Thesis

Advisor: Assoc. Prof. Dr. Ali Volkan AKKAYA

Energy storage systems are an inevitable part of future energy systems with the world switching to renewable energy sources and smart grid technologies. A reversible solid oxide cell (ReSOC) system is an electrochemical power to gas to power system poised to serve as an intermediary between energy demand and supply. The power generation is the fuel cell (SOFC), and the power storage is the electrolysis (SOEC) mode. In this study, a small scale ReSOC system comprising of the ReSOC stack and balance of plant (BOP) components (such as compressor, heat exchangers, tanks, etc.) is modeled using the electrochemical and thermodynamic relations. Engineering Equation Solver (EES), a powerful tool for thermodynamic analysis by FChart is used for the modeling and analysis of the ReSOC system. The performance of both the cell and the stack were validated with literature data. The energy and exergy analysis of the stack and system was carried out using performance metrics such as power, energy and exergy efficiency, exergy destruction, roundtrip efficiency, and exergetic performance coefficient. The system was further analyzed at base case conditions using the Levelized cost of storage (LCOS) and storage cost method. The result of the analysis carried out in this thesis can be summarized as follows. The stack overall performance is better than the system overall performance primarily because of the extra power consumption by the BOP components. Furthermore, the performance of the system is not only dependent on the system operating condition but also on the method of operating the stack and the composition of the reactant gas in the system. The SOEC mode (83% and 78% exergy and energy efficiency, respectively) performs better than the SOFC mode (68% and 65% exergy and energy efficiency, respectively) both exergetically and energetically and the system had a roundtrip efficiency of 0.51 at the base case. The economic analysis results showed that for both storage cost and LCOS, the system considered in this study is competitive with conventional battery storage technologies and flow batteries. With a storage cost of 13 cents/kWh and LCOS of 32 cents/kWh, the system is expected to be competitive with large scale compressed air energy storage systems after performance improvements. Exergoeconomic analysis showed that the major drivers of the exergetic cost rates are the storage tanks and ReSOC stack capital costs. The SOFC mode of operation had a better exergoeconomic performance than the SOEC mode of operation despite the SOEC having a better exergy performance.

Keywords: Reversible solid oxide cell, modeling, exergy, energy storage cost, exergoeconomy

OZET

Tersinir Katı Oksit Pili Sisteminin Modellenmesi ve Analizi

Muiz Adekunle AGBAJE

Makine Mühendisliği Bölümü

Yüksek Lisans Tezi

Danışman: Doç. Dr. Ali Volkan AKKAYA

Dünyanın yenilenebilir enerji kaynaklarına ve akıllı şebeke teknolojilerine daha çok önem vermesi ile birlikte, enerji depolama sistemleri geleceğin enerji sistemlerinin önemli bir parçası olacaktır. Enerji talebi ve arzı arasında bir aracı olarak görev yapan Tersinir Katı Oksit Hücre (TeKOH) sistemi, elektrokimyasal güçten gaza-gazdan güce dönüşüm sistemidir. Elektrik güç üretimi katı oksit yakıt hücresi (KOYH) modunda gerçekleşirken, gaz olarak enerji depolama elektroliz (KOEH) modu ile sağlanır. Bu çalışmada, bir TeKOH modülü ve diğer sistem bileşenlerinden (kompresörler, ısı değiştiricileri, depolama tankları gibi) oluşan küçük ölçekli bir TeKOH sistemi, elektrokimyasal ve termodinamik ilişkiler kullanılarak modellenmiştir. Bu model Engineering Equation Solver (EES) yazılımı ile kodlanarak, TeKOH modülünün ve sistemin analizi için kullanılmıştır. Hem hücrenin hem de modülün performansı literatür verileriyle doğrulanmıştır. TeKOH modülünün ve sistemin enerji ve ekserji analizleri, güç, enerji ve ekserji verimleri, ekserji yıkımı, gidiş-dönüş verimi ve ekserjetik performans katsayısı gibi performans ölçütleri kullanılarak gerçekleştirilmiştir. Ayrıca, sisteme ait depolama maliyeti bir değere getirilmiş maliyet yöntemi ile belirlenmiş ve analiz edilmiştir. Son olarak, SPECO yöntemi kullanılarak TeKOH sisteminin ekserjo-ekonomik analizi gerçekleştirilmiştir. Tez kapsamında yapılan analizlerin temel sonuçları şu şekilde belirtilebilir. Yardımcı sistem bileşenlerinin ekstra güç tüketimi nedeniyle, TeKOH modülünün genel performansının sistemin genel performansından daha iyi olduğunu göstermektedir. Ayrıca, sistemin performansı sadece sistemin çalışma koşullarına değil, aynı zamanda TeKOH modülünün çalıştırma yöntemine ve sistemdeki reaktant gazın komposizyonuna da bağlı olduğu görülmüştür. KOEH modu (ekserji ve enerji verimleri sırasıyla %83 ve %78), hem enerji hem de ekserji performansları açısından KOYH modundan (ekserji ve enerji verimleri sırasıyla %68 ve %65) daha iyi performans göstermektedir ve TeKOH sistemi temel çalışma koşullarında % 51'lik bir gidiş-dönüş verimliliği sağlamaktadır. Bir değere getirilmiş enerji depolama maliyeti (32 sent/kWh) TeKOH sistemin geleneksel pil depolama teknolojileri ve akış pilleri ile rekabet edebileceğini göstermiştir. 13 sent/kWh depolama maliyeti ve 32 sent/kWh bir değere getirilmiş maliyeti ile, sistemin performans iyileştirmelerinden sonra büyük ölçekte basınçlı hava enerji depolama (BHED) sistemleriyle rekabet edebilme potansiyeli mevcuttur. Ekserjo-ekonomik analizleri, birim ekserji maliyetinin değerini etkileyen en önemli sistem bileşenlerin depolama tankları ve TeKOH modülünün olduğunu göstermiştir. KOEH çalışma modunun daha iyi bir ekserji performansına sahip olmasına rağmen, KOYH çalışma modunun KOEH çalışma modundan daha iyi bir ekserjo-ekonomik performansa sahip olduğu görülmüştür.

Anahtar kelimeler: Tersinir katı oksit pili, modelleme, ekserji, enerji depolama maliyeti, ekserjo-ekonomi

---

1
INTRODUCTION

1.1 Literature Review

Several studies have been carried out on the performance and analysis of reversible solid oxide cells (ReSOC). The underlying work being the design of solid oxide fuel cell (SOFC) and electrolysis cell (SOEC) made this a possibility and has supported the development of ReSOC systems over time. Though more studies are focused on SOFC systems compared to SOEC systems, the research on ReSOC is gaining traction fast, owing to its potentially high energy density and roundtrip efficiency. A comprehensive review detailing ReSOC for sustainable energy is studied by Mogensen et al [1]. In the review article, a comparison between various energy storage systems was done and the characteristics of the ReSOC system were investigated. The present drawbacks encountered in ReSOC systems which include the cell support, degradation in the electrodes and electrolytes, and carbon deposition in cases where carbonaceous fuels are used are discussed. The application of ReSOC systems for transportation and grid stabilization was also reviewed in the paper. In conclusion, the researchers noted the attractiveness of the ReSOCs systems and the need for demonstration projects as the next phase of the technology. Song et al [2] studied the roles of ReSOC in the design and evaluation of technological tools in applications of sector-coupling of energy systems. The economic benefits, material development, and electrochemistry of ReSOC were discussed in the paper. In conclusion, the researchers stated that even though ReSOC can be coupled with existing power systems for a hydrogen-based system there is still the need to develop cells with low internal resistance and long-term stability.

Mathematical models give a first-hand perspective into the behavior of the ReSOC and give room for further analysis to understand the behavior of the cell under varying circumstances. Mathematical model validation with experimental data and performance of this model was carried out by Kazempoor et al [3]. In the study, a ReSOC was modeled using the same method for the SOFC and SOEC operating modes but changing the sign on the current density. Nernst Equation, activation, ohmic, and concentration losses in the cell were used to characterize the model. The model shows good agreement with experimental data and further analysis was carried out. ReSOC stacks designed for a 150kW system was evaluated by Königshofer et al [4]. In the comprehensive experimental study, the stack was operated using system-relevant gas mixtures. It was shown that high hydrogen partial pressures in the electrolysis mode presented lower diffusion losses but in the fuel cell mode, low fuel partial pressure resulted in higher losses. Maria et al [5] carried out an analysis on a 3D stack model using the homogenous Multiphysics modeling approach. The stack consisted of 100 cells and analysis was done using G-Prom and CFD software. They concluded that homogenous modeling consumes less time and less computational power compared to conventional 3D model simulation. Results from stack modeling show that generally there is additional voltage loss in ReSOC stacks when compared to cell internal losses primarily due to the interconnection between the cells when scaling up to the stack. The 3D stack and system performance analysis with the 0-D balance of plant components carried out by Yuqing et al. [6], it was demonstrated that excess air ratio decreases both stack and system efficiency of a ReSOC. In the analysis, where they developed a ReSOC system model in gProms Model Builder software for distributed scale energy storage application by scaling from cell to stack to system, a roundtrip efficiency of 72.3% and 58.3% for stack and system respectively was achieved. The Ph.D. thesis by Christopher Wendel [7] at the Colorado School of mines on the design and analysis of ReSOC systems for energy storage covers a broad range of the characteristics of ReSOC systems. Thermodynamic and economic analysis of a bulk scale and distributed scale system was carried out. He demonstrated that the system could have a roundtrip efficiency of up to 74% and a storage cost of 2.6 ¢/kWh. The effect of different configurations of the system on the roundtrip efficiency of the system was also investigated. Though the system looks promising, there is a need for a further and more detailed analysis of the system before it can be fit for practical applications.

The possibility of the use of metal hydride tanks for hydrogen and heat storage in a ReSOC system was analyzed in a novel design by Van-Tiep et al [8]. The effect of waste steam and the temperature of the metal hydride tank on the roundtrip efficiency of the system was studied. MgH2 was used for the high temperature (HTMH) and LaNi5 was used in the low-temperature metal hydride (LTMH) tank. The results showed higher roundtrip exergy efficiency for the low-temperature metal hydride and almost equal roundtrip efficiency when heat recovery was not done in the system. Also, the HTMH has the potential function of both the LTMH and external heat utilization. Another study by Van-Tiep et al [9] raised the efficiency of a ReSOC system for distributed electrical energy storage by coupling the system with waste heat. The analysis was done using EBSILON Professional Commercial software. The results showed that the temperature of the waste steam has little effect on the roundtrip efficiency of the system and the hydrogen concentration in the SOEC modes affects the roundtrip efficiency due to the balance of plant components. Nicolas and Masoud [10] showed that polygeneration systems where ReSOC is used for hydrogen production as a means of energy storage and Solar collectors for power generation could achieve a high system efficiency of 19.3% compared to conventional systems with an efficiency of around 18%. The system comprised of Dish-sterling solar collectors and parallel trough collectors, a ReSOC System for hydrogen production and storage, and a freshwater desalination system. The system was simulated for a 24hr 500kW electricity production and freshwater production. 3281Sm^3 of H_2, 8466L of freshwater, and 12MWh of electricity were recorded from the system at the end of the 24h simulation. The system efficiency could increase to 26.3% after modifications are made to the desalination process. Chen et al [11] carried out an analysis on a ReSOC system with methanation for grid stabilization. The study is aimed at showing how promising the power to gas concept is. The system consisted mainly of three parts: the ReSOC subsystem, the methane synthesis subsystem, and the system controller. Surplus energy from the grid was used to generate hydrogen via electrolysis and for methane synthesis, this gas is then used for electric power generation when required. The system showed power-to-gas efficiency of 85.34% and a gas-to-power efficiency of 46.95%. According to the study, a roundtrip efficiency of above 70% shows that the ReSOC system with methane synthesis is capable of grid balancing.

As important as the thermodynamic performance and feasibility of thermodynamic systems are, the most influential factor in the commercialization of any new technology is the economic performance or characteristic of the system. Several approaches have been utilized in literature to characterize the economic or thermoeconomic performance of energy systems. Among such are the total revenue requirement (TRR) [12], specific exergy cost (SPECO) [12], [13], capital cost [14], Levelized cost (LCOS) [15]–[17], and storage cost method [7], [18]. The specific exergy cost approach was introduced by Lazaretto and Tsatsaronis [19] and it has proven to be a very important tool in exergoeconomic analysis. Young et al. [12] used both the TRR and SPECO method for the economic and exergoeconomic analysis of a SOFC based cogeneration system. The TRR method estimated the Levelized cost of electricity of the system as 0.34 \$/kWh, which was about three times higher than the regular electricity cost. The researcher attributed the high LCOE primarily to the high purchased cost of the SOFC stack. The SPECO on the other hand yielded a product's specific exergy cost of 0.24 \$/kWh. However, summing the specific cost of fuel, system construction and operation's specific cost, and the cost of electricity in auxiliary components and specific exergy cost of streams leaving the system yielded a cost equivalent to the Levelized cost calculated in the TRR method. Calise et al. [14] used the capital cost approach with exergy to optimize the design of a hybrid system involving a solid oxide fuel cell (SOFC) and gas turbine based on the plant's total lifecycle cost. The system's yearly overall cost was then used to optimize the system only at the design point. The parameter used for the optimization was the cost of fuel. The optimal design point occurred at a fuel price of 0.20 \$/Nm^3. The storage cost method was used by researchers at the pacific northwest national laboratory [18] to compare electrical energy storage technologies to shed light on the status of energy storage technologies and the challenges faced by electrochemical energy storage systems. The review paper which focused more on battery storage technology as an electrochemical energy system highlighted the potentials and economic considerations for electrochemical energy storage devices.

Recent research on ReSOC stacks and systems has focused on the integration of ReSOC systems with existing infrastructure such as grid stabilization applications and carbon utilization. Motylinski et al [20] developed a dynamic model of a ReSOC system for grid energy balancing. They used wind data for electricity production to simulate uneven electricity production. They also studied the effect of the dynamic operation of both the ReSOC stack and system. They used mode switching strategies to show that alternate operation of the system in SOEC and SOFC modes enable the system to perform grid energy balancing continuously. Another successful application of the ReSOC system for integration into existing infrastructure was carried out by Reznicek and Braun [21]. The study which is part of a series of research work on ReSOC systems [22]–[25] showed the feasibility of integrating ReSOC systems with natural gas pipeline and carbon capture infrastructure. The natural gas pipeline provided the fuel during the SOFC mode, and the exhaust gas of this mode was stored in the CO_2 pipeline. In the electricity storage mode, CO_2 gas from the CO_2 pipeline or carbon capture infrastructure was converted to synthetic gas using excess electricity from renewable sources and injected into the natural gas pipeline. The 50MWe system produced synthetic natural gas at 81% efficiency and carbon dioxide at 69% efficiency. The researchers concluded that it might is more economically favorable to operate ReSOC systems with integration to pipelines than as standalone systems. The system is also predicted to be competitive with prevailing energy storage technologies and natural gas peaker plants.

Summarily, the operation and performance of the ReSOC stack and system are dependent on numerous factors. Researchers have tried to understand the operation of the stack using cell properties and distinct approaches such as numerical, computational, and experimental. ReSOC systems are high potential energy storage systems and are gaining attention due to the flexibility it provides and its high efficiency. The costs of ReSOC systems are still high primarily because of the high initial cost. This is expected to improve over time as new and cheaper cell materials are being researched.

The literature review has shown that studies has been carried out on the performance analysis of both ReSOC and ReSOC systems with more studies carried out at the cell and stack level. However, the studies have only focused on the electrochemical and thermodynamic performance based on the first law of thermodynamic analysis using the energy and mass balance equations. Energy or thermodynamic systems in general involves the combination of various equipment and components for the operation of the systems. Energy or first law-based analysis are aimed at using system energy generation or consumption to determine the system performance. However, for performance improvement in energy systems, analysis needs to be done by combining both the first and second law of thermodynamics. On the research of ReSOC systems, only a few studies have employed the method of exergy analysis to characterize the performance or even improve the performance of ReSOC systems. Thereby, this study will contribute to the research of ReSOC system by using both the first and second law of thermodynamics to carry out exergy and exergy-based analysis of the system. The exergy-based analysis will be performed for both the thermodynamic and economic aspects of the system. This will give an overview of the important metrics for improving both the system performance and system costs.

1.2 Objective of the Thesis

This study aims to extensively model and analyze the operation and performance of a kilowatt-scale solid oxide cell system as a gas-to-power-to-gas system for energy generation and energy storage. To objectives carried out to achieve this aim includes:

1. Electrochemical and thermodynamic modeling, simulation, validation, and analysis of a single ReSOC and stack.
2. Thermodynamic modeling and parametric analysis of a ReSOC system based on the validated stack using energy and exergy approach.

3. Economic and exergoeconomic analysis of the ReSOC system using the LCOS and SPECO approach, respectively.

1.3 Hypothesis

The design of ReSOC is rooted in the individual design of solid oxide fuel cells and solid oxide electrolysis cells. A ReSOC while functioning both as a fuel cell and as an electrolysis cell is expected to display distinct properties and characteristics in both modes albeit the same cell. The hypothesis for this study is that while on a first look, it seems rational to use one cell for two distinct but highly complementing purposes, what are the implications of this design? This thesis will therefore provide an answer to the following questions:

1. What are the similarities and differences in the performance of a ReSOC system in the power generation and power storage mode?
2. How do the operating conditions affect the system performance in both modes of operation?
3. What is the economic performance of the system, how does it compare with similar systems that serve the same purpose?
4. What is the distribution of exergy destruction in the system; which components have the highest exergy destruction?
5. What is the outlook on the system's economic and thermodynamic performance?

1.4 Scope of the Study

The present chapter has brought the reader up to date concerning development and research studies that have been carried out about ReSOC and ReSOC systems. Therefore, to achieve the objectives stated and provide answers to the questions in this hypothesis, the rest of this thesis is structured such that in chapter 2, the evolution of energy technologies, CO_2 emissions from energy sources, and a brief insight on the future energy systems is given. Here, the reason for the need for energy storage technologies is presented and the different energy storage technologies are also given. Electrochemical systems are defined, the different types of electrochemical energy systems and their operations are also given. Lastly, the reversible solid oxide cell is introduced as a bi-directional electrochemical energy system. The classification of solid oxide cells, areas of application, and the advantages of the ReSOC systems are explained.

Chapter 3 details the modeling, validation, and analysis of a standalone reversible solid oxide cell and stack. The cell model was based on the electrochemical operation and the cell materials, while the stack model was based on a repetitive cell unit. Electrochemical reactions such as the reforming water-gas shift and redox reactions are modeled to characterize the gas conversion in the ReSOC and stack. The operating parameters included the current, current density, Nernst voltage, overpotentials, gas concentration, oxygen content in air, equilibrium constant, fuel utilization factor, stoichiometric air factor, power/power density, thermoneutral voltage, efficiency, and roundtrip efficiency. Furthermore, the method of simulating the cell and the stack was described, and the simulation software was also introduced. The cell properties, cell and stack validation results, cell performance, and stack analysis results were given in the last parts of the chapter.

The stack model derived from chapter 3 is used in the system model presented in chapter 4 and the energy and exergy analysis of the stack and system is also presented. The system is described, and the balance of plant components was detailed and modeled based on mass, energy, and exergy balance. The system performance metrics for both the energy and exergy performance of the system are presented. Afterward, a parametric study of the effect of operating parameters on system and stack exergy performance is also carried out.

In chapter 5, the cost of the system is analyzed by estimating the capital, operation, and maintenance cost of all system components. The method of LCOS is used to characterize the economic property of the system and the results are compared with the cost of other storage systems presented in the literature. The exergoeconomic analysis of the system is carried out in chapter 6 using the capital costs derived from chapter 5 and the SPECO method. In the last chapter, the study is concluded and the questions in the hypothesis were answered based on the system analysis results.

2

ENERGY STORAGE & REVERSIBLE SOLID OXIDE CELL (RESOC)

2.1 The need for energy storage

By consensus, global warming and climate change are some of the biggest modern problems. This motivates the controversy-ridden but widely accepted decisions of reducing greenhouse gas emissions by world leaders. This is the highlight of the 2015 Paris agreement signed by 194 nations to slow down the rate at which the earth is warming up [26]. Despite this, reducing it has been a great challenge over the years. Major sources of greenhouse gas emissions especially CO_2 are from energy generation, agriculture and land use, and industrial activities [27], [28]. The most prominent among the solution poised for reducing emissions include switching to carbon-free energy generation sources and carbon capture, utilization, and storage (CCUS) technologies. While carbon-free energy sources such as wind and solar add virtually nothing to the existing CO_2 in the atmosphere, CCUS will reduce the existing amount of CO_2 or prevent the emission of newly produced CO_2 to the atmosphere for storage in caverns or utilization in the industrial process, energy storage, etc. Also, the prospect of using CO_2 in rocket engines for space missions has been proposed by researchers [29]. Figure 2.1 shows the monthly average for global CO_2 emissions from 1980 to 2021 [30].

According to Daniel Yergin, author of “The New Map: Energy, Climate, and the Clash of Nations” [31], the maturity of new energy technology takes a long time before it can completely replace or even almost replace existing technologies. A vivid example is the replacement of coal-fired power plants. Energy and power generation has been known to be the highest producer of CO_2 in the atmosphere and a lot of work has been done to reduce CO_2 emission during power generation. If we expect carbon-free or low carbon sources to replaces existing carbon-ridden technologies, it will take a while.

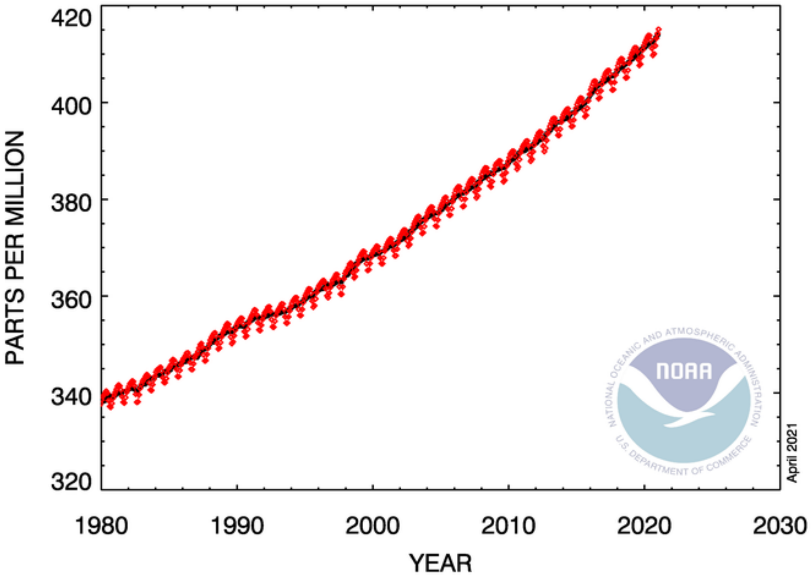

Figure 2.1 Global Monthly CO_2 Emission. Source: NOAA [30]

Meanwhile, apart from the problem of carbon reduction, another important problem for the future of energy is the increasing energy demand. Reports from the International Energy Agency predict total global energy demand to rise by 150% from 23,031 TWh in 2018 to 34,562 TWh by 2040 under the sustainable development scenario [32]. Energy efficiency improvement has proven to be a possible solution reducing total energy demand [33], but economic improvement comes with increased energy consumption with or without efficiency improvement. Carbon-free energy sources or renewable energy sources such as wind and solar have the technical potential to provide the world's energy but not without improvement to their current technology. Also, the unsteadiness of solar irradiation and wind speeds will cause instability on the supply side of the energy system. Furthermore, on the demand side of the energy system, intraday and interseason variation in energy demand makes it difficult to match an already fluctuating energy supply directly with unsteady energy demand.

As energy generation evolves, there is the need for the development of sophisticated energy storage systems to maintain the balance between the source and sink, otherwise described as keeping the demand to supply ratio at unity. To effectively balance energy supply with demand, the need for an intermediary cannot be overemphasized. The intermediary here, in the form of energy storage systems, will store energy during excess supply and produce energy during excess demand.

Future energy systems will be dominated by renewable energy technologies and smart energy grid systems. Efficient electrical energy storage and power-to-gas solutions could play a substantial role in increasing the penetration of fluctuating renewable energy resources, thus mitigating the worst impacts of climate change, and in integrating different energy grids and infrastructures. Balancing energy supply and demand is only one of the roles of energy storage. For example, electrical energy could be stored in form of fuel such as hydrogen or as thermal energy for use in other sectors such as transportation or chemical industry and residential heating, respectively. Electrical energy is the most used form of energy, so much that in so many contexts, the term "energy" is synonymous with "electrical energy". However, storing energy directly as electrical energy is costly and inefficient, and as a result, energy is mostly stored as precursors to electrical energy, in other words, fuel [34].

In a carbon-free or low-carbon energy ecosystem whereby precursors such as coal and other hydrocarbons cannot be used for energy storage, a change in the dynamics of energy storage technologies is inevitable. Energy storage technologies can be mechanical, thermal, electrochemical, and chemical. Properties used in characterizing energy storage mediums or systems include density (power and energy), time (storage, self-discharge, response, charge, and discharge), size, cost, efficiency, etc. Table 2.1 shows the different types of energy storage technologies available [34], [35].

2.2 Electrochemical energy systems

Electrochemistry is a branch of science that studies the relationship between chemical reactions and the flow of electric current. It explains how chemical reactions cause current flow or the reverse where the flow of current leads to a chemical reaction. Conversely, electrochemical energy systems employ the principle of electrochemistry for energy applications.

Table 2.1 Energy Storage Technologies [34], [35]

Storage Technology	**Sub-type**
Mechanical	Pumped hydro energy storage system
	Compressed air energy storage systems
	Flywheel energy storage system
	Liquid air energy storage system
	Advanced rail energy storage
	Groundbreaking energy storage
Thermal	Sensible heat thermal energy storage
	Latent heat storage
	Solar ponds
Electrochemical	Battery Energy Storage
	Flow batteries
	Electrolyzer
Chemical	Power to gas
	Large scale hydrogen storage
	Reversible endothermic chemical reactions
	Traditional energy storage (Natural gas, oil, coal)
Electrical	Supercapacitors
	Electromagnetic energy storage

Electrochemical cells like cells in general are the most fundamental part of an electrochemical system. This is the part where the basic chemical reaction and the flow of electricity occurs. Typically, an electrochemical cell consists of two electrodes and an electrolyte. The reduction reaction takes place at the cathode electrode and the oxidation reaction takes place at the anode electrode [36]. The configuration is such that the electrolyte is sandwiched between the anode and the cathode, and the two electrodes are connected by a conductor which connects the electrodes to the electric load or the electric power source, depending on the type of cell and the operation of the cell. A basic reaction that can occur in an electrochemical cell is the redox reaction of hydrogen and water. Equation 2.1 is the electrochemical reaction of hydrogen and oxygen to form H_2O.

$$H_2 + 0.5O_2 \overset{electricity}{\Longleftrightarrow} H_2O \qquad \Delta H = \pm 247 kJ/mol \quad (2.1)$$

The half-reactions at the anode and cathode are given in Equations 2.2 and 2.3, respectively.

$$H_2 + O^{2-} \leftrightarrow H_2O + 2e^- \quad (2.2)$$

$$0.5O_2 + 2e^- \leftrightarrow O^{2-} \quad (2.3)$$

Equation 2.1 is the chemical reaction showing the combustion of hydrogen to produce steam/water and the splitting of steam to produce hydrogen and oxygen. ΔH is the specific enthalpy of the reaction per mol of reactants and products. In the forward reaction, electricity is produced when it takes place in a fuel cell and the reverse reaction takes place in an electrolysis/electrolyzer cell to consume electricity and produce hydrogen. Different electrochemical cells have unique reactions that can take place in them based on the electrode-electrolyte material and configuration and the temperature of operation. Figure 2.2 shows the different types of electrochemical cells and their energy conversion direction.

Electrochemical energy devices that are used for electricity production converts chemical energy to electrical energy like X-to-power devices. Electricity storage application of electrochemical energy devices involves the reverse of the electricity production devices by converting electrical energy to chemical energy like the power-to-X devices. Bi-directional electrochemical energy devices act as a power-to-X-to-power device capable of energy storage and energy production.

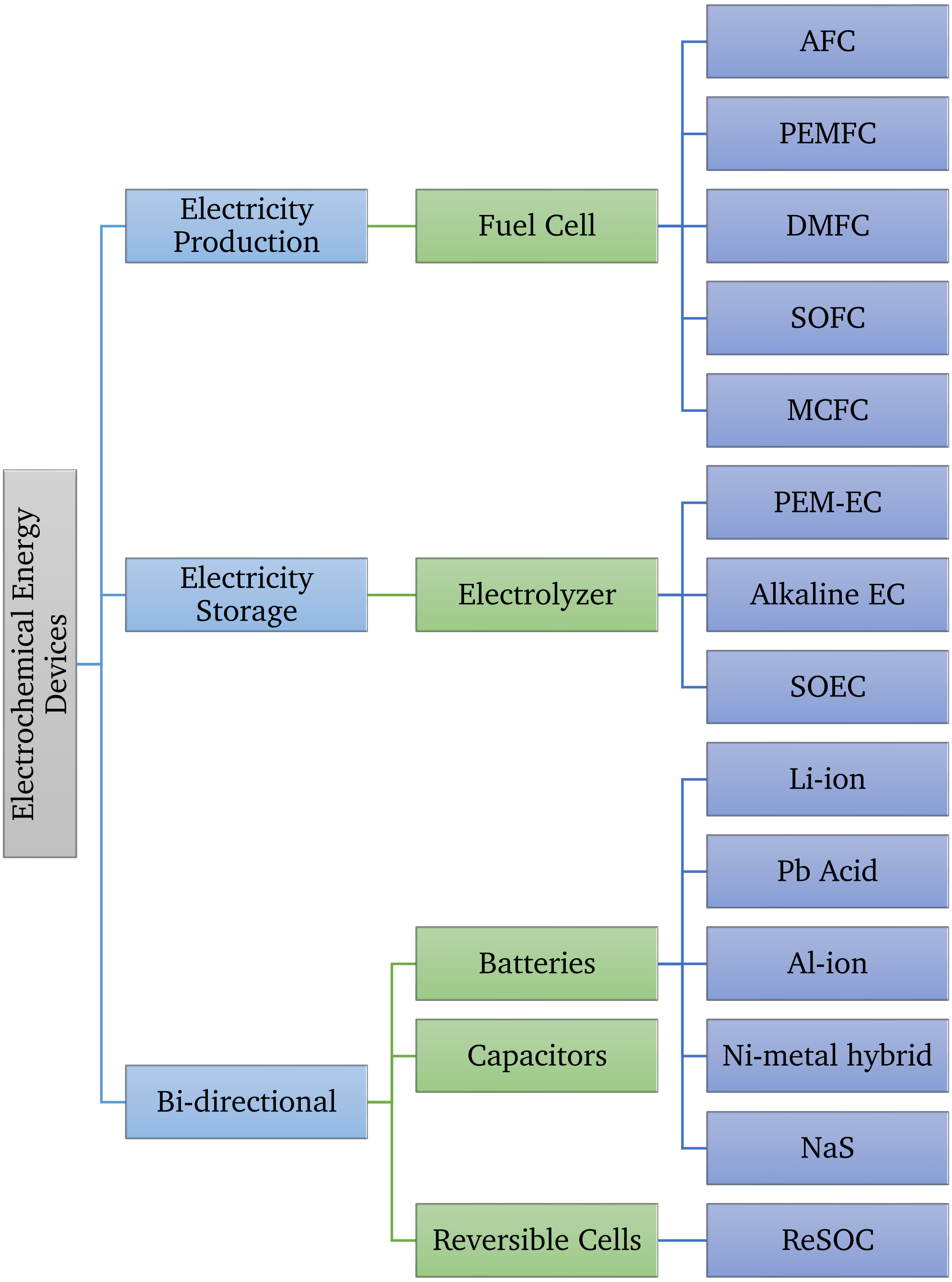

Figure 2.2 Electrochemical energy devices

2.3 Reversible Solid Oxide Cell (ReSOC)

Solid oxide fuel cell (SOFC) is a subject of interest due to its high power, high efficiency, and fuel flexibility compared to other fuel cells. Due to its high operating temperature [37], the probability of carbon deposition in the cell when using carbon-based fuels is low compared to other electrochemical cells. Methane which is a vast available natural gas can be used effectively in a SOFC without causing carbon deposition in the cell. The possibility of other gas such as syngas, biogas, and CO has been established in the literature. SOFC has been largely divided into two types based on their operating temperature, the High-Temperature SOFC (HT-SOFC) and Intermediate-Temperature SOFC (IT-SOFC). Due to the high operating temperature of the SOFC, they produce large amounts of heat, and this heat can be stored and used for other purposes, thus making them a good cogeneration device. Figure 2.3 shows the electrochemical reactions in a channel-level ReSOC for the fuel cell and electrolyzer mode of operation using syngas as the fuel gas[7].

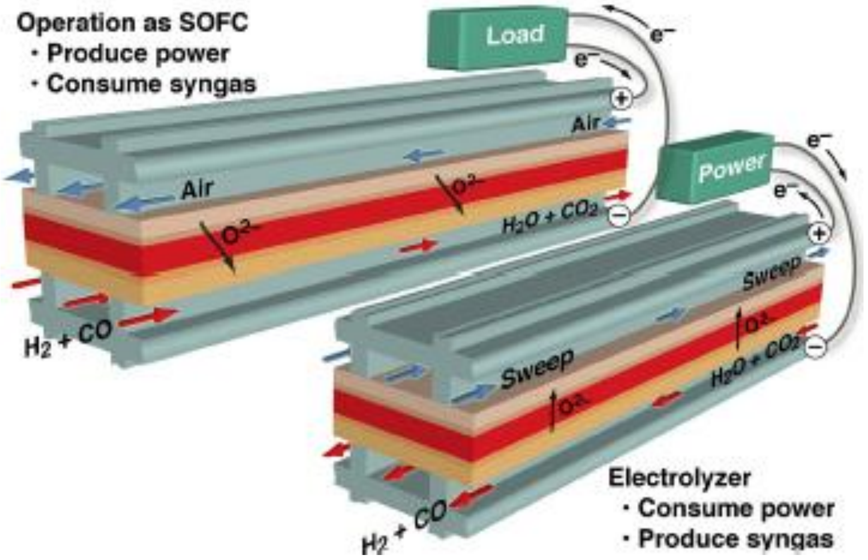

Figure 2.3 Graphical representation of a reversible solid oxide cell at the channel level in both fuel cell and electrolysis mode of operation [7].

As previously defined, fuel cells are used to generate electricity, and electrolyzer cells are used for electrical energy storage. A Reversible Solid Oxide Cell (ReSOC) is an electrochemical cell that combines the ability of SOFC for energy generation/gas to power and a Solid Oxide Electrolysis Cell (SOEC) for energy storage/power to gas in a single cell. Its uniqueness is that one cell or stack performs the entire function of both the power to gas and the gas to power application. A Reversible Solid Oxide Cell System thereby is an energy system that comprises a ReSOC stack and other balance of system components such as compressors, turbine, heat exchangers, storage tanks, pumps, etc. Thus, forming a compact system that functions as an energy storage system and an energy generation system. Solid oxide cells have been classified in the literature as shown in Table 2.2.

Table 2.2 Solid Oxide Cells Classifications (Adapted from [37])

Classification criteria	**Types**
Operating temperature	• Low-temp. SOC (LT-SOC) (500 ^{O}C–650 ^{O}C) • Intermediate SOC (IT-SOC) (650^{O}C–800^{O}C) • High-temp. SOC (HT-SOC) (800 ^{O}C–1000 ^{O}C)
Cell and stack designs	• Planar SOC (Flat-planar, radial-planar) • Tubular SOC (Micro-tubular, tubular) • Segmented-in-Series (Integrated-planar) SOC
Type of support	• Self-supporting (anode-supported, cathode-supported, electrolyte-supported) • External-supporting (interconnect supported, porous substrate supported)
Flow configuration	• Co-flow • Cross-flow • Counter-flow
Fuel reforming type	• External reforming SOC (ER-SOC) • Direct internal reforming SOC (DIR-SOC) • Indirect internal reforming SOC (IIR-SOC)

With the development of smart grids and the inevitable shift towards renewable energy production, there is the need for a reliable intermediary between energy demand and supply that can balance the difference and respond to both sides. Energy storage systems are systems designed to match the lag in the demand and supply of energy. ReSOC systems are proposed devices capable of converting electrical energy into chemical fuels, through electrolysis, and chemical fuels into electricity, through electrochemical oxidation. Though there are other types of fuel cells and electrolytic cells (proton exchange membrane, alkaline, direct methane, etc.), a major advantage of these systems is that the same ReSOC stack operates as both energy storage device (SOEC) and energy-producing device (SOFC) primarily due to its high operating temperature, thus making it economical compared to other fuel cell and electrolytic cell technologies.

The introduction of ReSOC systems to energy grids promises a more stable, more efficient, cost-effective, and long-lasting energy system. Though still in the early stage of research, its potentials are immense. Preliminary simulation results have shown that ReSOC systems are bound to become cheaper and even more efficient over time before it gets to the full deployment stage, thanks to the discovery of more efficient and less expensive electrode catalysts materials used in the cell itself and storage tanks. Apart from the ReSOC stack and the storage tanks (in some cases), the ReSOC system balance of plant components (compressor, expander, heater, etc.) are matured, familiar, and quite simple technology, making the system easy to deploy and even very reliable.

Energy storage systems (electrical energy storage systems) are characterized by cost, efficiency, storage capacity (energy density), and widespread availability. None of the presently available energy storage systems is without its downside; pumped hydroelectric energy storage system is limited by geographic location and size, the battery system is limited by cost, duration of storage, and energy density while compressed air energy storage is limited by cost, scalability, and geographic location [3], [23], [38], [39]. Power to gas systems combat the problem of power density and storage efficiency, effectively. In power-to-gas-to-power (or Power-to-X-to-power) systems, energy can be stored in a gas (fuel), and the gas is used in power generation. The advantage of this system is its high roundtrip efficiency compared to other energy storage systems. This makes the ReSOC system not only attractive but necessary for research to diversify our choices of energy storage solutions and to provide a more practical solution for the situation at hand (balancing energy systems or grids). Reversible solid oxide cell systems are well suited for energy management applications as both power and energy capacity are expected to be easily scalable. ReSOC systems also advantage in that they can be applied on a wide range from community-scale to distributed and grid-scale energy systems [40]–[44].

According to LUX research [45], the global energy storage market will hit $546 billion by 2035, and this will be facilitated by investment in diverse energy storage technologies. Innovation in energy storage systems is one of the major drivers in future energy technologies. The proposed ReSOC energy system is expected to be applicable for both distributed and grid-scale energy storage applications as well as industrial and urban central heating applications. The benefit of the system includes:

2.3.1 Cost-Benefit

Capital costs of a ReSOC system have been estimated between 233 to 317$/kWh and the cost of energy storage at 3 – 11 cents/kWh [46]–[50]. In comparison with other available energy storage systems, the storage cost of the ReSOC system is cheaper than a conventional battery and compressed air and competitive with pumped hydroelectric energy storage systems [49].

2.3.2 Renewable integration

With the increased penetration of renewable energy technologies in the global energy market and the resolution of various governments to maximize their potential in renewable energy generation via solar, wind, and geothermal sources for energy independence and security. ReSOC systems can be used as a buffer between renewable sources and energy consumptions to produce 100% clean energy. ReSOC systems can be operated with hydrogen and steam for a zero-carbon operation.

2.3.3 Distributed scale energy storage

Distributed scale energy systems are usually installed to operate at average capacity to reduce loss during off-peak energy demand conditions and to provide maximum possible energy supply during peak energy demand periods. This mismatch can be corrected by the means of energy storage technologies at the megawatt (MW) scale and with excellent time-shift properties. The proposed

ReSOC System is applicable at such scales for quick response and effective time-shift energy applications [23].

2.3.4 Large scale energy storage systems

Pumped hydroelectricity, compressed air, and Reversible solid oxide cell systems are the only energy storage technologies that have been technologically feasible for bulk scale power management and energy applications. ReSOC systems at this scale not only provide a better alternative to energy storage mix but also cost-competitive with other energy storage technologies at the bulk scale of application [46], [49], [51].

2.3.5 Smart Grid Application

For grid stabilization applications, the proposed system is expected to achieve a system roundtrip efficiency of 70%. This eases the stress on-peak electricity demand and load leveling. Future grids are expected to level energy supply with energy demand in opposite to the current systems available. ReSOC systems are scalable and can operate at a range of current densities. Thus, making them useful for intermittent power management systems crucial for smart grid applications.

2.3.6 Industrial & heating applications

Due to the high operating temperature of solid oxide cells, waste heat generated from the system can be used for residential heating purposes or industrial applications. The system can also be used for industrial syngas production [50]. The novelty of the system also lies in its ease of coupling with other power systems for a more efficient and economical energy system.

For industrial applications, ReSOCs can be used for heat and electricity generation and storage, primarily due to their high roundtrip efficiency of up to 70% at the system level and high operating temperature of over 600 ^{O}C [51]. Also, ReSOCs have the advantage of a wide variety of working fuels (H_2, H_2O, Syngas, CH_4) when compared to other cells used for the same purpose and have been demonstrated to be efficient to produce industrial syngas when operating in the electrolysis mode. Because RESOCs can use carbon-based fuels, they can be combined with gas turbines or afterburners for even more power generation when operated in fuel cell mode [52]. Studies have also shown the feasibility of combining ReSOC systems with carbon capturing and storage systems for efficient CO_2 sequestration and possible reuse for energy storage in electrolysis mode [49].

Efficient electrical energy storage and power-to-gas solutions could play a substantial role in increasing the penetration of fluctuating renewable energy resources, thus mitigating the worst impacts of climate change, and in integrating different energy grids and infrastructures. Some researchers have also demonstrated the feasibility of combining the ReSOC system with nuclear power generation systems. A large part of the capital costs of the ReSOC system was associated with the ReSOC stack and the storage tanks. This implies that advances in the stack materials and reduction of stack cost will lead to a further reduction in capital cost of ReSOC systems making them more suitable and economical for practical real-life use.

3
MODELING, VALIDATION, AND ANALYSIS OF RESOC STACK

3.1 Modeling

In this chapter, the ReSOC cell and stack considered in this study are described. ReSOC materials and properties, fuel constituents, governing electrochemical relations, and stack performance parameters are presented. Further, electrochemical and thermodynamics analysis of the cell and stack is carried out. As discussed in the introductory chapter of this thesis, a ReSOC is a high-temperature electrochemical cell that operates at temperatures of 500°C and above to store (SOEC Mode) and generate (SOFC Mode) electricity using steam and hydrogen or a combination of CO, CO_2, CH_4, $H_{2,}$ and H_2O. This high operating temperature requires special materials for the ReSOC and stack to operate efficiently and to withstand the accompanying thermal stress. Here, the cell electrode and electrolyte materials are as in [7], [53]. The electrolyte material is LSGM while the oxide electrode was produced from an LSCF-GDC functional layer with an LSCF current collector. The fuel electrode was fabricated from Ni infiltrate LSCM with a Ni infiltrated SLT support layer. There exist a potential of carbon deposition and cell carbon poisoning when the cell is operating on carbonaceous fuels such as CH_4 or syngas or CO. This carbon deposition probability can be eliminated by selecting the fuel gas mixture considering the carbon deposition boundary as shown on a C-H-O ternary diagram. A detailed explanation of the C-H-O ternary diagram can be found in [54]–[56]. The fuel composition for this study was selected following [7] and ensuring hydrogen to carbon ratio was maintained to avoid the carbon deposition region as recommended by the author.

The ReSOC stack is a collection of various homogenous cells connected either in series or parallel. Modeling and characterization of the stack are like the cell, especially in terms of performance and operating parameters. However, due to limitations imposed by the flow rate, the term stoichiometric factor or the excess air ratio is included in the stack modeling. A diagram of a typical ReSOC stack with the fuel and oxidant inlet and outlet positions is shown in Figure 3.1.

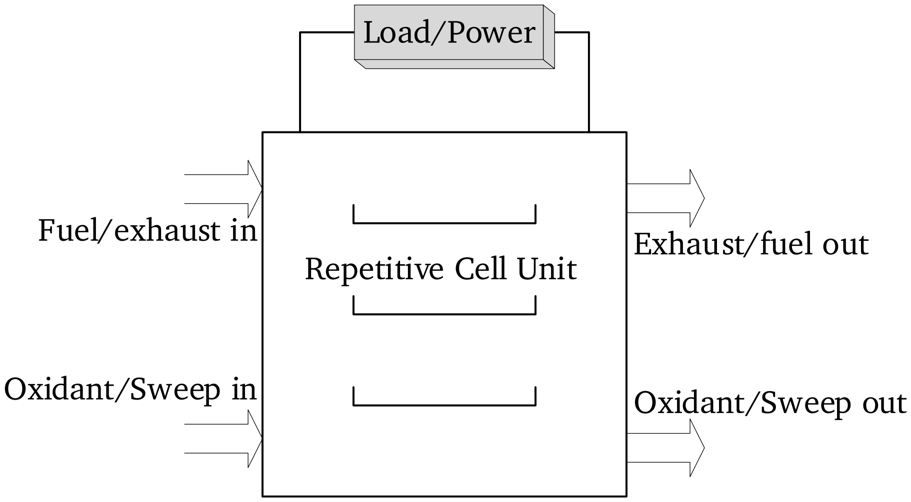

Figure 3.1 ReSOC stack reactant and product for power-producing fuel cell and fuel-producing electrolysis mode. Components are indicated as fuel cell mode/electrolysis cell mode.

The universal reactions taking place in a ReSOC is the oxidation (or reduction), methanation (or reforming), and water-gas shift (or reverse water-gas shift) reactions. Table 3.1 describes these reactions and their specific enthalpies in both modes of operation. In fuel cell mode the oxidation, reforming and water-gas shift reactions occur while in electrolysis mode reduction, methanation, and reverse water-gas shift occur. However, depending on the temperature at the axis of the cell and the reactant compositions, both water-gas shift and reverse water-gas shift can occur at different locations in the cell in one mode of operation. An advantage of the high operating temperature of the ReSOC is the ability to carry out internal reforming in the cell itself in the absence of a methane reformer. As shown in Table 3.1 a ReSOC can carry out both external and internal reforming.

Table 3.1 Reactions in a ReSOC Operating on Carbonaceous Fuel

Reaction	**Specific Enthalpy @298 K & 1 atm**	**Forward (SOFC Mode)**	**Reverse (SOEC Mode)**
$CH_4 + H_2O \Leftrightarrow 3H_2 + CO$	224 kJ/mol	Steam reformation	Methanation
$CO + H_2O \Leftrightarrow H_2 + CO_2$	36 kJ/mol	Water-gas shift	Reverse water-gas shift
$H_2 + 0.5O_2 \Leftrightarrow H_2O$	247 kJ/mol	Oxidation	Reduction

Some research claims that direct oxidation of CO and reduction of CO_2 can occur in ReSOCs [57], but in this study water-gas shift and reverse water-gas shift are taken to be the prominent pathway for this reaction to occur. This is due to the fast kinetics of ReSOCs which enables them to achieve near-equilibrium within the cell thus, product composition is not expected to be affected by the direct conversion of CO/CO_2. Also, the cell performance is dominated by the activation overpotential, and the diffusion losses do not significantly influence the cell performance as will be shown later. For these, only steam and hydrogen electrochemical conversion is assumed for this model. However, a more intrinsic study must consider the impact of direct CO/CO_2 electrochemical redox. The electrochemical redox half-reactions as considered in this study are defined for the fuel and oxidant electrodes in Equations 3.1 and 3.2, respectively. The cell-level electrochemical reactions and electron transfer are shown in Figure 3.2.

$$H_2 + O^{2-} \Leftrightarrow H_2O + 2e^- \tag{3.1}$$

$$0.5O_2 + 2e^- \Leftrightarrow O^{2-} \tag{3.2}$$

3.1.1 Mass Balance

The balances in the ReSOC and stack are dominated by the chemical and electrochemical reactions. The reactions are highly dependent on the inlet gas compositions. These inlet gas compositions after undergoing chemical and electrochemical changes form the exit gas composition of the ReSOC or stack.

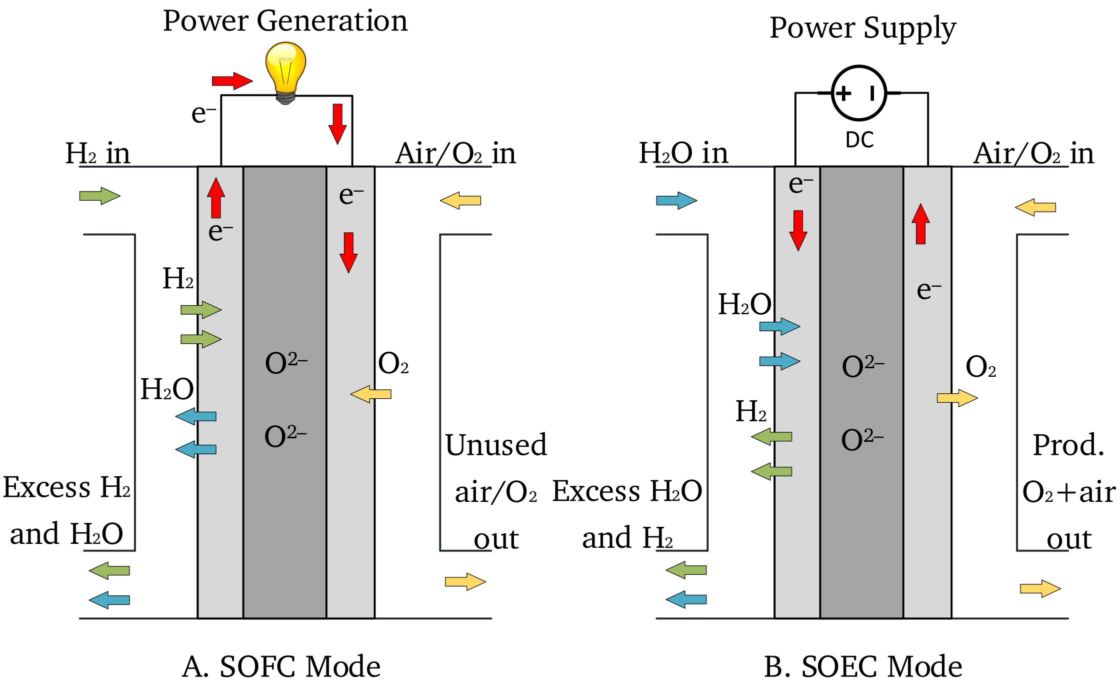

Figure 3.2 ReSOC operating in a) SOFC mode b) SOEC mode

The ReSOC considered in this study operates on a carbonaceous gas mixture containing at least two of the following gases: H_2, H_2O, CO, CO_2, CH_4, O_2, and N_2. Generally, the mole balance in the ReSOC is expressed as in Equations 3.3 to 3.9.

$$\dot{n}_{H_2,in} - \dot{n}_{H_2,out} = -3\dot{Y}_r - \dot{Y}_s + \dot{Z} \quad (3.3)$$

$$\dot{n}_{H_2O,in} - \dot{n}_{H_2O,out} = \dot{Y}_r + \dot{Y}_s - \dot{Z} \quad (3.4)$$

$$\dot{n}_{CO,in} - \dot{n}_{CO,out} = -\dot{Y}_r + \dot{Y}_s \quad (3.5)$$

$$\dot{n}_{CO_2,in} - \dot{n}_{CO_2,out} = -\dot{Y}_s \quad (3.6)$$

$$\dot{n}_{CH_4,in} - \dot{n}_{CH_4,out} = \dot{Y}_r \quad (3.7)$$

$$\dot{n}_{O_2,in} - \dot{n}_{O_2,out} = \dot{Z}/2 \quad (3.8)$$

$$\dot{n}_{N_2,in} - \dot{n}_{N_2,out} = 0 \quad (3.9)$$

$\dot{n}_{i,in}$ & $\dot{n}_{i,out}$ is the corresponding inlet and outlet molar flow rate, $\dot{Y}_r$ is the rate of the reforming reaction, $\dot{Y}_s$ is the rate of the water-gas shift reaction and $\dot{Z}$ is the rate of the redox electrochemical reaction. Equations 3.3 to 3.9 represent the reactions taking place in the fuel cell mode (forward reactions of Table 3.1). For the electrolysis mode where the reverse reaction takes place, the sign of the parameters on the right-hand side of the Equations needs to be reversed. Simply multiplying the inlet and outlet molar flow rate gives the mass flow rate for the gas species.

3.1.2 Fuel and Reactant Utilization Factors

The fuel utilization factor here is defined as the ratio of the amount of hydrogen utilized to the amount of equivalent hydrogen supplied to the ReSOC or stack in the SOFC mode. In the SOEC mode, it is referred to as the reactant utilization factor which is the ratio of oxygen produced from the reaction to the equivalent oxygen available in the reactant gases supplied to the ReSOC or stack. The fuel utilization factor (U_f) and the reactant utilization factor (U_r) as defined in this model is given by Equations 3.10 & 3.11, respectively.

$$U_f = \frac{\dot{n}_{H_2,converted}}{\dot{n}_{H_2,in} + \dot{n}_{CO,in} + 4\left(\dot{n}_{CH_4,in}\right)} \tag{3.10}$$

$$U_r = \frac{\dot{n}_{O_2,produced}}{2\left(\dot{n}_{H_2O,in} + \dot{n}_{CO,in} + 2\left(\dot{n}_{CO_2,in}\right)\right)} \tag{3.11}$$

Equation 3.10 contains hydrogen and other hydrogen-producing gases at the denominator. The denominator terms represent the methane in the reforming reaction, the carbon monoxide in the water-gas shift reaction, and the hydrogen of the electrochemical reaction.

It should be stated that the fuel utilization factor in the SOFC mode is not necessarily equal to the reactant utilization factor of the SOEC mode even if the stack is operating at the same current density and under the same operating condition for both modes of operation. However, in a closed system whereby the exit gas of the fuel cell mode is the inlet gas of the electrolysis cell mode and vice versa, the value of one does affect the value of the other in any mode of operation. This is because the fuel utilization measures the extent of oxidation of the fuel gases while the oxidant production measures the extent of reduction of the exhaust gases in the fuel cell mode and electrolysis mode, respectively. Thus, less oxidation in the fuel cell mode will amount to less reduction in the electrolysis mode.

3.1.3 Stoichiometric factor or excess air ratio

This is the ratio of the amount of oxygen supplied to the cell to the amount of oxygen required for the electrochemical reaction in the cell in the SOFC mode. For the electrolysis mode, the excess air ratio is the ratio of the rate of oxygen supplied to the cell to the oxygen produced in the cell. Here, the essence of supplying external air or oxygen to the cell is to drag the oxygen produced from the electrochemical reaction in the cell out through the exit channel. Since the oxygen will be produced at the reaction site, the produced oxygen needs to be driven out by a sweep gas. Also, supplied-air or oxygen to the cell provides thermal management in the stack. This will be discussed in further sections. Equations 3.12 and 3.13 define the excess air ratios for the SOFC and SOEC modes, respectively.

$$\lambda_{O_2,SOFC} = \frac{\dot{n}_{O_2,in}}{\dot{n}_{O_2,in} - \dot{n}_{O_2,out}} \tag{3.12}$$

$$\lambda_{O_2,SOEC} = \frac{\dot{n}_{O_2,in}}{\dot{n}_{O_2,out} - \dot{n}_{O_2,in}} \tag{3.13}$$

3.1.4 Current in a ReSOC

The current produced in ReSOC is one of the most fundamental characteristics of the rate of the electrochemical reaction in the cell. The electrochemical reaction is a product of the charge transfer/electron generation or consumption in the cell. And according to Faraday's law, the current is the rate of charge transfer. The relationship between current and charge transfer is shown in Equation 3.14.

$$i = \frac{dQ}{dt} \tag{3.14}$$

Where i is current, Q is the charge, and t is time. Representing the number of electrons transferred in an electrochemical reaction by n, and converting mole of electrons to charge using the Faraday's constant and introducing the rate of the electrochemical reaction in mol/s. The current is defined as Equation 3.15.

$$i = nF\dot{Z} \tag{3.15}$$

Where n is the number of electrons transferred in the electrochemical reaction, F is the Faraday's constant (96485 coulomb/mole) and $\dot{Z}$ is the rate of the electrochemical reaction in mol/s which is equivalent to the rate of hydrogen/steam conversion in the redox reaction. It should be noted that only the electrochemical reaction rate is involved in the current production process. In this case the H_2-O_2 redox reaction rate.

3.1.5 Nernst Voltage

The Nernst voltage also referred to as the open-circuit voltage (OCV) is the minimum (SOEC mode) or maximum (SOFC Mode) operating voltage of the ReSOC at its operating temperature and pressure for a specific reactant gas mixture. In other words, it is the ideal operating voltage of the cell where the performance is at the maximum theoretical efficiency regardless of the mode of operation. It is characterized by the change in Gibb's free energy of the reaction. Gibb's free energy of an electrochemical process is defined as the maximum reversible electrochemical work associated with the process to reach equilibrium at constant temperature and pressure. Mathematically, it is the difference between the change in enthalpy and entropy change of the process, defined as in Equation 3.16:

$$G = H - TS \tag{3.16}$$

For a chemical reaction, the Gibbs free energy is defined in terms of the enthalpy and entropy changes of the reaction. The change in Gibbs free energy of a reaction is shown in Equations 3.17 & 3.18.

$$\Delta\hat{g}(T) = \Delta\hat{h} - T\Delta\hat{s} \tag{3.17}$$

$$\Delta\hat{g} = \hat{g}_{products} - \hat{g}_{reactants} \tag{3.18}$$

Where H is the enthalpy, T is the temperature at which the reaction takes place, S is the entropy and $\hat{h}$ & $\hat{s}$ is the enthalpy and entropy change of the reaction per unit mole of the reactants and products.

Work is done in an electrochemical cell through the movement of electrons through a potential difference [58]. Equation 3.19 relates the work in an electrochemical cell to the Gibbs free energy.

$$W_{ele} = -\Delta\hat{g} \tag{3.19}$$

Also, Equation 3.20 defines the relationship between the electrochemical work and the electromotive force.

$$W_{ele} = nFE \tag{3.20}$$

Combining Equations 3.19 & 3.20 gives the relationship between the Gibbs free anergy and the electromotive force as shown in Equation 3.21.

$$-\Delta\hat{g} = nFE \tag{3.21}$$

Thus, the reversible voltage generated for an electrochemical reaction is given in Equation 3.22. The reversible voltage is the voltage at which an electrochemical reaction is at equilibrium.

$$E = -\frac{\Delta\hat{g}}{nF} \tag{3.22}$$

Where n is the number of electrons transferred, F is the Faraday's constant of 96485 coulomb/mole, and E is the electromotive force or potential difference in the cell.

In a reacting gas mixture, the Gibbs free energy of the reaction at constant temperature and pressure is expressed as a function of the partial pressure of the reactant and product gases as defined in Equation 3.23. Equation 3.24 is a general chemical reaction showing the corresponding products and reactants species.

$$\Delta\hat{g}_T = \Delta\hat{g} + RT\ln\frac{p_M^m \cdot p_N^n}{p_A^a \cdot p_B^b} \tag{3.23}$$

$$aA + bB \Leftrightarrow \mathrm{mM} + \mathrm{nM} \tag{3.24}$$

Where the reactant gases A and B form products M and N. The stoichiometric coefficients are written with the italicized, lowercase letters a, b, m, and n. R is the universal gas constant 8.314 J/mol-K. p_i^j is the partial pressure of the corresponding gas in the flow stream. Expressing Equation 3.23 in terms of voltage and using the relation in Equation 3.22 yields the Nernst potential as defined in Equation 3.25.

$$E_{Nernst} = E - \frac{RT}{nF}\ln\frac{p_M^m \cdot p_N^n}{p_A^a \cdot p_B^b} \tag{3.25}$$

The Nernst Equation defines the maximum voltage a fuel cell or minimum voltage an electrolysis cell can achieve for a specific gas mixture at its operating temperature and pressure.

For the forward reaction in the reduction/oxidation process of H_2, H_2O, and O_2 gases in a ReSOC (Equation 3.26), the Nernst Voltage is defined by Equation 3.27.

$$H_2 + 0.5O_2 \Leftrightarrow H_2O \tag{3.26}$$

$$E_{Nernst} = E - \frac{RT}{nF} \ln \frac{p_{H_2O}}{p_{H_2} \cdot p_{O_2}^{0.5}} \tag{3.27}$$

The partial pressure of a gas species is related to the molar fraction of the gas as expressed in Equation 3.28. Using Equation 3.28 in Equation 3.27, the Nernst voltage can be expressed as a function of the molar fraction of the gas species, assuming the pressure at the oxide and fuel electrodes is the same as the ReSOC operating pressure. The resulting expression is given as Equation 3.29.

$$p_i = X_i \cdot P_{tot} \tag{3.28}$$

$$E_{Nernst} = E - \frac{RT}{nF} \ln \left(\frac{X_{H_2O}}{X_{H_2} \cdot X_{O_2}^{0.5}} \sqrt{\frac{1}{P_{cell}}} \right) \tag{3.29}$$

Equation 3.29 shows the relationship between the Nernst voltage, cell operating temperature, and cell operating temperature explicitly. X_i is the molar fraction of the respective gas species and P is the pressure in bar.

3.1.6 Chemical equilibrium constant

In the Equation for the Gibbs free energy of a chemical reaction, the term represented by the partial pressure is called the reaction quotient. The reaction quotient, K, is defined in Equation 3.30 as:

$$K = \frac{p_M^m \cdot p_N^n}{p_A^a \cdot p_B^b} \tag{3.30}$$

The value of K at which the forward and reverse reactions occur at the same rate is called the equilibrium constant of the reaction. The equilibrium constant is derived from the Gibbs free energy of the reaction and expressed in Equation 3.31 as:

$$\ln K = \frac{-\Delta \hat{g}}{RT} \tag{3.31}$$

This constant is useful in calculating equilibrium compositions of products for a particular reaction under any operating temperatures and pressure.

As mentioned in Table 3.1, reactions in a ReSOC include reformation, methanation, water-gas shift, and reverse water gas shift reactions. Equilibrium constants of the reformation and water gas shift reactions are calculated in Equations 3.32 & 3.33, respectively. The corresponding Gibbs free energy of the reformation and water gas shift reactions is expressed in Equations 3.34 & 3.35, respectively. While Equations 3.32 to 3.35 represent the forward reactions as shown in the table, the reverse reactions can be determined by simply substituting the reactants for the products and vice versa. Equation 3.36 is the same as Equation 3.15, the difference being that the term in the former uses specific values per mole of the respective gas species.

$$K_r = \frac{X_{H_2}^3 \cdot X_{CO}}{X_{CH_4} \cdot X_{H_2O}} P^2 \tag{3.32}$$

$$K_s = \frac{X_{CO_2} \cdot X_{H_2}}{X_{CO} \cdot X_{H_2O}} \tag{3.33}$$

$$\Delta \hat{g}_r = 3\hat{g}_{H_2} + \hat{g}_{CO} - \hat{g}_{CH_4} - \hat{g}_{H_2O} \tag{3.34}$$

$$\Delta \hat{g}_s = \hat{g}_{CO_2} + \hat{g}_{H_2} - \hat{g}_{CO} - \hat{g}_{H_2O} \tag{3.35}$$

$$\hat{g}_i = \hat{h}_i(T) - T \cdot \hat{s}_i(T, P) \tag{3.36}$$

3.1.7 Cell Overpotentials

Overpotentials in solid oxide cells are caused by several factors such as the activation energy of the reaction, the electrical conductivity of the cell materials, the gas diffusivity, structure of the cell materials, interconnects between cells, leakages between cells, etc. However, the most prominent overpotentials are the activation, ohmic, and concentration overpotentials of the cell and thus will be the only ones considered for this study.

3.1.7.1 Activation Overpotential

This is the overpotential caused by the energy required for the reactants to cross the free energy barrier, become activated, and in turn form products [59]. This energy is called the activation energy. The activation energy is the minimum energy required for electrochemical reactant species to form a product. To overcome this energy barrier, an electrochemical cell sacrifices some voltage (fuel cell mode) or requires additional voltage (electrolysis mode). The activation overpotential is related to the current density through the Butler-Volmer Equation given in Equation 3.37.

$$\frac{j}{j_{0,i}} = e^{\left(\frac{\alpha_{i,a} nF\eta_{act,i}}{RT}\right)} - e^{\left(-\frac{\alpha_{i,c} nF\eta_{act,i}}{RT}\right)} \tag{3.37}$$

Where j is the cell current density, $j_{0,i}$ is the exchange current density of the electrode, i denotes fuel electrode or oxidant electrode, n=2 in the fuel electrode and 4 in the oxidant electrode, α is the charge transfer coefficient or electrode symmetry factor usually between 0 and 1.

The current density is the amount of current passing through the cell per unit active cell area. It is the most widely used parameter in characterizing the performance of a fuel cell and defining the operating condition of the cell. Since the current scales with cell size, the current density is a universal term that can be used regardless of cell or stack size. The current density multiplied by the cell active area gives the current passing through or generated by the cell or stack. However, unlike the current in the cell, the current density is independent of the cells being connected in series or parallel. Since separate reactions occur at the electrodes as shown in Equations 3.1 and 3.2, the total activation potential is contributed from both the fuel electrode and the oxide electrode. Equation 3.38 defines the total activation overpotential in a ReSOC cell.

$$\eta_{act} = \eta_{act,FE} + \eta_{act,OE} \tag{3.38}$$

FE denotes fuel electrode and OE denotes oxide electrode. In the same manner, the exchange current densities are defined separately at each electrode. The exchange current density is the “equilibrium current density”. It is the current density at which both the forward and reverse electrochemical reactions are taking place at the same rate. The exchange current density is dependent on reactant concentration as will be shown in Equations 3.39 and 3.40. The exchange current density is defined as in Ref. [53].

$$j_{0,FE} = j_{0,FE}^{ref} \left(\frac{p_{H_2}}{P_0}\right)^{0.5} \left(\frac{p_{H_2O}}{P_0}\right)^{0.5} e^{\left(-\frac{E_{act,FE}}{RT}\left(\frac{1}{T}-\frac{1}{T_{ref}}\right)\right)} \tag{3.39}$$

$$j_{0,OE} = j_{0,OE}^{ref} \left(\frac{p_{O_2}}{P_0}\right)^{0.2} e^{\left(-\frac{E_{act,OE}}{RT}\left(\frac{1}{T}-\frac{1}{T_{ref}}\right)\right)} \tag{3.40}$$

Where a, b, c, T_{ref}, $j_{0,i}^{ref}$ and $E_{act,i}$ are constants defined in the reference literature [53], p_i is the partial pressure of the gas species. The partial pressures are the values calculated at the triple phase boundary (TPB) in the concentration overpotential.

3.1.7.2 Concentration Overpotential

This is due to the diffusion of the reactants and products through the porous electrode structures. Like the activation overpotential, the total concentration overpotential is a sum of the overpotentials at the fuel and oxidant electrode. The difference of the molar concentrations between the electrode surface and the reaction site is modeled using the Fickian diffusion and the mole fractions are used to estimate the concentration overpotential [3]. Equations 3.41 to 3.43 show the total concentration overpotential, concentration overpotential at the fuel electrode, and concentration overpotential at the oxide electrode, respectively.

$$\eta_{conc} = \eta_{conc,FE} + \eta_{conc,OE} \tag{3.41}$$

$$\eta_{conc,FE} = \frac{RT}{2F} \ln\left(\frac{X_{H_2,cha} \cdot X_{H_2O,TPB}}{X_{H_2O,cha} \cdot X_{H_2,TPB}}\right) \tag{3.42}$$

$$\eta_{conc,OE} = \frac{RT}{4F} \ln\left(\frac{X_{O_2,cha}}{X_{O_2,TPB}}\right) \tag{3.43}$$

The subscript cha denotes the molar fraction of the gas supplied to the cell and TPB is the molar fraction at the triple phase boundary or the reaction site in the cell. In the stack, an intermediary concentration, defined as the surface concentration is added to account for the difference in the concentration between the stack entry and the cell surface before the triple phase boundary of the cell. The surface concentration is defined as in [60]. Equations 3.44 to 3.46 give the concentration at the triple phase boundary as defined in [61].

$$X_{H_2O,TPB} = X_{H_2O,cha} + \frac{RT\delta_{FE} j}{2FPD_{H_2O}^{eff}} \tag{3.44}$$

$$X_{H_2,TPB} = X_{H_2,cha} - \frac{RT\delta_{FE}j}{2FPD_{H_2}^{eff}} \tag{3.45}$$

$$X_{O_2,TPB} = \frac{1}{d_{O_2}} + \left(X_{O_2,cha} - \frac{1}{d_{O_2}}\right) \cdot exp\left(-\frac{RT\delta_{OE}j}{4FPD_{O_2}^{eff}}\right) \tag{3.46}$$

δ_{OE} and δ_{FE} are the oxidant electrode and fuel electrode thickness (m) respectively. D_i^{eff} is the effective diffusivity of the gas in the flow stream, j is the current density in the cell. The term d_{O_2} in Equation 3.46 is the oxygen effective diffusivity ratio defined in Equation 3.47 as:

$$\frac{1}{d_{O_2}} = \frac{D_{O_2,kn}^{eff}}{D_{O_2,kn}^{eff} + D_{O_2-N2}^{eff}} \tag{3.47}$$

The diffusivity of the gases is calculated from the Knudsen diffusion and binary diffusion coefficient [43] and given in Equations 3.48 to 3.53.

$$\frac{1}{D_k^{eff}} = \frac{1}{D_{k,kn}^{eff}} + \frac{1}{D_{k-m}^{eff}} \tag{3.48}$$

$$D_{k,kn}^{eff} = \frac{\xi}{\tau} \cdot D_{k,kn} \tag{3.49}$$

$$D_{k-m}^{eff} = \frac{\xi}{\tau} \cdot D_{k-m} \tag{3.50}$$

$$D_{k,kn} = \frac{d_p}{3}\sqrt{\frac{8RT}{\pi M_k}} \tag{3.51}$$

$$D_{k-m} = \frac{1.43 \cdot 10^{-3} \cdot T^{1.75}}{P\left(\frac{2}{M_{k-m}}\right)^{0.5} \cdot \left(v_k^{1/3} + v_m^{1/3}\right)^2} \tag{3.52}$$

$$M_{k-m} = \frac{1}{M_k} + \frac{1}{M_m} \tag{3.53}$$

$\{when\ k\ is\ H_2;\ m\ is\ H_2O\ and\ vice\ versa\}$

Where d_p is electrode pore diameter, M is the molar mass of the gas, v is the special fuller's diffusion volume, D_{k-m} is the binary diffusion of specie m into k, $D_{k,kn}$ is the Knudsen diffusion, ξ is electrode porosity and τ is electrode tortuosity.

3.1.7.3 Ohmic Overpotential

This overpotential is due to the electrical and ionic conductivity of the cell materials. It follows ohm's law and is defined in Equations 3.54 to 3.56.

$$\eta_{ohm} = j \cdot R_{cell} \tag{3.54}$$

$$R_{cell} = R_{OE} + R_{FE} + R_{EL} \tag{3.55}$$

$$R_i = \delta_i/\sigma_i \tag{3.56}$$

R_{cell} is the total electric area-specific resistance of the cell, subscript EL represents electrolyte, FE is the fuel electrode, OE is the oxide electrode, and σ is the conductivity (electric or ionic). The conductivity of the electrode and electrolyte materials is given in the literature.

3.1.8 Operating Voltage

The cell operating voltage is governed by the difference between the Nernst voltage and the cell overpotentials as defined by Equation 3.57.

$$V_{cell} = E_{nernst} - \eta_{ohm} - \eta_{act} - \eta_{conc} \tag{3.57}$$

The operating voltage in the stack is different from the individual cell operating voltage [62]. This additional voltage is attributed to further losses between cell interconnects when scaling up to a stack. In this study, this loss is attributed as η_{sta} and its area-specific resistance (ASR) is taken to be 0.10 Ωcm^2 is defined in references [14 & 15]. The corresponding additional stack overpotential is determined by this ASR multiplied by the current density. Thus Equation 3.58 defines the stack operating voltage as:

$$V_{sta} = E_{nernst} - \eta_{ohm} - \eta_{act} - \eta_{conc} - \eta_{sta} \tag{3.58}$$

V_{sta} is not the overall stack operating voltage but rather the corresponding operating voltage of an individual cell when operating in a stack. It can be referred to as the “effective cell operating voltage”. This must be noted when calculating stack power and power density, to avoid humongous mistakes. It should be noted that in the fuel cell mode, current density and overpotentials are positive, and in the electrolysis cell mode of operation, negative. This leads to an operating voltage lesser than the Nernst voltage in the fuel cell mode of operation and a higher than the Nernst voltage in the electrolysis cell mode of operation.

3.1.9 Power and Power Density

The electrical power generated (Fuel Cell mode) or consumed (Electrolysis Cell mode) in the ReSOC is a product of the cell operating voltage and current. Defined in Equation 3.59 as:

$$\dot{W}_{cell} = V_{cell} \cdot i \tag{3.59}$$

The cell power ($\dot{W}_{cell}$) is expressed in Watts or Kilowatts. The Power in the stack on the other hand is a product of the effective cell voltage in the stack, the cell current, and the total number of cells in the stack. Equation 3.60 defines the stack power in both modes of operation as:

$$\dot{W}_{stack} = \sum_{no\ of\ cells=1}^{m} (V_{sta} \cdot i) \tag{3.60}$$

The stack power ($\dot{W}_{stack}$) is expressed in Watts or Kilowatts. Where m is the total number of cells in the stack. It can be defined as no of cells per module multiplied by the number of modules or number of cells connected in series multiplied by the number of cells connected in parallel depending on the stack configuration. In this study, the total number of cells was considered as a total without giving respect to the stack configuration.

The power density in the cell, like the current density, is the electrical power generated or consumed by the cell per unit surface area of the cell. The unit can be in W/cm^2 or kW/m^2. This relationship is shown mathematically in Equation 3.61. The surface area is the total surface area of the cell which sometimes can be different from the cell active surface area. In this study, however, the cell surface area has been taken to be equal to the active surface area for simplicity.

$$Pd_{cell} = \frac{\dot{W}_{cell}}{Cell\ Surface\ Area} = V_{cell} \cdot j \tag{3.61}$$

3.1.10 Heating Value of Reactant and Product gases

The heating value of a gas is the energy content of the gas per unit mass or mole of the gas compound. The unit is kJ/mol or MJ/kg. Examples of such gas with heating values are alkanes, hydrogen, carbon monoxide, ammonia, etc. In this study, the lower heating values were used in calculating the heating values of respective gases because the ReSOC and stack operating temperature are beyond the vaporization temperature of liquid H_2O. For a gas mixture, the heating value of the gas is the sum of the heating value of the containing gases with their respective mass. In Equation 3.62, the lower heating value of a gas mixture containing H_2, H_2O, CO, CO_2, and CH_4 is shown. The mass here is represented as a rate; hence, the total heating value is also a rate. Integrating this over a period will give the total heating value produced or consumed by a ReSOC or Stack. Since H_2O and CO_2 have no energy content, they are not included in the total heating value of the gas mixture.

$$\dot{W}_{LHV} = \left(\dot{m}_{H_2} \cdot LHV_{H_2}\right) + \left(\dot{m}_{CO} \cdot LHV_{\mathrm{CO}}\right) + \left(\dot{m}_{CH_4} \cdot LHV_{CH_4}\right) \tag{3.62}$$

LHV stands for lower heating value. This relationship is used in estimating the total rate of the heating value of the reactant and product gas in the SOFC and SOFC mode of the ReSOC and stack in this study.

3.1.11 Energy balance in a ReSOC Stack

The energy balance follows the general convention for a steady flow process. In the fuel cell mode, electrical energy is produced, and it is consumed in the electrolysis mode. The energy balance for the fuel cell mode and electrolysis mode as applied in the stack is given in Equations 3.63 and 3.64, respectively.

$$\sum_i \left(\dot{n}_i \cdot \hat{h}_i\right)_{in} = \sum_i \left(\dot{n}_i \cdot \hat{h}_i\right)_{out} + \dot{W}_{stack,SOFC} \tag{3.63}$$

$$\sum_i \left(\dot{n}_i \cdot \hat{h}_i\right)_{in} + \dot{W}_{stack,SOEC} = \sum_i \left(\dot{n}_i \cdot \hat{h}_i\right)_{out} \tag{3.64}$$

$\dot{n}_i$ is the molar flow rate of individual gas species (mol/s), $\hat{h}$ is the specific enthalpy (J/mol) and $\dot{W}$ is the electrical energy (Watts).

3.1.12 Thermoneutral Voltage

The thermoneutral voltage is the voltage required for net heat generation in a ReSOC stack. It is the enthalpy change associated with the electrochemical reaction per unit of charge transferred. The thermoneutral voltage has been employed in literature for electrolysis and co-electrolysis thermal management studies. Since ReSOCs may be employed for heat and power cogeneration purposes, the thermoneutral voltage is useful in calculating stack inlet gas temperatures to avoid overheating the stack and to predict stack heat characteristics. Equation 3.65 is the mathematical definition of the thermoneutral voltage.

$$V_{TN} = -\frac{\Delta\hat{h}}{nF} \tag{3.65}$$

Where, $\Delta\hat{h}$ is the enthalpy change of the reaction. For a steam/hydrogen reaction at 800°C, the thermoneutral voltage is 1.42V. In an electrochemical redox reaction, the thermoneutral voltage can be expressed in terms of the rate of the reaction as shown in Equation 3.66.

$$V_{TN} = -\Delta\hat{h}_{redox} \cdot \frac{\dot{Z}}{i} \tag{3.66}$$

Where, r_{redox} is the rate of the redox reaction and i is the current.

Since ReSOCs are compatible with carbonaceous reactants, in the case where the reactant gas is a mixture of gases whereby reactions such as the reforming and water gas shift take place in the ReSOC, the thermoneutral voltage is expressed considering the enthalpy of all occurring reactions. The heat produced from one reaction can be provided as required heat for the next reaction at the ReSOC operating conditions. For this study, the thermoneutral voltage is defined as in Equation 3.67.

$$V_{TN} = -\left\{\left(\Delta\hat{h}_{redox} \cdot \frac{\dot{Z}}{i}\right) + \left(\Delta\hat{h}_{shift} \cdot \frac{\dot{Y}_s}{i}\right) + \left(\Delta\hat{h}_{reform} \cdot \frac{\dot{Y}_r}{i}\right)\right\} \tag{3.67}$$

To avoid the need for an external heat source in a ReSOC stack, the relationship between the electrolysis and fuel cell mode operating voltage and the thermoneutral voltage is recommended as in Equation 3.68.

$$V_{EC} > V_{TN} > V_{FC} \tag{3.68}$$

Where V_{FC} and V_{EC} are the operating voltage of the ReSOC in the fuel cell and electrolysis cell mode, respectively at the selected operating current density. The heat requirement of the ReSOC stack is calculated from the thermoneutral voltage in Equation 3.69.

$$\dot{Q} = i\left(V_{op} - V_{TN}\right) \tag{3.69}$$

In the SOEC mode of operation, heat is generated for a positive $\dot{Q}$ and external heat is required for a negative $\dot{Q}$, while for the SOFC mode reverse is the case. Most importantly, the current is taken as positive for both modes of operation. The heat requirement or heat generation in the stack is reflected in the temperature change of the oxidant in the stack. If heat is generated in the stack, the temperature of the oxidant increases across the stack and vice versa. This leads to a corresponding enthalpy change in the oxidant. This enthalpy change in the oxidant is equivalent to the heat requirement or generation in the ReSOC stack.

3.1.13 Performance Metrics in the ReSOC and Stack

Since the electrolysis and fuel cell mode of the ReSOC stack is expected to operate independently of each other, the energy efficiencies of both modes are separately defined based on the respective inputs and outputs.

3.1.13.1 ReSOC Efficiency

In the SOFC mode, for the ReSOC stack, the only output is the electrical power, and the considered input is the heating value of the fuel gas. The practical energy efficiency of a typical solid oxide fuel cell contains three parts: thermal efficiency, electrical efficiency, and fuel utilization efficiency [59]. The energetic efficiency of the cell and stack in the fuel cell mode of operation is given in Equation 3.70.

$$\eta_{FC} = \frac{\dot{W}_{SOFC}}{\sum \dot{W}_{LHV,in} + \max\left(0, \dot{Q}_{FC}\right)} \tag{3.70}$$

$\dot{W}_{SOFC}$ is the rate of electrical power generation in the ReSOC stack (Equation 3.59), $\dot{W}_{LHV,in}$ represents the rate of LHV of the fuel inlet gases to the ReSOC stack (Equation 3.61) and, $\dot{Q}_{FC}$ is the rate of heat required or generated in the stack (Equation 3.68). Equation 3.69 best expresses the efficiency when the ReSOC or stack operates at a constant inlet gas flow rate and varying fuel utilization factor. In a study where the fuel utilization factor is constant, but the inlet gas flow rate is varied, the lower heating value corresponding power should be expressed as the difference between the inlet and exit gas flow rate to be able to better express the effect of the fuel utilization factor.

In the SOEC mode, alongside the heating value of the produced fuel gas and electrical power consumption in the stack, the heat requirement of the stack is also considered in the energy efficiency calculation. At high operating current densities where the device requires external heating (this will be explained in the further sections), the efficiency of the stack will exceed 100% if the heat requirement of the stack is not taken into consideration. The stack efficiency is thus defined as in Equation 3.71:

$$\eta_{EC} = \frac{\sum \dot{W}_{LHV,prod}}{\dot{W}_{SOEC,in} - \min(0, \dot{Q}_{EC})} \tag{3.71}$$

$$\sum \dot{W}_{LHV,prod} = \sum \dot{W}_{LHV,out} - \sum \dot{W}_{LHV,in} \tag{3.72}$$

Where, $\dot{Q}_{EC}$ is the rate of external heat supplied to the stack and $\dot{W}_{LHV,prod}$ is the rate of the heating value of the produced fuel gases in the electrolysis mode.

3.1.13.2 Roundtrip Efficiency

One of the most crucial parameters in characterizing an energy storage system is roundtrip efficiency. The roundtrip efficiency is the percentage of the total stored energy of a system that can be recovered from the system. In other words, it is the ratio of the total energy recovered in a system to the total energy stored in the system.

In a system operating at a steady state, the roundtrip efficiency can be defined in terms of system power as the ratio of power discharged from the system to the power charged into the system. It is impractical however to design energy storage systems based on power roundtrip efficiency. This is due to fluctuations in the operation of real systems. However, power roundtrip efficiency is a key tool for system optimization and selecting system design, minimum, and maximum operating conditions since characterizes the performance of the system while in operation. Since gas storage tank sizing is not covered in the scope of this study, the stack and system operating power is used to characterize the roundtrip efficiency. For a ReSOC stack, the theoretical or maximum roundtrip efficiency is defined in Equation 3.73 according to the energy required for electrolysis and energy generated from the fuel cell.

$$\eta_{RT,Theoretical} = \frac{Max\ Energy\ Generation\ in\ Fuel\ Cell}{Min\ Energy\ utilisation\ in\ Electrolysis\ Cell} \tag{3.73}$$

As earlier described, thermodynamically, the maximum work generated in the fuel cell is the Gibbs free energy of the reaction, and the minimum energy required for electrolysis is the change in enthalpy of the reaction. Thus, theoretical roundtrip for the reversible electrochemical reaction is given in Equation 3.74 and the relationship between the change in enthalpy, Gibbs free energy, and entropy is given in Equation 3.75.

$$\eta_{RT,Theoretical} = \frac{\Delta G}{\Delta H} \tag{3.74}$$

$$\Delta H = \Delta G + T\Delta S \tag{3.75}$$

The above Equation for the maximum roundtrip is applicable for all cases of a negative entropy change. In rare cases where there is a positive entropy change, the inverse of the equation is applicable for the theoretical roundtrip efficiency of the stack. A positive entropy change indicates an endothermic reaction with a $T\Delta S$ amount of heat required to account for the difference between the enthalpy change and the maximum work output from the reaction. Equation 3.76 describes the theoretical roundtrip efficiency for a positive entropy change in the reaction.

$$\eta_{RT,Theoretical,\Delta S>0} = \frac{\Delta H}{\Delta G} \tag{3.76}$$

A 100% roundtrip efficiency will thus indicate that all the chemical energy in the gas can be converted to electricity in the fuel cell mode and that all the electricity supplied to the electrolyzer can be converted to the chemical energy of the fuel.

As discussed earlier, the stack performance is characterized by the operating voltage. To express the roundtrip efficiency in terms of power rather than energy, a constraint of operating time is placed on both modes of operation. Recall from Equation 3.14 that the current in the ReSOC is the rate of charge transferred. To unify both operating modes, the charge transfer for both modes of operation is taken as equal, and they are assumed to operate for the same duration. Hence, in Equations 3.77 and 3.78, the constraint for this model is given as:

$$SOFC_{duration} = SOEC_{duration} \tag{3.77}$$

$$i_{SOFC} = i_{SOEC} \tag{3.78}$$

In this light, the actual stack roundtrip efficiency is defined as Equation 3.79:

$$\eta_{RT,stack} = \frac{\dot{W}_{SOFC}}{\dot{W}_{SOEC}} \tag{3.79}$$

$\dot{W}_{SOFC}$ and $\dot{W}_{SOEC}$ is the power generation and consumption in the stack in the SOFC mode and SOEC mode, respectively.

3.2 Simulation Procedure and Model Validation

The ReSOC and stack model was carried out using the Equations introduced in Section 3.1. First, the ReSOC was modeled, and the results are extrapolated for the stack model. In modeling the ReSOC, parameters such as cell active area, excess air ratio, and energy balance were not considered. This is because the cell model was limited to performance evaluation and to determine the operating range of the cell. The stack model followed the same procedure as the cell model except for parameters such as stack operating voltage and stack power (Equations 3.58 & 3.60). All models are carried out using Engineering Equation Solver (EES) software. A snapshot of the coding process in EES software is given in Figure 3.3.

Figure 3.4 and Figure 3.5 show the model process for the cell and stack, respectively. In the cell, first the operating conditions such as pressure, temperature, fuel utilization ratio, and current density were determined. Then the inlet gas compositions (fuel and oxidant) were determined. In the modeling of this study, the reactant gas compositions were taken as in reference [7]. These are used to calculate the equilibrium gas compositions on the exit side of the cell. The equilibrium composition and operating temperature and pressure are used to calculate the Nernst voltage and the fuel utilization is used to calculate the reaction rate in the electrochemical reaction. The reaction rate is used to calculate the cell current. Thermoneutral voltage was estimated from the reforming, water-gas shift, and redox reaction rates. The current density and other cell properties were used to calculate the overpotentials in the cell, then the cell operating voltage. A graph of the current density against the operating voltage is sketched through parametrization to characterize the cell performance.

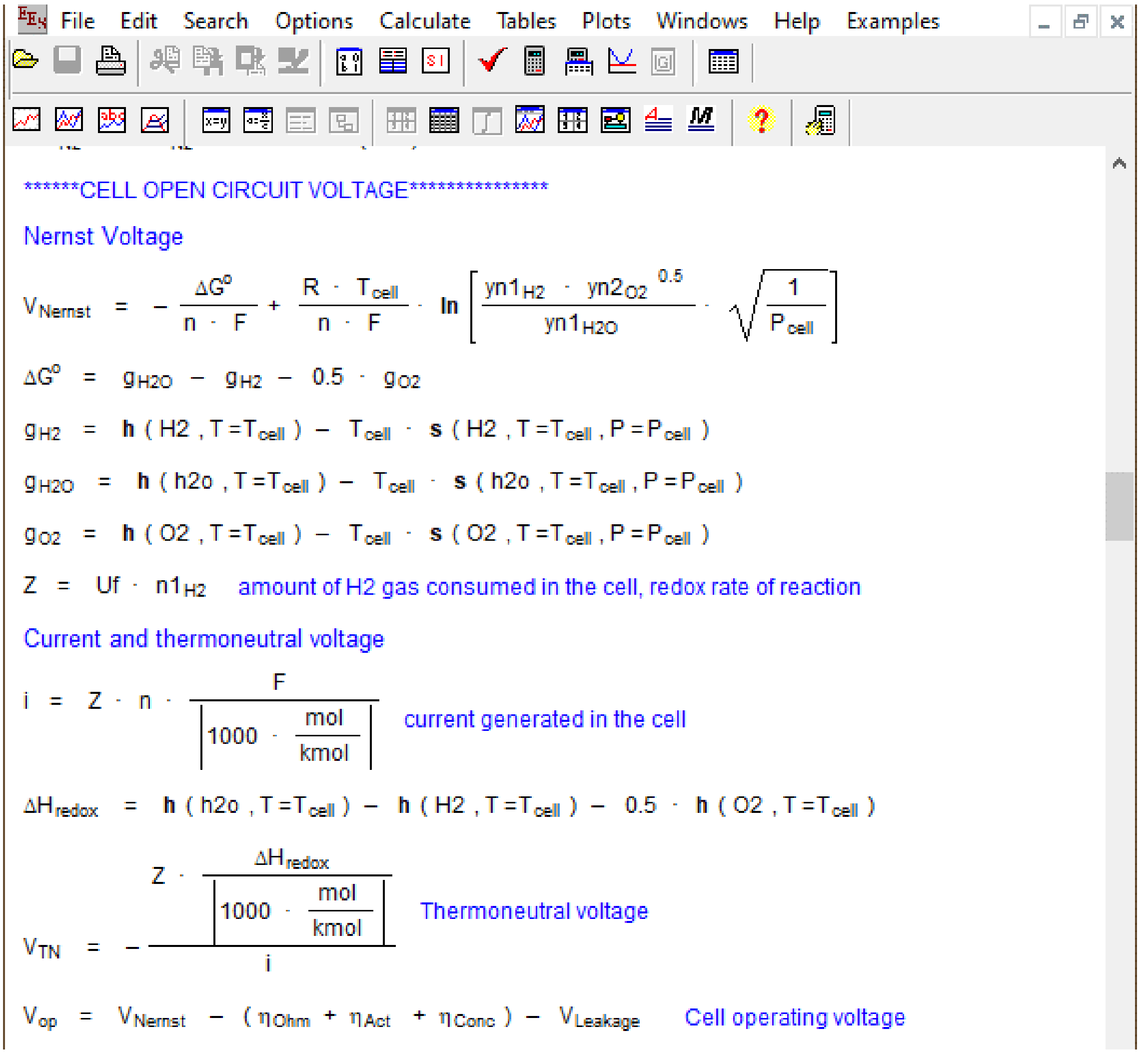

******CELL OPEN CIRCUIT VOLTAGE***************

Nernst Voltage

$$V_{Nernst} = -\frac{\Delta G^o}{n \cdot F} + \frac{R \cdot T_{cell}}{n \cdot F} \cdot \ln\left[\frac{yn1_{H2} \cdot yn2_{O2}^{0.5}}{yn1_{H2O}} \cdot \sqrt{\frac{1}{P_{cell}}}\right]$$

$$\Delta G^o = g_{H2O} - g_{H2} - 0.5 \cdot g_{O2}$$

$$g_{H2} = \mathbf{h}(H2, T = T_{cell}) - T_{cell} \cdot \mathbf{s}(H2, T = T_{cell}, P = P_{cell})$$

$$g_{H2O} = \mathbf{h}(h2o, T = T_{cell}) - T_{cell} \cdot \mathbf{s}(h2o, T = T_{cell}, P = P_{cell})$$

$$g_{O2} = \mathbf{h}(O2, T = T_{cell}) - T_{cell} \cdot \mathbf{s}(O2, T = T_{cell}, P = P_{cell})$$

$Z = Uf \cdot n1_{H2}$ amount of H2 gas consumed in the cell, redox rate of reaction

Current and thermoneutral voltage

$$i = Z \cdot n \cdot \frac{F}{\left|1000 \cdot \frac{mol}{kmol}\right|}$$ current generated in the cell

$$\Delta H_{redox} = \mathbf{h}(h2o, T = T_{cell}) - \mathbf{h}(H2, T = T_{cell}) - 0.5 \cdot \mathbf{h}(O2, T = T_{cell})$$

$$V_{TN} = -\frac{Z \cdot \frac{\Delta H_{redox}}{\left|1000 \cdot \frac{mol}{kmol}\right|}}{i}$$ Thermoneutral voltage

$$V_{op} = V_{Nernst} - (\eta_{Ohm} + \eta_{Act} + \eta_{Conc}) - V_{Leakage}$$ Cell operating voltage

Figure 3.3 Model Coding in Engineering Equation Solver Software

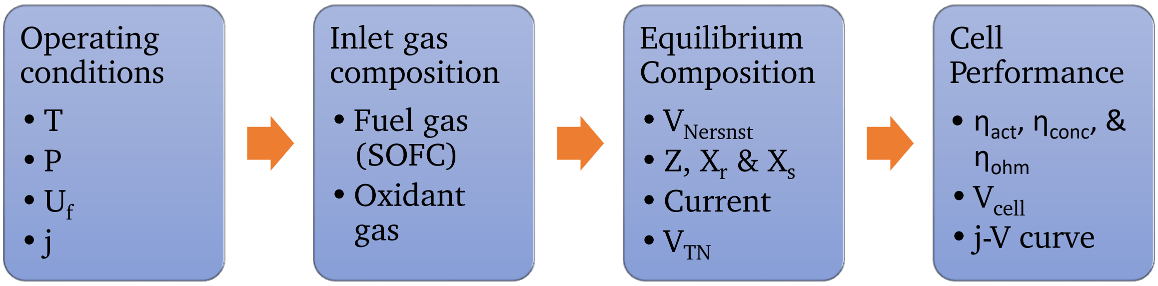

Figure 3.4 Modeling Process of ReSOC

In the stack simulation, a similar approach is taken. Among the operating conditions, the excess air ratio was included as a preselected parameter. A step is added between selecting operating conditions and inlet gas compositions as indicated in Figure 3.5. In this step, the stack is sized to give a complete overview of the stack. Also, to determine the equilibrium composition, an iterative method is used until the inlet gas composition of the fuel cell mode is equal to the exit gas composition of the electrolysis mode. This was made possible by simulating each mode separately and readjusting the fuel cell inlet compositions for each run. This iteration was done in EES using the “PROCEDURE” and “UNTIL” functions in EES.

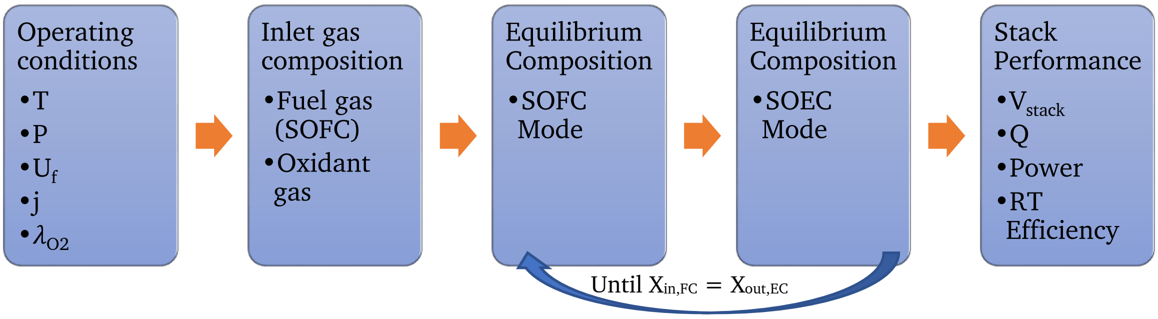

Figure 3.5 Stack Simulation Process

The properties of the ReSOC and stack used in modeling and validation analysis are given in Table 3.2. Cell properties and operating conditions are as given in reference [7], other references are stated accordingly.

The SOFC and SOEC region of operation for different gas compositions and operating temperatures were validated with data from the literature. The validation results as shown in Figure 3.6 for the cell shows a good agreement with the reference literature for the range of current densities considered. The H_2-H_2O plot has an inlet gas containing 50% H_2 and 50% H_2O by mole while the Syngas plot contained 25% H_2, 38% H_2O, 12% CO_2, and 25% CH_4 by mole. The cell was operated at 1.01325 bar pressure and the corresponding temperature is indicated in the plot. In both the H_2-H_2O plot and the syngas plot, the inlet air is assumed to comprise 20% oxygen and 80% Nitrogen per mole as stated in the reference literature. In a ReSOC stack operating with carbonaceous fuels, the most important species in the reaction is H_2, CH_4, CO, CO_2, H_2O, and O_2. The stack operating parameters as used in the validation model is given in Table 3.3.

Table 3.2 Single ReSOC Properties [7]

	Fuel Electrode	**Oxidant Electrode**	**Electrolyte**
ξ	0.26	0.3	-
τ	3	3	-
d_p	$1 * 10^{-6}$ [m]	$1 * 10^{-6}$ [m]	-
δ_i	0.065 [cm]	0.0040 [cm]	0.0016 [cm]
σ	10 $[(\Omega\text{-cm})^{-1}]$	300 $[(\Omega\text{-cm})^{-1}]$	$\frac{5.17 * 10^6}{T} e^{\left(-\frac{93800}{RT}\right)} [(\Omega \cdot \text{cm})^{-1}]$
$j_{0,i}^{ref}$	1.56 $[\text{A/cm}^2]$	0.25 $[\text{A/cm}^2]$	-
$E_{act,i}$	60 [kJ/mol]	162 [kJ/mol]	-
$\alpha_{i,a}$	0.4	0.5	-
$\alpha_{i,c}$	0.6	0.5	-
v_{H_2}	6.12 [65]	$v_{O_2} = 16.3$ [65]	-
v_{H_2O}	13.1 [65]		
T_{ref}	873 [K]		
P_o	1.01325 [bar]		

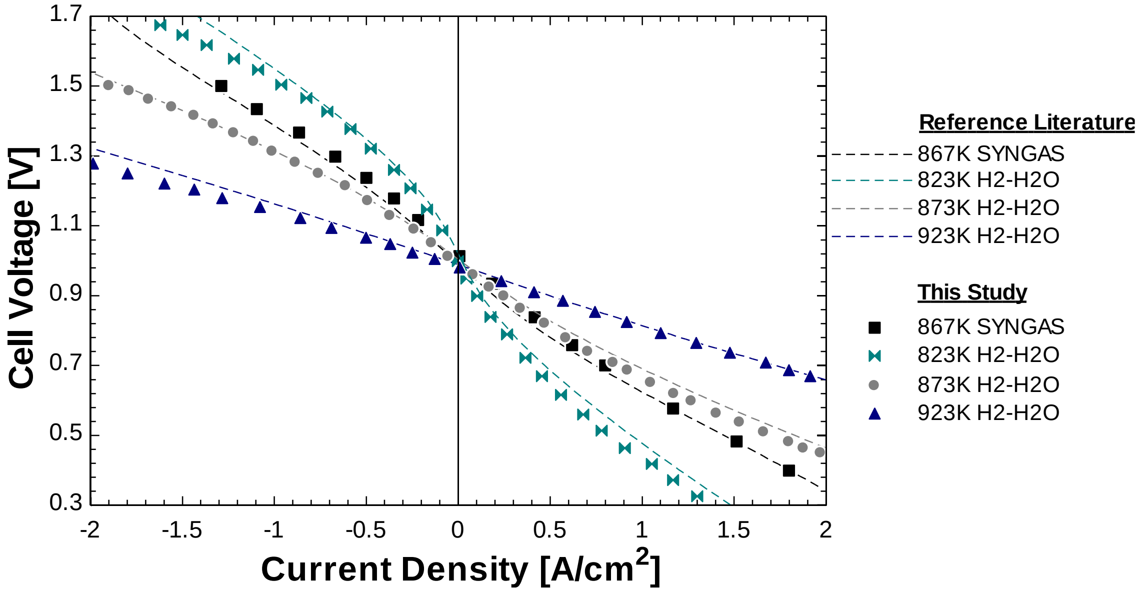

Figure 3.6 ReSOC model validation with literature experimental study in [7]

Table 3.3 Input parameters for stack performance validation

Stack Input Parameters	
T_{op}	873 [K]
P_{op}	1.01325 [bar]
j	±0.2 [A/cm^2]
λ_{O2}	2.245 [SOFC] 0.934 [SOFC]
U_f	0.65
U_r	0.44
Active Area	534760[cm^2]

Furthermore, the stack model was also validated with data from existing literature for a specific reactant gas combination. The iterative method presented in Figure 3.5 was used in determining the inlet gas compositions and the result of the simulation is presented in Table 3.4. The results from the stack model agree very well with existing literature data. As shown in Table 3.4, the percentage absolute difference between the performance results in the reference literature and this study stood below 1%. While the percentage difference of the inlet gas molar fractions (input data) was as high as 8%, the effect of this was very minimal on the performance of the stack as seen in the temperature and mass flow rate tables. The high percentage difference in the inlet gas molar fraction can be attributed to their low nominal value. It can be observed from the validation table that the molar fractions with low nominal values have the highest percentage differences in both the SOFC and SOEC mode of operation. Since this does not affect the performance of the stack much. The validation result for the stack performance is within an acceptable range. This stack model is used throughout this study in analyzing and characterizing a ReSOC stack. Figure 3.7 shows a schematic representation of a ReSOC stack showing the inlet and outlet streams of the reactants and oxidant sides of the stack. The stream designation is the same as indicated in the validation results shown in Table 3.4.

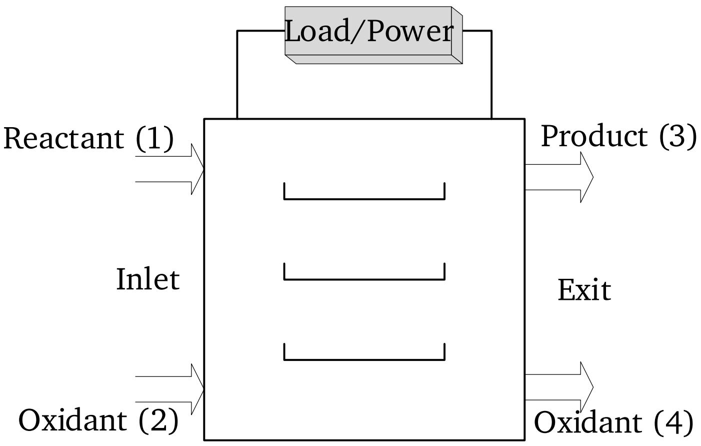

Figure 3.7 Schematic diagram of a ReSOC stack showing inlet and exit streams

3.3 Analysis Results and Discussion

The performance of an electrochemical cell is mostly characterized by the j-V curve for the cell and the corresponding activation, concentration, and ohmic overpotential in the cell. For the ReSOC considered in this study, the performance is characterized using the same reactant gas for both fuel cell and electrolysis cell mode. In the cell performance analyzed in this section, the same cell properties presented in section 3.1 were used. The cell operating temperature and the inlet gas compositions however are different. In the ReSOC performance analysis presented, the cell was operated at a constant fuel utilization of 0.65 and operated at various current densities in both modes of operation. The ReSOC is simulated up to the limiting current density and the corresponding graphs are plotted. The inlet gas contained 25% CO, 25% H_2, 25% H_2O, and 25% CO_2 by mole. Air is assumed to contain 21% and 79% Oxygen and Nitrogen, respectively.

Figure 3.8 is the j-V performance curve for the ReSOC at 923K and 1.10325 bar operating temperature and pressure, respectively. The fuel cell mode of operation had a higher limiting current density compared to the electrolysis mode. The limiting current density in the fuel cell and electrolysis cell mode is 2.619 A/cm^2 and 1.48 A/cm^2, respectively. The maximum power density of 1.129 W/cm^2 in the fuel cell mode occurred at 2.07 A/cm^2 current density.

Table 3.4 Stack model validation with results presented in the literature.

Parameters	% cell product composition by mole					Temperature (K)				Flow rate (g/s)				V_{op} (V)	Stack Power (kW)
						Inlet		Exit		Inlet		Exit			
	H_2	CH_4	H_2O	CO	CO_2	T_1	T_2	T_3	T_4	m_1	m_2	m_3	m_4		
SOFC Mode of Operation															
Reference [7]	32.4	0.5	50.7	3.5	13.0	823	733	883	883	4.17	85.51	13.02	76.65	0.936	100
This- Study	32.78	0.47	50.21	3.25	13.28	823	733	885.3	885.3	4.15	85.47	13.02	76.60	0.938	100.3
Absolute Difference	0.38	0.03	0.49	0.25	0.28	0	0	2.3	2.3	0.03	0.13	0.02	0.13	0.002	0.2
% difference	1.17	6	0.97	7.14	2.15	0	0	0.3	0.3	0.72	0.15	0.15	0.17	0.21	0.2
SOEC Mode of Operation															
Reference [7]	67	20.3	9.4	2.5	0.9	801	817	874	867	13.02	35.57	4.17	44.43	1.119	119.6
This Study	67.73	19.9	8.72	2.71	0.93	801	817	867	867	13.02	35.56	4.15	44.43	1.121	119.9
Absolute Difference	0.73	0.4	0.68	0.21	0.03	0	0	0	0	0.02	0.05	0.03	0.05	0.002	0.2
% difference	1.09	1.97	7.23	8.4	3.33	0	0	0.8	0	0.15	0.14	0.72	0.11	0.18	0.17

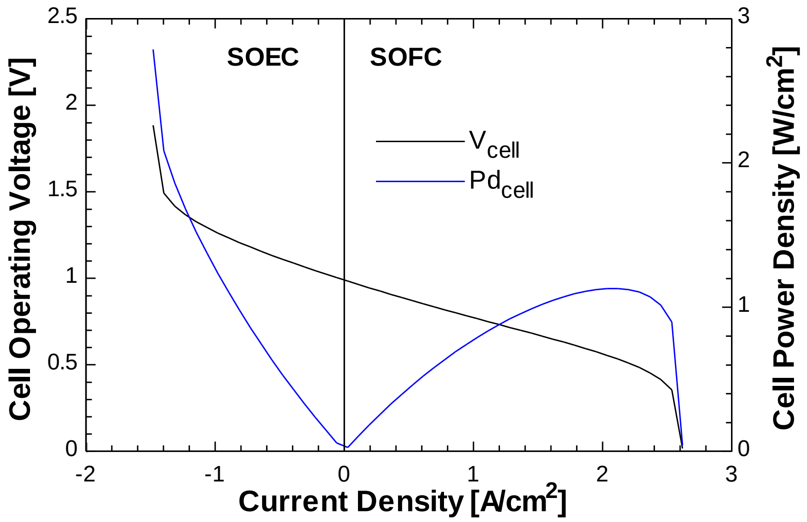

Figure 3.8 j-V performance curve for ReSOC

While the power generation in the fuel cell mode diminished as the cell approached limiting current density, the power further increased in the electrolysis cell mode as the cell approached limiting current density. This is a typical characteristic of a fuel cell and electrolysis cell. The overpotential in the ReSOC which serves as the losses in the cell is plotted in Figure 3.9. The overpotentials in both modes are dominated by the ohmic and the activation overpotentials. However, the concentration overpotential becomes dominant as the cell approaches the limiting current density.

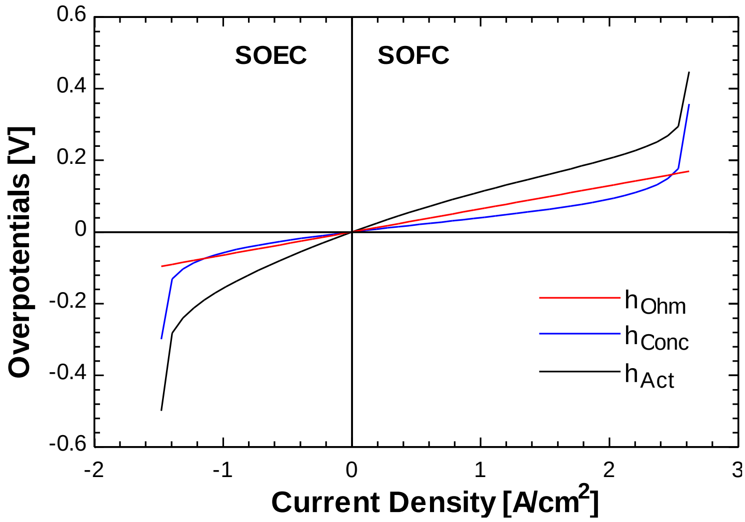

Figure 3.9 ReSOC Overpotentials in fuel cell and electrolysis mode.

This shows that while at lower current densities, the portion of the concentration overpotential might be very less compared to the activation overpotential, but at high current density, it is just as important or even most important among the overpotentials. Using the ReSOC stack derived from the validation model above, the performance of the stack in both the fuel cell and electrolysis mode has been characterized. In the performance analysis, the stack is taken to operate at a constant inlet mass flow rate for the SOFC mode, and the fuel utilization and reactant utilization factor varied accordingly. In operating the stack, the fuel cell mode is first operated. The exit gas from the fuel cell mode serves as the inlet gas for the electrolysis mode. Also, the model is constrained so that the electrolysis outlet gas is the same as the fuel cell inlet gas. Therefore, at the end of each cycle, the gas returns to its initial composition. This will allow for multiple gas reuse and is favorable for standalone ReSOC stacks. The SOFC inlet gas for the base case contained 19.78% CH_4, 67.6% H_2, 2.76% CO, 8.89% H_2O, and 0.97% CO_2 by mole. Air is used as the oxidant and is assumed to contain 21% and 79% Oxygen and Nitrogen by mole, respectively. The operating temperature of the base case is 873 [K] and the operating pressure is 1.01325 [bar].

Figure 3.10a shows the current-voltage of a single ReSOC stack showing the fuel cell and the electrolysis cell mode of operation. Different inlet mass flow rates are considered to compare how the stack performance varied under different inlet mass flow rates. The right axis of Figure 3.10a shows the power density of the cell as defined in Equation 3.61. The behavior of the stack at the considered inlet mass flow rates possesses some similarities and differences in the fuel cell and electrolysis cell mode. A higher mass flow rate indicates a higher limiting current density because more fuel is available for the reaction even at higher current densities. Therefore, for the stack to be operable at a higher current density, it is only logical to increase the inlet mass flow rate. Because the exit gas from the fuel cell mode is the inlet gas for the electrolysis cell mode, the electrolysis cell mode performance will be highly dependent on the performance of the fuel cell mode. The cell operating voltage of a higher mass flow rate is higher than that of a lower mass flow rate as the stack nears its operating limiting current density. At 0.2 A/cm^2 current density for example, at 5g/s inlet gas flow rate the corresponding operating voltage is 0.945V and 1.128V for the SOFC and SOEC modes, respectively while at 15 g/s the operating voltage is 0.965V and 1.155V for the SOFC and SOEC modes, respectively. While a higher operating voltage is desirable for the SOFC mode, the reverse is the case for the SOEC mode.

Corresponding overpotentials for the considered mass flow rates at operating conditions of 873K temperature and 101.325kPa of pressure are shown in Figure 3.10b. It should be noted that the SOFC mode operation is limited by the SOEC mode operation of the ReSOC stack. The limiting current density of an electrochemical cell is determined by the concentration overpotential as explained in [59]. As operating current density increases, the reactant composition at the reaction sites tends toward zero. As the electrolysis mode reaches the limiting current density, gas conversion stops, hence the fuel cell mode cannot be continued since the prior electrolysis mode could not occur, thereby limiting the ReSOC stack. This phenomenon is specific to the method of operating the ReSOC stack considered for this research. This limitation might not occur in a stack where the fuel cell and electrolysis cell reactant gases are not related such as a system integrated into a natural gas pipeline and/or used for carbon capture.

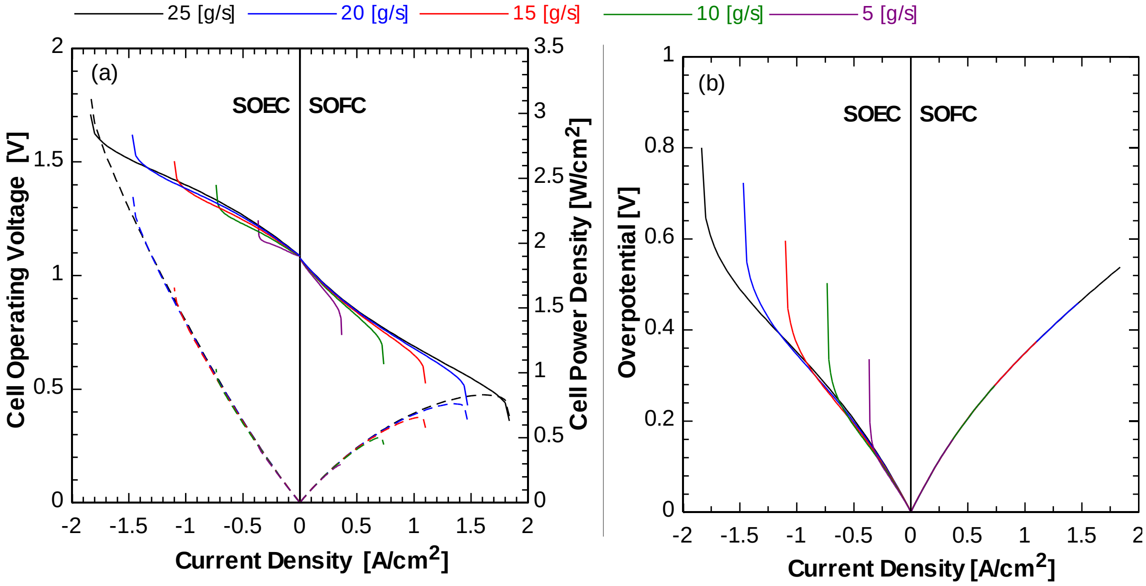

Figure 3.10 Performance of a single cell in the ReSOC stack at varying inlet mass flow rates

Despite the slight difference in operating voltage for both modes of operation, the operating current represented by the rate of reaction in Figure 3.11 is the same for both modes of operation. The electrochemical (redox) reaction rate is directly proportional to the ReSOC current as related in Equation 3.14. For all the reactions taking place in the cell, the rate is similar for both modes of operation. However, at different inlet mass flow rates, the reaction rate varied for the reformation and the water-gas shift reactions. Because the stack is operating at a constant inlet mass flow rate, the operating current density determines the fuel utilization in the stack. It is of course important to predetermine the fuel utilization factor while designing the ReSOC stack, but for analysis purposes, we can allow the stack to predetermine its utilization factor and select the best for design parameters.

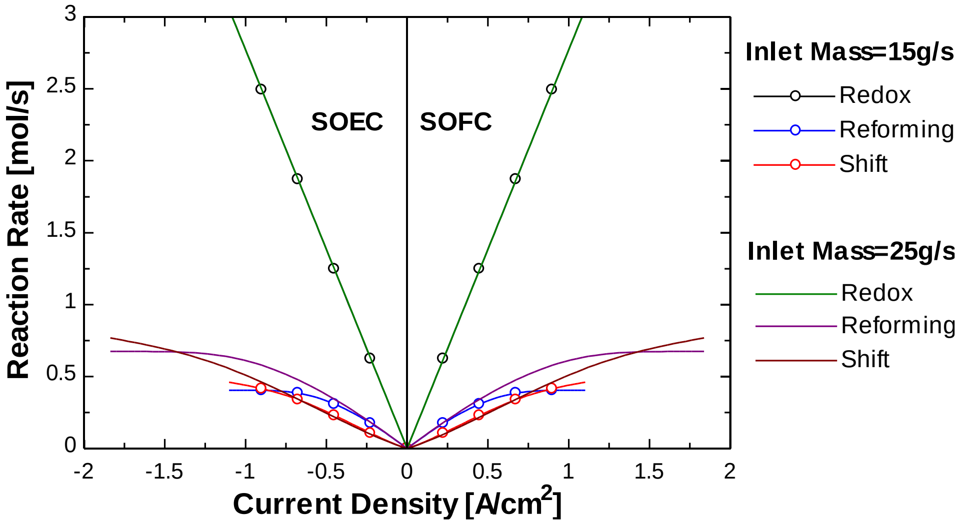

Figure 3.11 Chemical and electrochemical reaction rates at 15g/s and 25g/s inlet mass flow rates

Figure 3.12 shows the fuel utilization factor and the reactant utilization factor as a function of the operating current density in the fuel cell and electrolysis cell mode, respectively. To understand the effect of the utilization factor on stack performance, the power density of the stack is also plotted on the same graph. Fuel utilization on the SOFC mode increases linearly with the operating current density. The linear performance of the fuel utilization can be better understood from Equation 3.10. Since inlet gas fraction and inlet mass flow rate is constant and the number of moles of H_2 converted is the reaction rate, then the fuel utilization factor is directly proportional to the reaction rate which has been explained in Figure 3.11.

For the SOEC mode of operation, the reactant utilization starts linearly but approaches what seems to be a limit at 0.46 reactant utilization. The oxidant production rate unlike the fuel utilization rate is dominated by the water-gas shift rate of reaction. Equation 3.11 defines the reactant utilization factor and takes the H_2O, CO_2, and CO into consideration. From Table 3.1, CO, CO_2, and H_2O are all involved in the water gas shift reaction. The rate and extent of this reaction will to a large extent determine the amount of reactant available for the SOEC operation hence the reactant utilization factor.

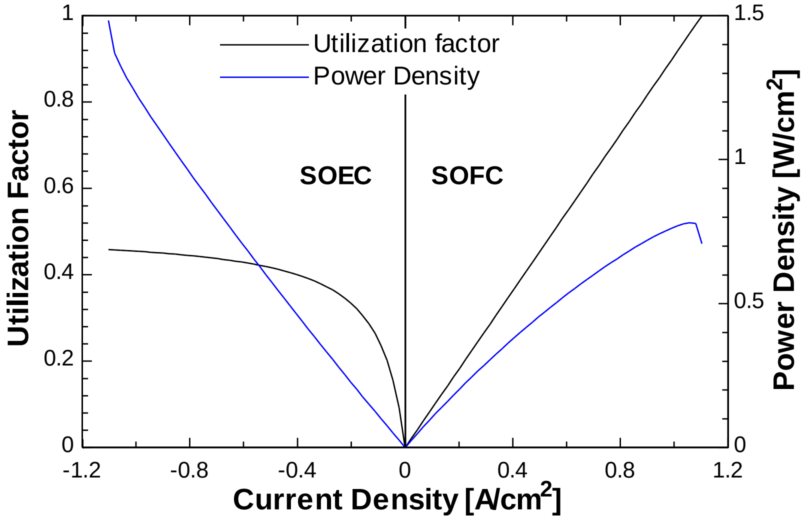

Figure 3.12 Current density vs Utilization factor and Power density

The conversion rate for the reformation and water-gas shift reactions increases as the inlet mass flow rate increases. However, since the electrochemical conversion rate is the same for all considered mass flow rates, this means that the same amount of gas is converted at every current density regardless of the mass flow rate, hence, lower efficiency at higher mass flow rates. In Figure 3.13, the stack performs better at lower mass flow rates compared to higher mass flow rates. This is because the stack performance is largely determined by the ratio of the reactant gas converted. A smaller amount of gas will be converted faster than a larger amount of gas due to the limited reaction sites available in the stack.

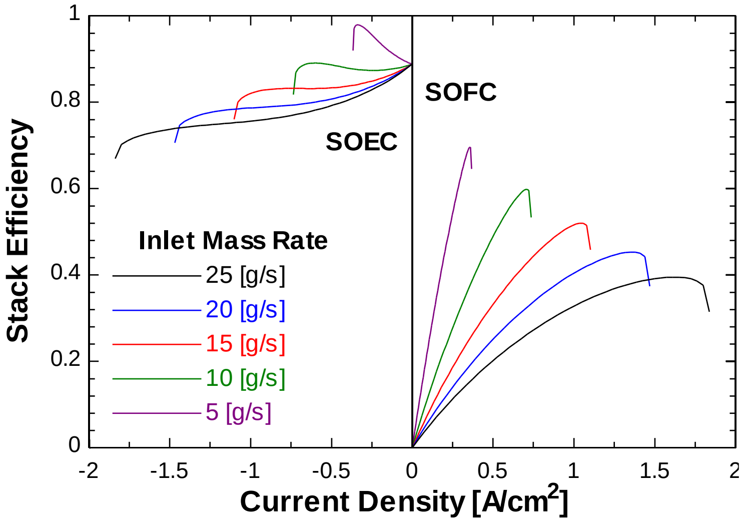

Figure 3.13 Stack Efficiency for both modes of Operation

Despite the large difference in the individual efficiency of the operating modes, the roundtrip efficiency gives a completely different story (Figure 3.14). Despite the difference in the individual performance in the SOFC and SOEC mode with the fuel cell mode efficiency reducing by more than four folds at 25 g/s flow rate compared to 5 g/s flow rate, the considered inlet mass flow rates in this study have similar roundtrip efficiencies. This implies that the stack reversible performance, i.e., the power generation to power consumption ratio to return inlet reactant gas to its original constituents is not dependent on the mass flow rate but the ReSOC stack. The roundtrip performance for the stack is similar at all inlet mass flow rates with the difference occurring at current densities close to the limiting value. This gives an advantage in the method of operation selected for the stack in this study. Since the unconverted fuel or exhaust gas in any mode of reaction is recoverable at the end of the cycle, then the individual efficiency of the operating mode is of little importance. Therefore, ReSOC stacks can easily be sized based on power characteristics at specific current density and a minimum reactant flow rate. The advantages of operating a ReSOC stack at a reactant flow rate higher than the design flow rate will be explained in the thermal management section of the stack electrochemical analysis.

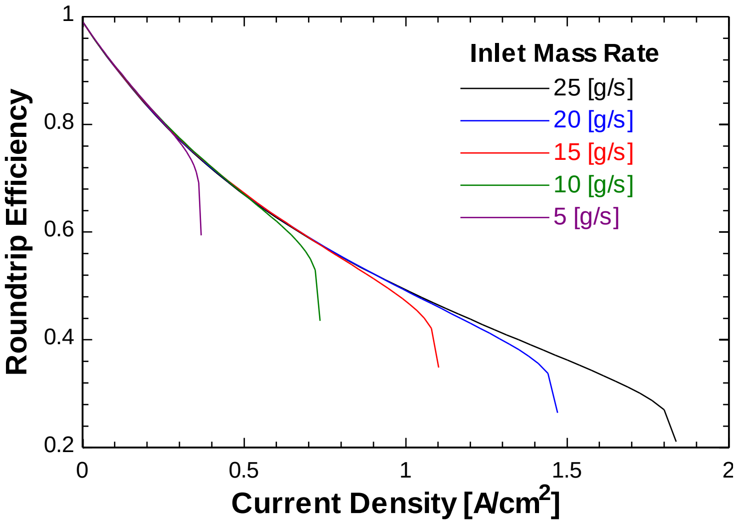

Figure 3.14 Stack roundtrip efficiency

In the temperature effect analysis, the reactant gas in the fuel electrode is assumed to enter the stack at 873 K temperature and exit at the stack operating temperature. On the air side, the inlet temperature is determined to form the stack energy balance Equation, and the exit temperature is also the same as the stack operating temperature. In this manner, the excess heat that may be required by the stack will be supplied through the inlet air to the stack. The stack was operated at a current density of ±0.2 A/cm^2 and the reactant gas composition is the same as used in the stack analysis above. For the pressure analysis, the stack is assumed to have uniform temperature throughout and all inlet and exit gas pressure are the same as the stack operating pressure.

The Nernst Voltage which is the ideal operating voltage of the ReSOC is influenced by both the operating temperature and pressure of the cell. The Nernst Voltage is dominated by the maximum reversible work in the cell defined by ΔG, the Gibbs free energy. The Gibbs free energy of the reaction is dependent on the thermodynamic state of the reaction environment which is the standard temperature and pressure at which the reaction takes place. The reaction quotient in the Nernst Equation is defined by the partial pressures of the reactant and product gases, and the T term is the stack operating temperature (see Equation 3.28). This explains the magnanimity of the operating temperature, operating pressure, and the gas mixture on the stack performance. The Nernst voltage increases with increasing operating pressure for both modes of operation as shown in Figure 3.15a. Both modes continue in the same direction and almost at the same rate for the pressure range considered. This interprets that, on a first look, increasing stack operating pressure is favorable for the ReSOC stack in power generation mode while the reverse is the case for the storage mode since a higher voltage means better performance for SOFC and poor performance for SOEC. The ideal operating voltage of the ReSOC stack in the power generation mode and storage mode for the temperature analysis behaves in the same pattern as in the pressure analysis (Figure 3.15b). The effect of operating temperature however on the stack is slightly different from that of the operating pressure. Both the fuel cell and the electrolysis cell mode of operation resulted in a quadratic graph for the range of temperature considered. As the operating temperature increased, the performance of the stack improved up to operating temperatures of about 950 K for SOFC and 1000 K for SOEC but from there onwards, performance deteriorated for both the SOFC and SOEC mode. One would expect the power in the stack to follow the same fashion as the ideal operating voltage but as it is can be seen from Figure 3.15b, it is different.

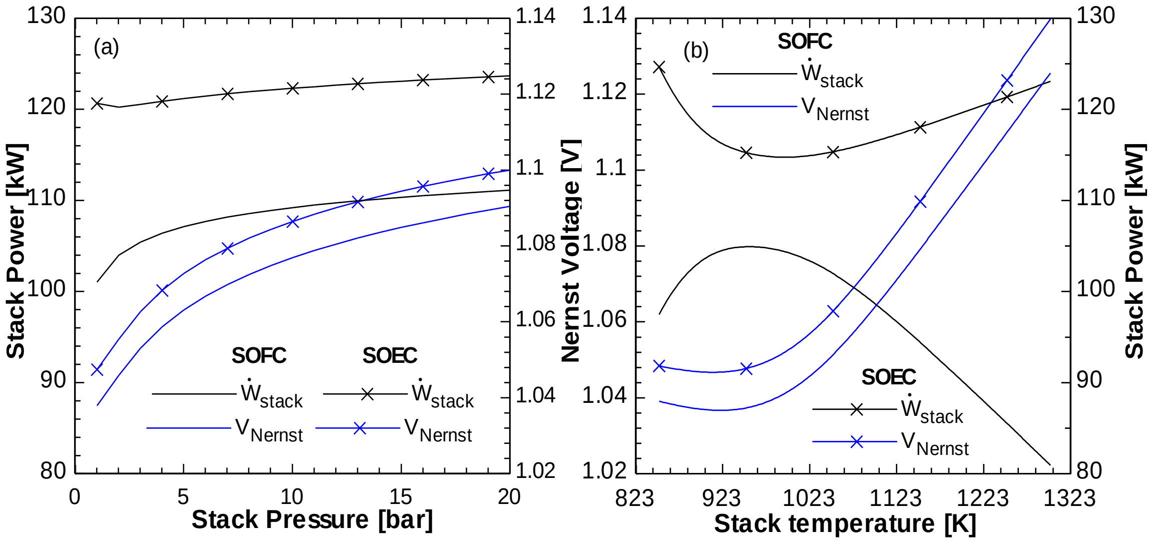

Figure 3.15 The effect of a) Operating pressure b) Operating temperature on the reversible voltage and power in the ReSOC stack for both modes of operation

The cell operating voltage in the stack and the total cell overpotential for both operating modes are shown in Figure 3.16. Increasing the stack operating pressure beyond 5 bar have little effect on the stack performance for both modes of operation. However, to reflect the power performance of the stack as seen in Figure 3.15b, the operating voltage has a quadratic curve for both fuel cell and electrolysis mode of operation for a varying operating temperature. For the electrolysis cell mode, this behavior is caused by the ever-increasing Nernst voltage and the decreasing overpotentials. As overpotentials decrease, the operating voltage decreases, but because the Nernst voltage increased faster than the overpotentials, it reaches a point where the Nernst voltage dominates, and that forms the crest of the curve of the operating voltage. The cause of the Nernst voltage behavior is the inlet gas fraction. This phenomenon will be explained sooner.

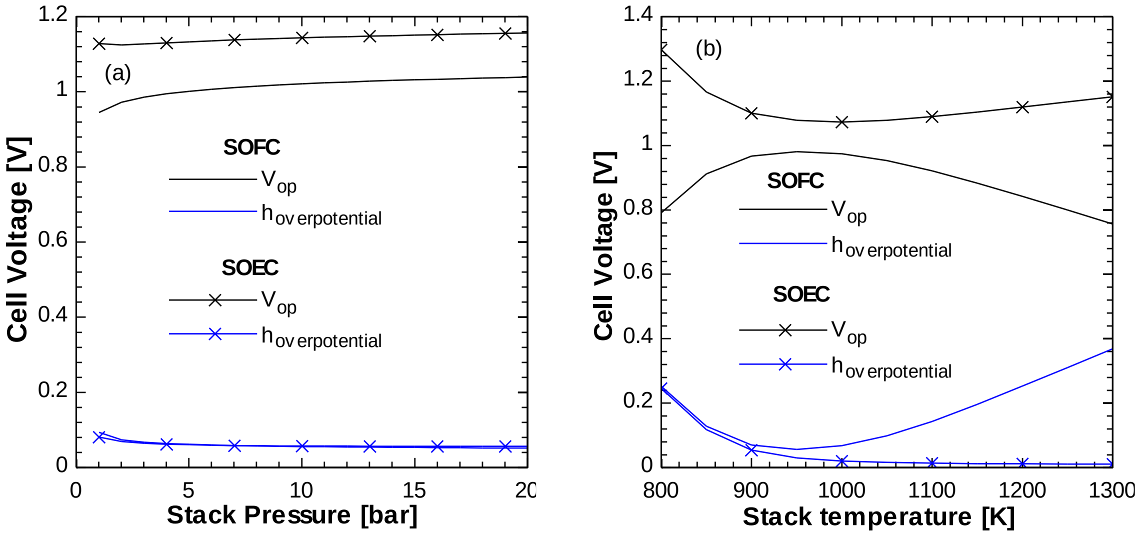

Figure 3.16 The effect of a) Operating pressure b) Operating temperature on the cell operating voltage and overpotentials in the ReSOC stack for both modes of operation

For the fuel cell mode, the overpotentials increase with increasing operating temperature in contrary to the electrolysis cell mode. In the same manner, as the electrolysis cell mode, this is the reason for the behavior of the operating voltage graph for increasing operating temperature. Figure 3.17 shows the performance of the overpotentials in the fuel cell mode for increasing stack operating temperature. The reason for the increased overpotentials in the stack is the increased concentration overpotentials at the stack operating current density. This phenomenon is unexpected for a solid oxide cell stack. This behavior of the stack is because of the modeling method employed in this study. The gas mixture can change based on the operating conditions of the stack to ensure that the stack can return the inlet gas constituent to its original mixture after every roundtrip cycle. Figure 3.18 shows the change in inlet gas molar fractions as a function of operating temperature to further buttress this point. This reflects in the stack efficiency and roundtrip efficiency as shown in Figure 3.19. Increasing the pressure is good for the stack roundtrip efficiency but increasing the temperature is only good if the power generation does not exceed the peak shown in Figure 3.16a.

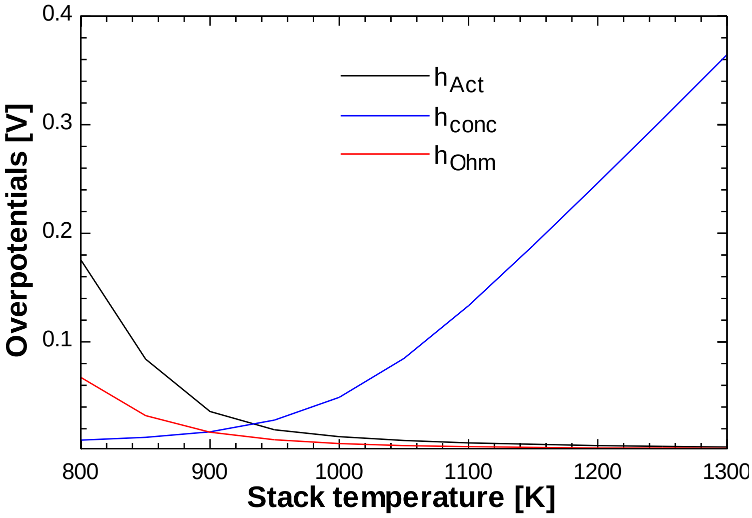

Figure 3.17 Overpotentials vs Stack temperature

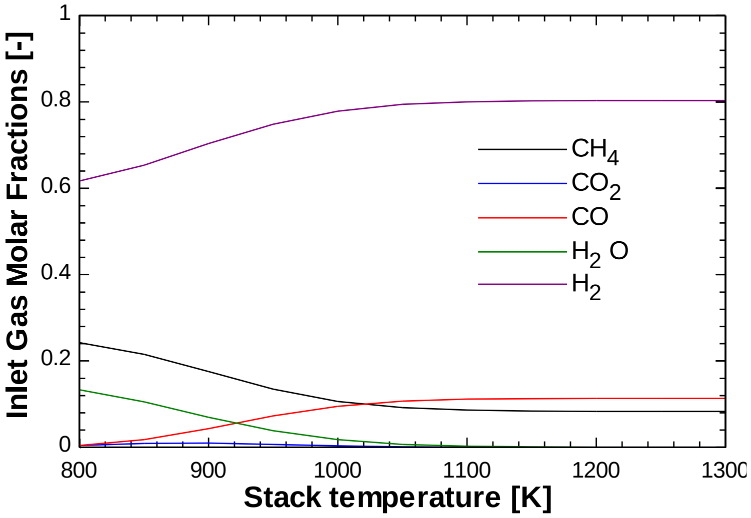

Figure 3.18 Inlet gas molar fraction vs Temperature

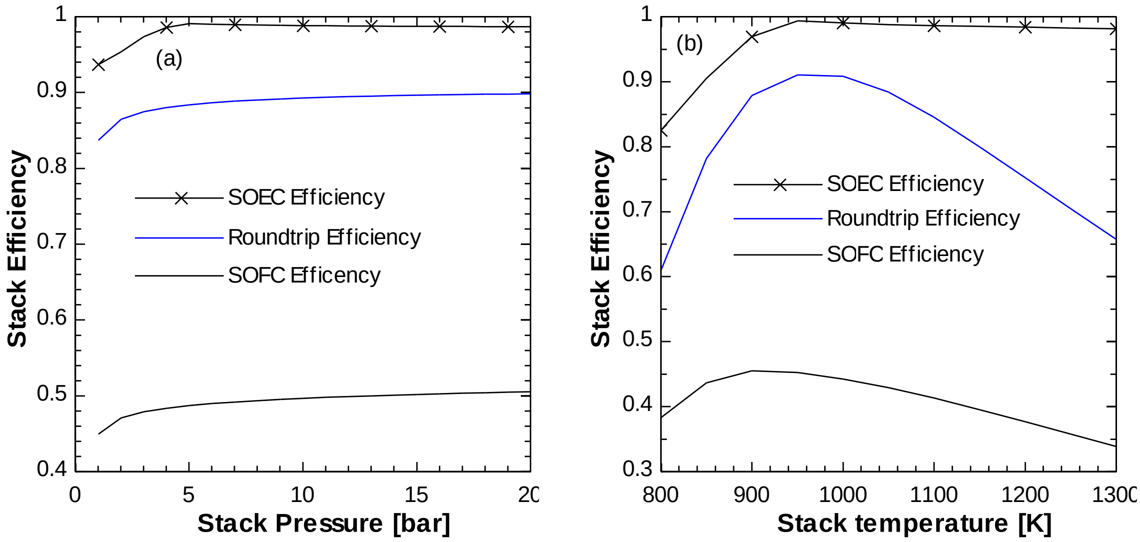

Figure 3.19 The effect of a) Operating pressure b) Operating temperature on the stack efficiency and roundtrip efficiency in the ReSOC stack for both modes of operation

The same characteristic is expected even if the inlet mass flow rate is increased or reduced. But the temperature or current density at which the stack records the best performance will be different for every specific inlet mass flow rate.

The pressure and temperature analyses show that increasing the stack operating pressure improves the overall performance of the stack for both operating modes, with the SOFC mode better than the SOEC mode regardless. Increasing the operating temperature has its pros and cons depending on the mass flow rate and operating current density. However, if the stack is not expected to return the inlet gas mixture to its original mixture after every cycle, a very different performance could be recorded. Furthermore, studies need to be carried out on concentration overpotentials to understand why pure fuels have higher concentration overpotentials than non-pure fuels.

A unique property of the solid oxide cells is their high operating temperature. Thus, it is very important to characterize the effect of temperature and temperature requirements on stack performance. The effect of the stack operating parameters on its heating requirements is used to characterize the thermal management in the stack. Thermoneutral and cell voltage for 10g/s inlet gas flow rate at different operating temperatures are shown in Figure 3.20. The stack heat is defined in Equation 3.69 by the thermoneutral voltage and the cell operating voltage. Since both modes operate separately and at different times, the heat generated in the SOFC mode of operation is not considered for reuse in the SOEC mode in this study. Though this is an option for reversible solid oxide cell systems that can be investigated in further studies. Figure 3.20A to Figure 3.20C shows the relationship among thermoneutral voltage, operating voltage, and the heat requirement of the stack at 873K, 923K, and 973K operating temperature and 1.01325 bar operating pressure.

In the SOFC mode of operation, there is a heating requirement in the stack generally at a current density below 0.25A/cm^2. This is the region where the cell voltage is above the thermoneutral voltage which is not desirable for the SOFC mode of operation. What this means is that at these current densities, due to the low redox rate of reaction, the heat produced from the redox reaction is not enough for the water-gas shift reaction to occur. In practical terms, for the inlet gas flow rate, operating the stack at these current densities should be avoided. In the SOEC mode, a 50K operating temperature increase from 873K to 923 K at operating current density beyond –0.55A/cm^2 requires up to 4kW of external heat for stack operation. The sudden drop in heating requirement as the operating current density approaches its limiting value is due to additional heat produced from the overpotentials in the stack. For 973 K operating temperature, at an operating current density of –0.36A/cm^2 heat produced in the stack equates to the heat required for the reactions to take place. The heat required increased to over 32kW at an operating current density of –0.69A/cm^2. This becomes a design issue as performance improvement through increased operating temperature might lead to a heating problem in the stack.

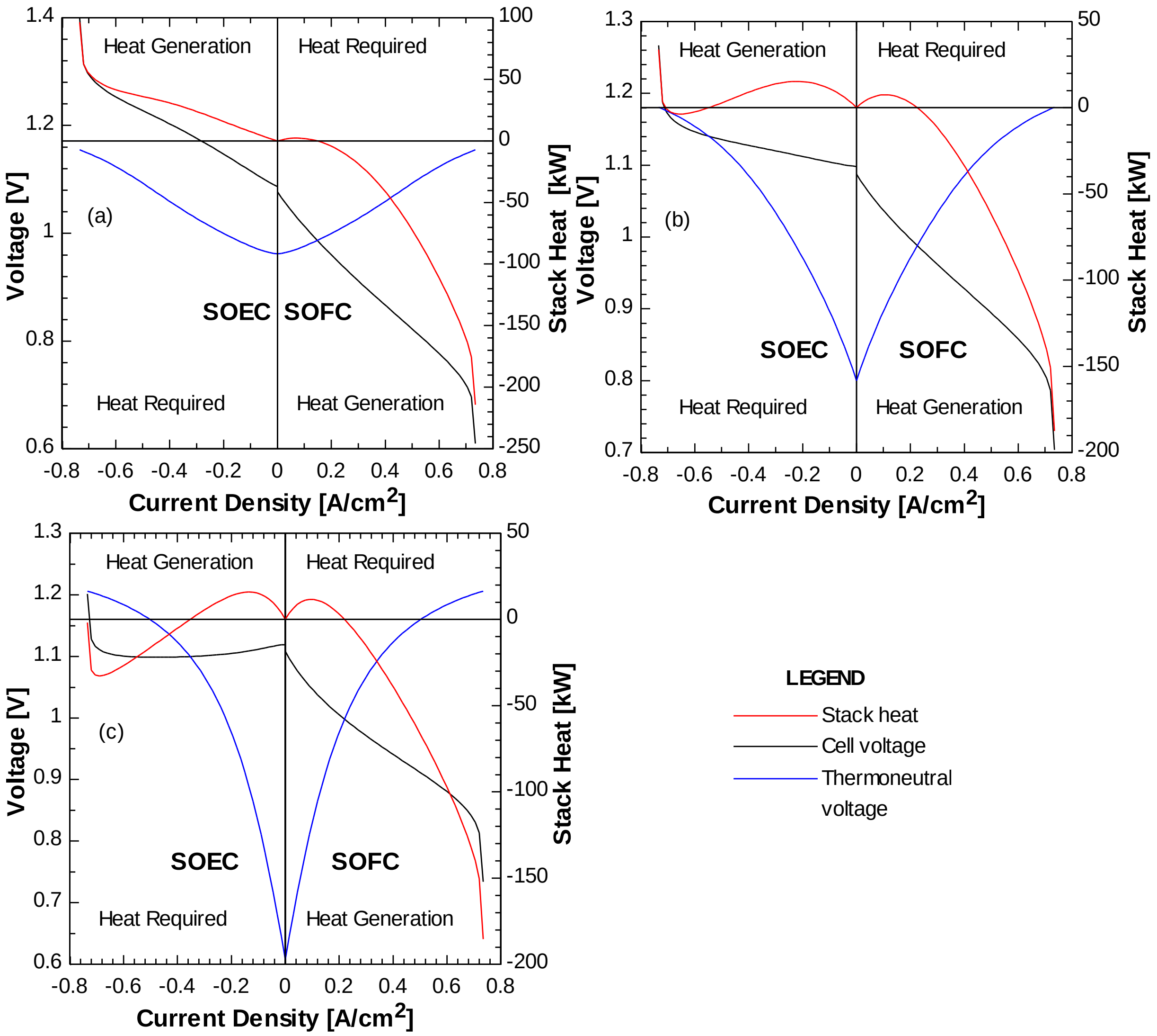

Figure 3.20 The relationship between the thermoneutral voltage and ReSOC stack thermal characteristics at a) 873K b) 923K c) 973 K operating temperature and 10 g/s inlet mass flow rate.

The energetic performance of the stack in terms of efficiency, energy production, and energy consumption has been discussed. The effect of parameters such as excess air ratio and operating current density on the stack temperature and the fuel utilization/oxidant production factor is next investigated for the ReSOC stack. These parameters are important especially for thermal management and degradation characterization in the stack. The temperature change of air at the stack oxidant electrode defined as $\Delta T_{air} = T_{air,out} - T_{air,in}$ with operating current density was investigated Figure 3.21. Where, $T_{air,in}$ and $T_{air,in}$ is the temperature of the oxidant gas at the inlet and outlet of the oxidant electrode, respectively. In the plot in Figure 3.21, the inlet flow rate of the gas was at 10g/s and the operating temperature was 973K.

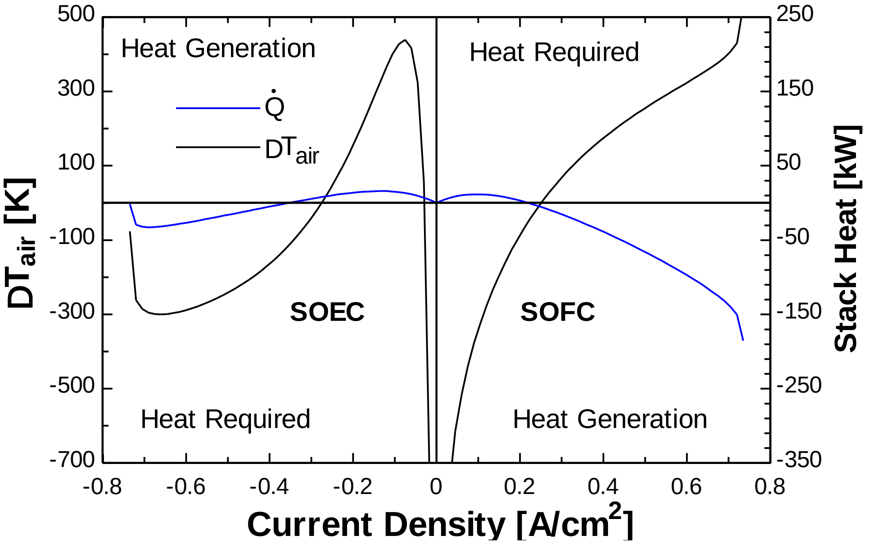

Figure 3.21 Relationship between ΔT_{air} and stack heat at 973 K operating temperature

The relationship between the temperature change and the stack heat was also plotted on the same graph. Since the air exit temperature is taken constant, only the inlet air temperature will change according to the energy balance in the stack. This response of air temperature with the heat requirement in the stack enables characterization of the thermal requirements of the stack from the stack energy balance even without operating the stack. As defined in Equation 3.80, a positive ΔT_{air} indicates heat generation in the stack while heat required will yield negative a negative ΔT_{air}. Evidently from the graph, the temperature difference was not zero at the same instance where the stack heat was zero. This difference is because the change in air temperature is merely a response to stack activities and not a direct measure of the reactions ongoing in the stack. The large temperature difference presented in Figure 3.21 possesses a problem of extremely high inlet air temperatures as the stack already operates at a high temperature. To mitigate this temperature difference, Figure 3.22 shows how the excess air ratio for the fuel cell and electrolysis cell mode of operation affects the temperature difference. The stack is operated at a 10g/s inlet mass flow rate, SOFC current density of 0.6A/cm^2, SOEC current density of 0.1A/cm^2, and 973K operating temperature.

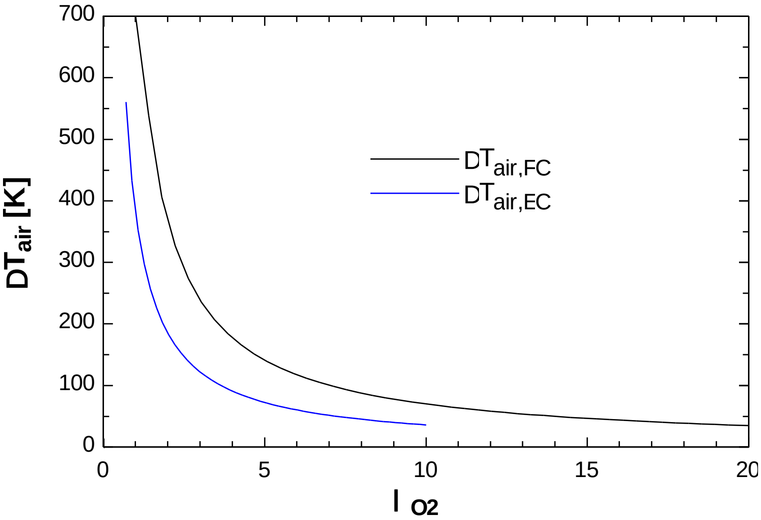

Figure 3.22 Excess air ratio vs ΔT_{air} at 973 K operating temperature

As the excess air ratio increases, ΔT_{air} reduces. This means that increasing the inlet mass flow rate will reduce the quality of heat required. Operating the stack with a higher inlet oxidant flow rate improves stack thermal performance.

4

RESOC SYSTEM MODELING AND EXERGY-BASED PERFORMANCE ANALYSIS

In this chapter, the ReSOC system considered in this study is introduced. The system operating technique and system components are explained and modeled using energy relations. The ReSOC stack model is the same as explained in the previous chapter. Other balance of plant components such as the compressors and heat exchangers are modeled using their energy relations. Furthermore, the exergy relations for individual components are given as well as the exergy performance parameters. The system performance is also described based on energy and exergy relations for both modes of operation. The roundtrip efficiency for the system is used to characterize energy storage systems is also given. The system performance at base case operation is presented showing the streams and the properties of each stream as it goes through the system. Also, the effect of the operating parameters such as the operating current density and fuel utilization ratio on system performance is given to show the acceptable range of operation in the system. The exergy performance analysis for the ReSOC stack and system is also presented.

4.1 System Description

In the system considered in this study, a reversible solid oxide cell stack was configured alongside other components to condition the stack inlet gases and utilize stack exit gases. The components ensure a steady constant gas flow rate in and out of the stack. The system balance of plant components are compressors, heat exchangers, heat recuperators, and storage tanks. The system modeled and analyzed in this study follows the system configuration of a stored vapor ReSOC system presented by Wendel and Braun [66]. The system is designed to operate in the same manner for both the SOFC mode and SOEC mode this allowing one system for both modes of operation. The difference in the system will be the operation of the ReSOC stack and the storage tanks.

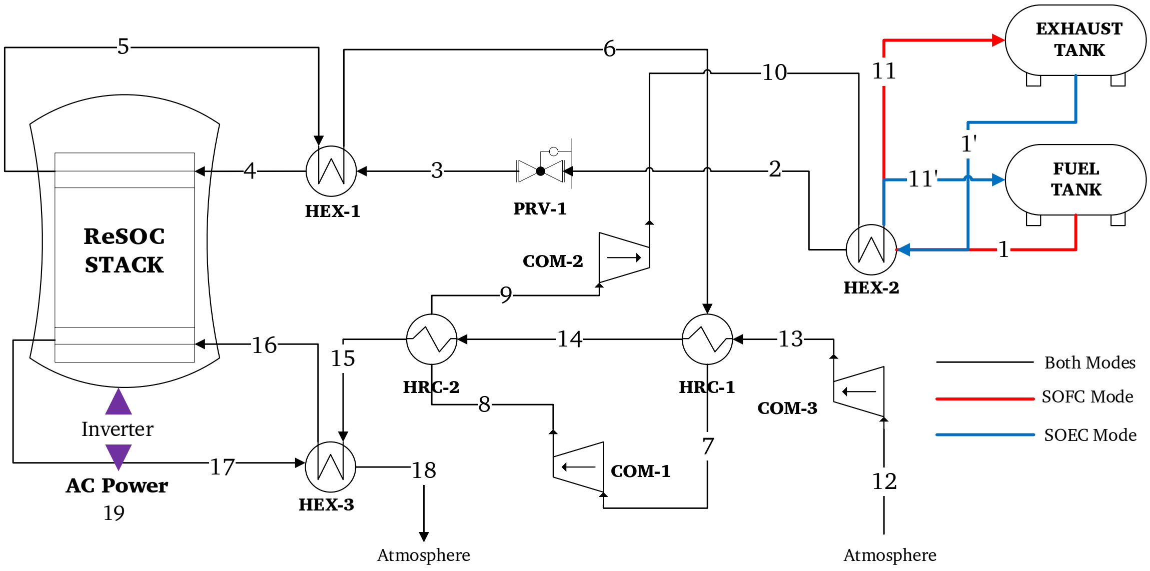

Figure 4.1 The Reversible Solid Oxide Cell (ReSOC) system showing the power generation and storage modes of operation.

On the reactant gas side in figure 1, the reactant gas flows from the fuel storage tank through the tank heat exchanger (HEX-2). The pressure at the exit of the heat exchanger is the same as the tank storage pressure. The pressure reduction valve (PRV-1) is used to adjust the flow pressure to match the stack operating pressure. That way the pressure reduction valve can also be used to set the stack operating pressure since the stack operating pressure has to match the inlet gas pressure. The reactant gas proceeds through the pressure reduction valve to the stack inlet heat exchanger (HEX-1). The reactant gas at the exit of the heat exchanger is at a temperature close to the stack operating temperature. This is the stack inlet gas which is at a pressure equivalent to the stack operating pressure and a temperature close to the stack average operating temperature. At the stack exit, the product gas from the chemical and electrochemical reaction leaves the stack and reenters the heat exchanger HEX-1. Between heat exchangers HEX-1 and HEX-2 is a combination of two intercoolers (HRC-1 & HRC-2) and two compressors (COM-1 & COM-2). The intercooler preheats the incoming air on the air side of the ReSOC system. The compressors cover the pressure difference between the stack operating pressure and the storage tank pressure. The stack product gas after being finally compressed to the storage tank pressure is used to preheat incoming gas from the storage tank. After losing some heat in HEX-2, the stack exit gas is finally stored in the storage tank. This last heat exchanger performs multiple functions: 1. It preheats the reactant gas 2. It lowers the storage temperature of the product gas to the possible minimum. It is important to store the product gas at the lowest possible temperature to reduce the insulation in the tank, hence the overall system cost. However, storing the gas at extremely low temperatures might condense the H_2O molecules in the gas mixture which will lead to complications not only in the storage tanks but also in the system. One way of overcoming the problem of storage temperature is to condense out most of the H_2O in the product gas and store it separately. In that case, the gas can be stored at room temperature without complications and the need for tank insulation. The downside to this is that the system will use more components (e.g., water storage tank, separator/mixer, etc.) and this can also lead to higher energy demand in the system. The energy demand will be from the separator, preheater, steam generator, mixer, etc. In this study, however, the storage tank temperature is higher than the vapor temperature of H_2O so the gas can be stored directly in the tank without the need for extra components in the system. In the SOFC mode, the tank supplying reactant gas to the system is the fuel tank and the stack exit gas is stored in the exhaust tank. In the SOEC mode, gas is supplied to the system from the exhaust tank and stored in the fuel storage tank. This is based on the relationship established in the stack model where the exit of the fuel cell mode is the inlet of the SOEC mode and vice versa.

On the air/oxidant side of the system, the inlet oxidant gas (air or oxygen) is fed to the system from a predetermined source. The source can be ambient air from the environment or a storage tank for specially prepared oxidant gas such as oxygen or treated air. In this study, ambient air is used as the oxidant gas. Air is assumed to contained 21% oxygen and 79% nitrogen and nitrogen is inert. The air blower creates a pressure difference thus allowing the required air inflow into the system. This slightly raises the temperature of the incoming air. Further, the temperature is raised in the first and second preheaters (HRC-1 & HRC-2) using heat from the product gas intercoolers. As the last pass before entering the stack. The heated air is passed through the air heat exchanger (HEX-3). After this stage, the air enters the ReSOC where the electrochemical reaction takes place. The air/oxidant gas is involved only in the electrochemical reaction. The excess/unused air leaves the stack through the exit channel of the air electrode. In an exothermic stack, the temperature of the air exiting the stack is higher than the inlet air temperature. The temperature difference at the oxidant inlet and exit electrode have been explained in the stack thermal management section. The exiting air and the incoming air to the stack undergo a heat transfer process in the air heat exchanger before the exit air is released to the ambient environment or used in a heat recuperation process in the case of a cogeneration system. In the fuel cell mode of operation, due to the oxidation process in the stack, the exit air from the system is lean in oxygen as compared to the ambient air. The amount of oxygen in the exit air is dependent on the stack operating current density and the fuel utilization factor in the stack.

4.2 Modeling System Components

The system proposed in this study contains compressors, heat exchangers, recuperators, and storage tanks as the balance of plant components. The fuel composition has been predetermined, thus eliminating the need for other components to prepare the fuel and/or exhaust gases or to make the stack tail gas appropriate for external use. The function of the compressor is to match the gas pressure to the stack operating pressure since the system is also considered for a pressurized operation. Another need for the compressors is due to the pressure difference between the storage tank and the ReSOC stack. The heat exchangers and recuperators on the other hand allow for the reuse of the thermal energy of the stack exit gas in the stack inlet stream of reactant gases. Also, heat exchangers are used for heating the inlet reactant gases to temperatures close to the stack operating temperature, avoiding the need for an external heat source in the system. The balance of plant components is modeled as a black body using mass balance and energy balance Equations. The storage tanks are modeled simply as sink and source.

The assumptions in the thermodynamic model carried out in this study includes:

1. Steady-state operation
2. Gases have ideal properties.
3. The chemical reaction reached equilibrium.
4. Reforming/Methanation reaction is internal.
5. H_2/H_2O redox is the only electrochemical reaction taking place.
6. No heat loss in the stack or any other system components
7. The cells in the stack are homogenous.
8. The exit gas from the fuel cell is the inlet gas of the electrolysis cell and vice versa.
9. There is no leakage of reactant gas in the stack.
10. Air contains 79% N_2 and 21% O_2 by mol.
11. Only physical and chemical exergy exists in flow streams.
12. 2% pressure-drop in system components.
13. The inverter efficiency is 95%.

4.2.1 ReSOC Stack

In addition to the stack modeling already detailed in the previous section, the stack exergy balance is introduced. The exergy balance in the stack is like the energy balance for both modes of operation. The difference lies in the exergy destruction term added in the exergy balance. Compressor consumes AC type electricity while ReSOC stack uses DC type. Inverters are used to convert electricity from DC to AC mode. Equation 4.1 shows the conversion formula used in converting the DC power in the ReSOC stack to AC power for both modes of operation.

$$AC\ power = inverter\ efficiency * DC\ power \tag{4.1}$$

Electrical power generated or consumed in the stack is converted to AC power using Equation 4.1 before used in system performance calculation and analysis. In the SOFC mode the exergy balance in the stack is as expressed in Equation 4.2:

$$\sum_i \dot{E}x_{fuel} + \sum_i \dot{E}x_{in,oxid} = \sum_i \dot{E}x_{exh} + \sum_i \dot{E}x_{out,oxid} + \dot{W}_{SOFC} + \dot{E}x_d \quad (4.2)$$

Where, $\dot{E}x_i$ is the exergy rate in W or kW, subscripts "fuel" is the inlet/reactant gas in the SOFC fuel electrode, "exhaust" is the product from the SOFC electrode, and "oxidant" is the gas at the SOFC fuel electrode. The oxidant can either be air or oxygen. $\dot{E}x_d$ is the exergy destruction rate and is a fundamental parameter in determining the exergetic performance of a process. Equation 4.3 gives the stack exergy balance in the SOEC mode.

$$\sum_i \dot{E}x_{exh} + \sum_i \dot{E}x_{in,oxid} + \dot{W}_{SOEC} = \sum_i \dot{E}x_{fuel} + \sum_i \dot{E}x_{out,oxid} + \dot{E}x_d \quad (4.3)$$

The SOFC exit gas is the SOEC inlet gas, thus here "exhaust" subscript represents the inlet/reactant gas in the SOEC fuel electrode, and "fuel" represents the product from the SOEC fuel electrode. The "oxidant" is the same as in the SOFC mode. The exergy rate of the gases is defined as in Equation 4.4.

$$\dot{E}x_i = \dot{m} \cdot ex_i \quad (4.4)$$

$\dot{m}$ is the mass flow rate of the gas in g/s and ex_i is the specific exergy of the gas in J/g. The specific exergy is defined in Equation 4.5 as the sum of the physical and chemical exergy of the gas species [52]. The specific physical and chemical exergy is also defined in Equations 4.6 and 4.7.

$$ex_i = ex_{ph} + ex_{ch} \quad (4.5)$$

$$ex_{ph} = \left(\hat{h} - \hat{h}_0\right) - T_0(\hat{s} - \hat{s}_0) \quad (4.6)$$

$$ex_{ch} = es_i^{ch} + RT_0 \cdot \ln(X_i) \quad (4.7)$$

$\hat{h}$ and $\hat{s}$ are the specific enthalpy and entropy of the gas at the stack operating conditions while $\hat{h}_0$ and $\hat{s}_0$ are the specific enthalpy and entropy of the gas at the surrounding conditions which is taken as a standard state of 298 K & 1atm temperature and pressure, respectively. T_0 is the standard state temperature, es_i^{ch} is the standard chemical exergy of the corresponding gas species, R is the universal gas constant, and X_i is the molar fraction of the gas.

The exergetic performance of a thermodynamic process is measured through the exergy efficiency and the exergy destruction rate. The exergy destruction rate has been defined in Equations 4.2 and 4.3. The exergy efficiency of the ReSOC stack is defined according to principles stated in [67] is given in Equation 4.8 ad 4.9 for the SOFC and SOEC modes, respectively.

$$\varepsilon_{SOFC} = \frac{\dot{W}_{SOFC}}{\left(\sum_i \dot{E}x_{fuel} + \sum_i \dot{E}x_{in,oxid}\right) - \left(\sum_i \dot{E}x_{exh} + \sum_i \dot{E}x_{out,oxid}\right)} \tag{4.8}$$

$$\varepsilon_{SOEC} = \frac{\sum_{i=Ch4,H2,CO} \dot{E}x_{fuel} - \sum_{i=CH_4,H_2,CO} \dot{E}x_{exhaust}}{\sum_i \dot{E}x_{exh} - \left(\sum_i \dot{E}x_{fuel} - \sum_{i=CH_4,H_2,CO} \dot{E}x_{fuel}\right) + \dot{W}_{SOEC}} \tag{4.9}$$

EPC for the SOFC and SOEC modes of operation for a ReSOC stack is defined in Equation 4.30 and 4.31, respectively.

$$EPC_{SOFC} = \frac{\dot{W}_{SOFC}}{\dot{E}x_{d,SOFC}} \tag{4.10}$$

$$EPC_{SOEC} = \frac{\sum_{i=Ch4,H2,CO} \dot{E}x_{fuel} - \sum_{i=CH_4,H_2,CO} \dot{E}x_{exhaust}}{\dot{E}x_{d,SOEC}} \tag{4.11}$$

4.2.2 Compressor

The compressor model in this study is characterized using the zero-dimensional model based on energy and mass balances. The mass and energy balance in the compressor is given in Equations 4.12 and 4.13.

$$\dot{m}_{in} = \dot{m}_{out} \tag{4.12}$$

$$\sum \dot{H}_{in} + \dot{W}_{comp} = \sum \dot{H}_{out} \tag{4.13}$$

$\dot{m}$ is the mass flow rate through the compressor in g/s, $\dot{H}$ is the enthalpy of the respective gas stream in J/s and $\dot{W}_{comp}$ is the electrical power consumed in the compressor in W. In the compressor model, the exit pressure is predetermined in the model. The performance of all the compressors selected in this study is characterized by the isentropic efficiency. Isentropic efficiency of the compressor is the ratio of the ideal work done by the compressor at isentropic conditions to the actual work done by the compressor. The compressors are assumed to operate at constant isentropic efficiency. Equation 4.14 defines the isentropic efficiency of a compressor based on the specific enthalpy of the inlet and outlet streams. The air blower on the oxidant side is modeled as a compressor.

$$\eta_{iso,comp} = \frac{\hat{h}_{out,s} - \hat{h}_{in}}{\hat{h}_{out} - \hat{h}_{in}} \tag{4.14}$$

$\eta_{iso,comp}$ is the isentropic efficiency of the compressor, $\hat{h}_{out}\&\hat{h}_{in}$ is the actual specific enthalpy of the inlet and outlet gas streams and $\hat{h}_{out,s}$ is the specific enthalpy of the outlet gas stream at the specific entropy of the inlet stream. The exergy balance in the compressor is defined in Equation 4.15. The exergy stream contains both physical and chemical exergy as defined in Equations 4.5 to 4.7.

$$\sum_i \dot{E}x_{in} + \dot{W}_{comp} = \sum_i \dot{E}x_{out} + \dot{E}x_{d,comp} \tag{4.15}$$

The exergy efficiency of the compressor is defined in Equation 4.16 as:

$$\varepsilon_{comp} = \frac{\sum_i \dot{E}x_{out} - \sum_i \dot{E}x_{in}}{\dot{W}_{comp}} \tag{4.16}$$

4.2.3 Heat exchanger and recuperator

The heat exchanger in this model is assumed to be a counter flow heat exchanger without mixing. Like the compressor, it is modeled using the mass balance, energy balance, and a performance metric. The heat recuperator and heat exchanger were modeled the same, thus the relationships established for the heat exchanger are the same as for the heat recuperator. The heat exchanger has two inlet and outlet streams, the hot and cold inlet stream, and the hot and cold outlet stream. The mass balance and energy balance for the heat exchanger/heat recuperator are as defined in Equations 4.17 and 4.18.

$$\sum \dot{m}_{in} = \sum \dot{m}_{out} \tag{4.17}$$

$$\sum \dot{H}_{in,cold} + \sum \dot{H}_{in,hot} = \sum \dot{H}_{out,cold} + \sum \dot{H}_{out,hot} \tag{4.18}$$

The mass balance Equation is the sum of all gas in each stream i.e., hot, and cold gas. The effectiveness of the heat exchanger is the ratio of the actual heat transfer to the maximum possible heat transfer in the heat exchanger. The effectiveness-NTU method is used for performance analysis characterization in this study. The effectiveness of a heat exchanger is defined in Equations 4.19 to 4.22 [68].

$$\in = \frac{q}{q_{max}} \tag{4.19}$$

$$q = C_{hot}\left(T_{hot,in} - T_{hot,out}\right) = C_{cold}\left(T_{cold,out} - T_{cold,in}\right) \tag{4.20}$$

$$C_i = \dot{m}_i \cdot c_{p,i} \tag{4.21}$$

$$q_{max} = C_{minimum}\left(T_{hot,in} - T_{cold,in}\right) \tag{4.22}$$

Where, $\in$ is the heat exchanger effectiveness, q is the heat transfer in the heat exchanger and q_{max} is the maximum possible heat transfer in the heat exchanger. C_i is the heat capacity for the respective gas stream in J/K, $\dot{m}_i$ is the mass flow rate in g/s, $c_{p,i}$ is the specific heat capacity in J/g-K and, $C_{minimum}$ is the least of the heat capacities between the hot and cold gases. The NTU, a short form for the number of transfer units is related to the heat capacity and the effectiveness as shown in Equations 4.23 to 4.25 [68].

$$NTU = \frac{UA}{C_{minimum}} \tag{4.23}$$

$$\in = \frac{1 - e^{[-NTU(1+C_{ratio})]}}{1 - C_{ratio} \cdot e^{[-NTU(1+C_{ratio})]}} \tag{4.24}$$

$$C_{ratio} = \frac{C_{minimum}}{C_{maximum}} \tag{4.25}$$

Where U is the overall heat transfer coefficient of the gases [69], A is the heat transfer area, and C_{ratio} is the heat capacity ratio. Exergy balance for the heat exchanger/recuperator is expressed as in Equation 4.26. The exergy efficiency of the heat exchanger is defined in Equation 4.27.

$$\sum_i \dot{E}x_{in,cold} + \sum_i \dot{E}x_{in,hot} = \sum_i \dot{E}x_{out,cold} + \sum_i \dot{E}x_{out,hot} + \dot{E}x_{d,HEX} \tag{4.26}$$

$$\varepsilon_{HEX} = \frac{\sum_i \dot{E}x_{out,cold} - \sum_i \dot{E}x_{in,cold}}{\sum_i \dot{E}x_{in,hot} - \sum_i \dot{E}x_{out,hot}} \tag{4.27}$$

4.2.4 Pressure reduction valve

The valve is used in controlling the stack inlet reactant pressure to match the stack operating pressure. Since the gases are stored at very high pressure, it is required that the pressure of the gas be stepped down to match the stack operating pressure. The pressure reduction valve operates isothermally thus no temperature reduction across the valve. The pressure drop however leads to entropy generation in the gas which in turn becomes exergy destruction. The energy and exergy balance across the pressure reduction valve is given in Equations 4.28 and 4.29, respectively. The exergy efficiency of the pressure reduction valve is as in equation 4.30.

$$\sum \dot{H}_{in} = \sum \dot{H}_{out} \tag{4.28}$$

$$\sum_i \dot{E}x_{in} = \sum_i \dot{E}x_{out} + \dot{E}x_{d,PRV} \tag{4.29}$$

$$\varepsilon_{PRV} = \frac{\sum_i \dot{E}x_{out}}{\sum_i \dot{E}x_{in}} \tag{4.30}$$

4.2.5 Storage Tanks

Storage tanks are modeled as a source and sink with constant properties. The fuel and exhaust tanks are taken to be at a constant pressure of 2 MPa for both modes of operation. The fuel gas is assumed to leave the fuel storage tank at a temperature of 550 K for the SOFC mode of operation and the exhaust tank temperature is determined by the system operating conditions. In the SOEC mode, the exhaust gas is assumed to leave the exhaust storage tank at a temperature of 550 K and the fuel tank temperature is determined by the system operating conditions.

4.3 System Performance Metrics

4.3.1 Energetic performance

In the ReSOC system, the parasitic power consumption by the balance of plant components in both generation and storage mode further reduces the system roundtrip efficiency. This is because more power will be required by the components in terms of thermal or electrical energy. This leads to increased electricity consumption in the SOEC mode and a reduced net power generation in the SOFC mode. The effect of this parasitic energy consumption affects the system roundtrip efficiency as shown in Equation 4.31. The ReSOC system roundtrip efficiency ($\eta_{RT,sys}$) is the ratio of the net electrical power generated in the SOFC mode to the gross electrical power consumed in the SOEC mode. In Equation 4.31,

$\sum \dot{W}_{BOP}$ is the sum of auxiliary parasitic electrical power consumption in the system for the respective mode of operation. It is defined in this study by Equation 4.32 as the sum of the electrical power consumed by the three compressors as shown in Figure 4.1.

$$\eta_{RT,sys} = \frac{\dot{W}_{SOFC} - \sum \dot{W}_{BOP,FC}}{\dot{W}_{SOEC} + \sum \dot{W}_{BOP,EC}} \tag{4.31}$$

$$\sum \dot{W}_{BOP} = \dot{W}_{comp1} + \dot{W}_{comp2} + \dot{W}_{comp3} \tag{4.32}$$

The system efficiency is defined for the fuel cell and electrolysis cell mode in Equations 4.33 to 4.36. Two individual alternatives were given for the system efficiencies for both modes of operation.

In the fuel cell mode, $\eta_{sys,1}$ assumes that the outlet stream from the system (exhaust gas) is stored and can be used for other purposes. Thereby the effective system input is the heat value rate of the converted fuel gases. $\eta_{sys,2}$ however, assumes that the fuel cell operation exit gas is a waste gas, hence, the input is the fuel entering the system.

In the electrolysis mode, $\eta_{sys,1}$ takes the difference between the system inlet and outlet steam as the product while $\eta_{sys,2}$ takes only the outlet stream as the system product and the inlet stream act as an input to the system alongside stack power and balance of plant components parasitic power consumption.

$$\eta_{sys,FC,1} = \frac{\dot{W}_{SOFC} - \sum \dot{W}_{BOP,FC}}{\sum \dot{W}_{LHV,in} - \sum \dot{W}_{LHV,out}} \tag{4.33}$$

$$\eta_{sys,FC,2} = \frac{\dot{W}_{SOFC} - \sum \dot{W}_{BOP,FC}}{\sum \dot{W}_{LHV,in}} \tag{4.34}$$

$$\eta_{sys,EC,1} = \frac{\sum \dot{W}_{LHV,out} - \sum \dot{W}_{LHV,in}}{\dot{W}_{SOEC,in} + \sum \dot{W}_{BOP,EC}} \tag{4.35}$$

$$\eta_{sys,EC,2} = \frac{\sum \dot{W}_{LHV,out}}{\sum \dot{W}_{LHV,in} + \dot{W}_{SOEC,in} + \sum \dot{W}_{BOP,EC}} \tag{4.36}$$

In Equations 4.33 and 4.34, the output of the SOFC mode of operation in the system is the net electricity production. The difference between the inlet and exit heat rates is taken as the system input since the outlet is stored for future use. In the SOEC mode, the system output is the heating value rate in the fuel produced from the conversion in the stack as shown in the numerator of Equations 4.35 and 4.36. The denominator is the total electric power consumed by the system in the operating mode. The system is configured as a standalone self-sustaining system, thus, heat from an external source is not expected. The only power input to the system is through the stack and the compressors.

4.3.2 Exergetic Performance

The exergy analysis is used in identifying irreversibilities in the system and for improving overall system performance. It helps in identifying the location and extent of loss in the quality of energy of a system. In addition to the total system exergy destruction rate, exergy efficiency, and exergetic performance coefficient as discussed in the ReSOC stack analysis section, the exergy destruction ratio is also introduced to characterize exergy performance at different locations in the system. Exergy balance for respective components in the system as used in this study is shown in Table 4.1. Another term introduced in characterizing the system exergy performance apart from the exergy efficiency is the exergetic performance coefficient (EPC). The method of EPC has been applied in the analysis of solid oxide fuel systems by Akkaya [52]. EPC measures the ratio of the exergy rate of the product from a thermodynamic process to the exergy destruction rate. It defines the value of a useful product in a process per unit exergy destroyed. Unlike the exergy efficiency that measures performance as a function of input, it measures performance as a function of internal processes, in this case, the exergy destruction rate.

Table 4.1 Exergy destruction rate of system components

ReSOC Stack	SOEC Mode	$\dot{E}x_{D,EC} = \dot{E}x_4 + \dot{E}x_{16} + \dot{E}x_{19} - \dot{E}x_5 - \dot{E}x_{17}$
	SOFC Mode	$\dot{E}x_{D,FC} = \dot{E}x_4 + \dot{E}x_{16} - \dot{E}x_{17} - \dot{E}x_5 - \dot{E}x_{19}$
HEX-1		$\dot{E}_{D,HX1} = \dot{E}x_3 + \dot{E}x_5 - \dot{E}x_4 - \dot{E}x_6$
HEX-2		$\dot{E}_{D,HX2} = \dot{E}x_1 + \dot{E}x_{10} - \dot{E}x_2 - \dot{E}x_{11}$
HEX-3		$\dot{E}_{D,HX3} = \dot{E}x_{15} + \dot{E}x_{17} - \dot{E}x_{16} - \dot{E}x_{18}$
HRC-1		$\dot{E}_{D,HRC1} = \dot{E}x_6 + \dot{E}x_{13} - \dot{E}x_7 - \dot{E}x_{14}$
HRC-2		$\dot{E}_{D,HRC2} = \dot{E}x_8 + \dot{E}x_{14} - \dot{E}x_9 - \dot{E}x_{15}$
COM-1		$\dot{E}x_{D,COM1} = \dot{E}x_7 + \dot{W}_{COM1} - \dot{E}x_8$
COM-2		$\dot{E}x_{D,COM2} = \dot{E}x_9 + \dot{W}_{COM2} - \dot{E}x_{10}$
COM-3		$\dot{E}x_{D,COM3} = \dot{E}x_{12} + \dot{W}_{COM3} - \dot{E}x_{13}$
PRV-1		$\dot{E}x_{D,CV1} = \dot{E}x_2 - \dot{E}x_3$
Storage Tanks	Fuel (SOEC)	$\dot{E}x_{D,TNK1} = \dot{E}x_{11'} - \dot{E}x_1$
	Exhaust (SOFC)	$\dot{E}x_{D,TNK2} = \dot{E}x_{1'} - \dot{E}x_{11}$

Equations 4.37 to 4.43 express the parameters used in characterizing the exergetic performance of the system.

$$\varepsilon_{sys,FC1} = \frac{\dot{E}x_{19} - \dot{E}x_{BOP}}{\dot{E}x_1 - \dot{E}x_{11}} \tag{4.37}$$

$$\varepsilon_{sys,FC2} = \frac{\dot{E}x_{19} - \dot{E}x_{BOP}}{\dot{E}x_1} \tag{4.38}$$

$$\varepsilon_{sys,EC1} = \frac{\sum_{i=Ch4,H2,CO} \dot{E}x_{11} - \sum_{i=CH_4,H_2,CO} \dot{E}x_1}{\dot{E}x_{19} + \dot{E}x_{BOP}} \tag{4.39}$$

$$\varepsilon_{sys,EC2} = \frac{\sum_{i=Ch4,H2,CO} \dot{E}x_{11}}{\dot{E}x_1 + \dot{E}x_{19} + \dot{E}x_{BOP}} \tag{4.40}$$

$$\dot{E}x_{BOP} = \dot{W}_{COM1} + \dot{W}_{COM2} + \dot{W}_{COM3} \tag{4.41}$$

$$\dot{E}x_{D,tot} = \sum_k \dot{E}x_{D,k} + \dot{E}x_{18} \tag{4.42}$$

$$Y_{D,k} = \frac{\dot{E}x_{D,k}}{\dot{E}x_{D,tot}} \tag{4.43}$$

$$EPC_{sys,FC} = \frac{\dot{E}x_{19} - \dot{E}x_{BOP}}{\dot{E}x_{D,tot}} \tag{4.44}$$

$$EPC_{sys,EC} = \frac{\sum_{i=Ch4,H2,CO} \dot{E}x_{11} - \sum_{i=CH_4,H_2,CO} \dot{E}x_1}{\dot{E}x_{D,tot}} \tag{4.45}$$

Equations 4.37 to 4.45 are the exergetic efficiency of the ReSOC system in both the power generation and storage mode of operation. In the same fashion as the energy efficiency has been defined, two alternatives for the exergy efficiency have also been presented. $\dot{E}x_{19}$ is the exergy of the AC electric power in the stack after conversion from DC type by the inverter. $\dot{E}x_{BOP}$ is the power consumed by the parasitic balance of plant components, in this case, the compressors as shown in Equation 4.41. All other exergy states represent the respective stream as shown in Figure 4.1. The system total exergy destruction, shown in Equation 4.42, is the sum of individual exergy destruction in the components and the exergy loss in the system. State 18 is the exergy loss in the system, and exergy loss in the tank is defined as the tank exergy destruction. Exergy destruction ratio, $Y_{D,k}$ is shown in Equation 4.43. Exergy performance coefficient for both modes of operation is represented in Equations 4.44 and 4.45.

4.4 Analysis Results and Discussion

The ReSOC system performance is characterized based on the energy and exergy methods. The performance metrics of the ReSOC system are like the ReSOC stack. A major change is the introduction of the balance of plant components in the ReSOC system analysis. The balance of plant power consumption is defined by the total power consumed by the compressors in the system. In the energy analysis of the system, the effect of the heat exchangers seems apparent because it only uses the thermal energy in the gas streams and does not require an auxiliary source of power input like the compressors. However, the heat exchanger is very crucial to the overall performance of the ReSOC stack in the system and the system thermal management. Also, in a situation where the system is designed for cogeneration purposes, the heat exchanger performance will have a more obvious effect on the system performance. The effect of the heat exchangers' performance on the system performance is however easily expressed in the exergy analysis of the system even while considering only the electrical performance.

The performance characteristic of the balance of plant components and the stack operating conditions for the base case system performance results in this study are shown in Table 4.2. The performance of the compressor is characterized by the isentropic efficiency and the heat exchanger/recuperator by the effectiveness. Since all system components are assumed to be adiabatic, there is no heat loss rate for any of the system components. To account for pressure loss in the pipe and system components, a 2% pressure drop was assumed for all the components in the system except the storage tank whose pressure is constant at both the inlet and outlet. Also, the temperature of the exit stream of both tanks is taken to be 550K. The difference between the inlet and exit enthalpies or exergy of the tank is taken as the heat loss or exergy loss for the tank in the performance analysis. The characteristics of the flow streams in the system base case performance are shown in Table 4.3 and Table 4.4 for the SOFC and SOEC modes of operation, respectively.

In the SOFC mode of operation, the fuel tank is assumed to be at a constant temperature of 550K while the exhaust tank temperature is determined from the system operation. In the SOEC mode, the exhaust tank is at a constant temperature of 550K, and the fuel tank temperature from the system performance. Air is assumed to contain 21% oxygen and 79% nitrogen. The atmospheric and dead state conditions are taken as 298K temperature and 101.325kPa. Since the excess air ratio is kept constant for both modes of operation, the heat requirement in the stack is satisfied by a temperature increase in the stack inlet air rather than increasing the inlet air mass flow rate.

Figure 4.2 to Figure 4.5 show the result of the system operation and balance of plant components' performance at the base case system operation for both SOFC and SOEC modes of operation. Also, the performance metrics of individual components such as the exergy destruction rate and exergy efficiency for the system and system components are presented for both modes of operation. In the stack, electric power is generated for the SOFC mode and consumed in the SOEC mode. For both modes of operation, the compressors consume electrical energy. The exergy destruction in the valve is a result of the pressure drop occurring in the valve.

Table 4.2 Performance Parameters of System Components

Parameter/ Component	Operating Mode	
	SOEC	SOFC
Isentropic Efficiency		
COM-1	0.85	0.85
COM-2	0.85	0.85
COM-3	0.84	0.84
Effectiveness		
HEX-1	0.64	0.70
HEX-2	0.58	0.80
HEX-3	0.80	0.62
HRC-1	0.46	0.26
HRC-2	0.38	0.27
Storage Tank Properties		
Storage pressure (kPa)	2000	2000
Exit Temperature (K)	550	550
ReSOC Stack operating parameters		
Temperature (K)	873	
Pressure (kPa)	101.325	
Current Density	±0.25	
Fuel utilization	0.60	
Inverter efficiency	0.95	
Pressure-drop in components	2%	

Table 4.3 SOFC mode base case result

Streams	$\dot{m}_i[g/s]$	$P[bar]$	$T[K]$	$\hat{h}_i[J/g]$	$\hat{s}_i[J/g.K]$	$ex_i[J/g]$
1	5.611	20.0	550	-4719	21.49	47131
2	5.611	19.6	790	-3547	23.28	47772
3	5.611	1.22	790	-3547	26.45	46827
4	5.611	1.19	897	-2986	27.14	47183
5	16.68	1.17	943	-9082	14.17	7655
6	16.68	1.14	865	-9271	13.97	7526
7	16.68	1.12	454	-10200	12.54	7027
8	16.68	5.38	698	-9660	12.66	7529
9	16.68	5.28	509	-10080	11.97	7315
10	16.68	20.4	850	-9306	12.42	7956
11	16.68	20.0	680	-9700	11.91	7712
12	106.7	1.01	298	0	6.88	4.284
13	106.7	1.27	321	23	6.90	24.48
14	106.7	1.24	463	168	7.28	56.40
15	106.7	1.22	527	234	7.41	80.76
16	106.7	1.19	783	509	7.85	227.6
17	95.65	1.17	943	692	8.07	346.8
18	95.65	1.14	667	385	7.69	152.6

Table 4.4 SOEC mode base case result

Streams	$\dot{m}_i[g/s]$	$P[bar]$	$T[K]$	$\hat{h}_i[J/g]$	$\hat{s}_i[J/g.K]$	$ex_i[J/g]$
1	16.68	20.0	550	-9990	11.44	7563
2	16.68	19.6	859	-9285	12.46	7963
3	16.68	1.22	859	-9285	13.93	7526
4	16.68	1.19	869	-9261	13.96	7538
5	5.611	1.17	874	-3110	27.02	47094
6	5.611	1.14	861	-3180	26.96	47041
7	5.611	1.12	443	-5207	23.79	45960
8	5.611	5.38	686	-4608	24.05	47022
9	5.611	5.28	610	-4434	23.5	46818
10	5.611	20.4	1083	-1971	24.93	48856
11	5.611	20.0	686	-4067	22.55	47469
12	44.40	1.01	298	0	6.88	4.453
13	44.40	1.27	322	236	6.9	24.48
14	44.40	1.24	570	280	7.49	103.3
15	44.40	1.22	614	326	7.58	124.5
16	44.40	1.19	1061	823	8.19	439.3
17	55.47	1.17	1173	943	8.26	531.7
18	55.47	1.14	821	545	7.87	269.0

Comparing system components' performance using the exergy efficiency and exergy destruction rate as shown in Figure 4.2 and Figure 4.3. It is obvious that high exergy destruction rate does not correspond to low exergy efficiency, rather it is dependent on the magnitude of the fuel and product streams in the components. A typical example is the storage tanks and the pressure reduction valve. While both components have similar exergy efficiency, the exergy destruction rates for each component are far from same. The energetic performance of the stack and compressors as well as the total system exergy destruction rate is shown in Figure 4.4. The result suggests that the power consumed by the compressors is very small compared to the power produced in the SOFC mode. However, the system exergy destruction rate in the SOFC mode of operation was almost half of the total power production. The effect of this is better understood in the EPC parameter result shown in Figure 4.6. System efficiency represented by the energy, exergy and roundtrip efficiencies is shown in Figure 4.5. For all the efficiency cases considered in both exergy and energy analysis, the SOEC mode of operation performed better than the SOFC mode of operation. While the energy and exergy efficiency of the SOEC mode in both efficiency scenarios considered had close values, the SOFC mode had very distinct values. This is because of the desired product in both modes of operation. The product in the SOEC mode is the gas while in the SOFC mode of operation it is electricity. Thus, gas storage improved the SOFC mode efficiency by reducing loss while it does not matter much for the SOEC mode of operation. The roundtrip efficiency suffered at the system level when compared to the stack roundtrip efficiency because of the power consumed in the compressors. To improve the roundtrip efficiency, more effort should be put in improving the performance of the SOFC mode of operation.

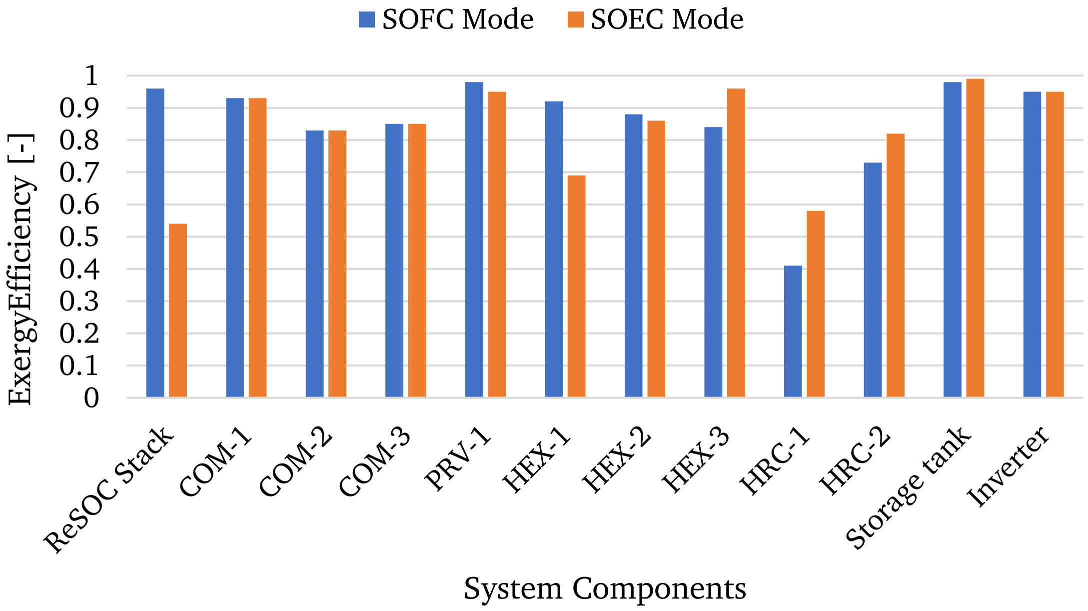

Figure 4.2 Exergy efficiency of system components at base case operating conditions

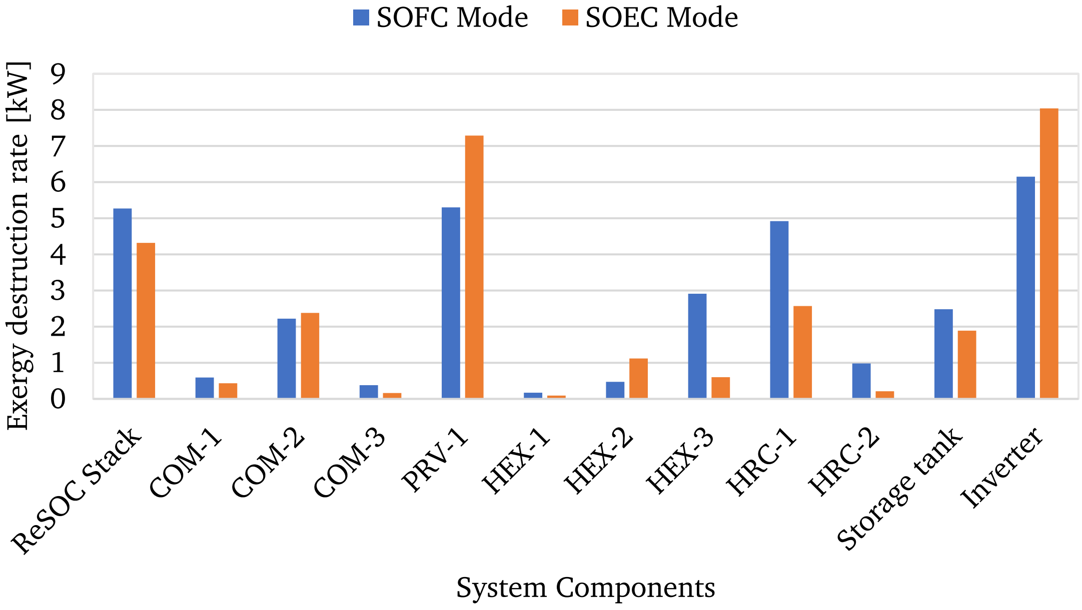

Figure 4.3 Exergy destruction rate of system components at base case operating conditions

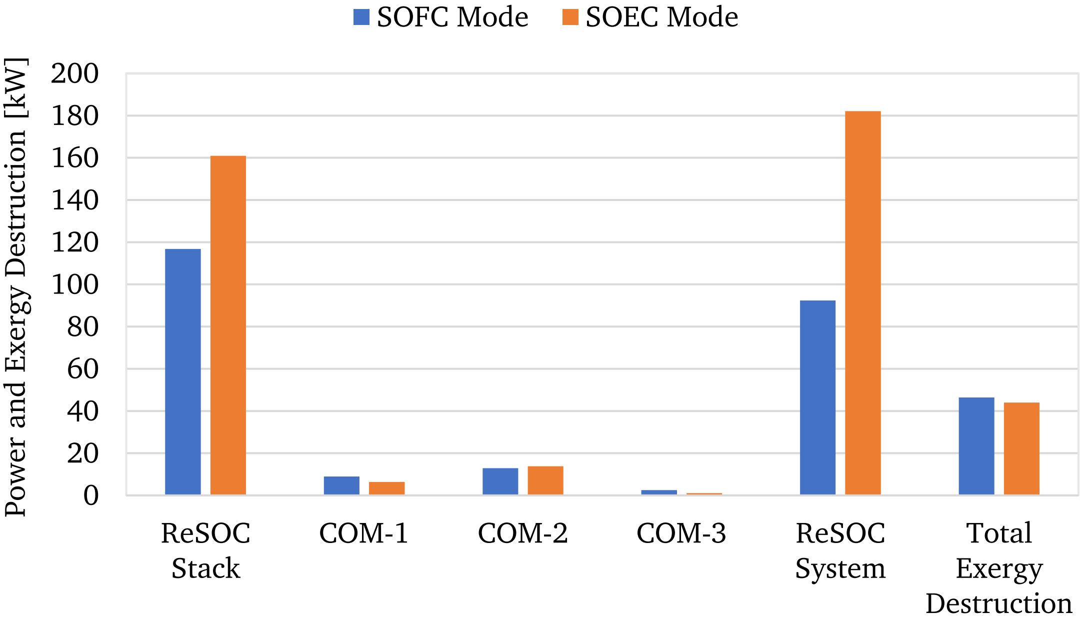

Figure 4.4 Stack, compressor & system power, and system total exergy destruction rate at base case operating conditions

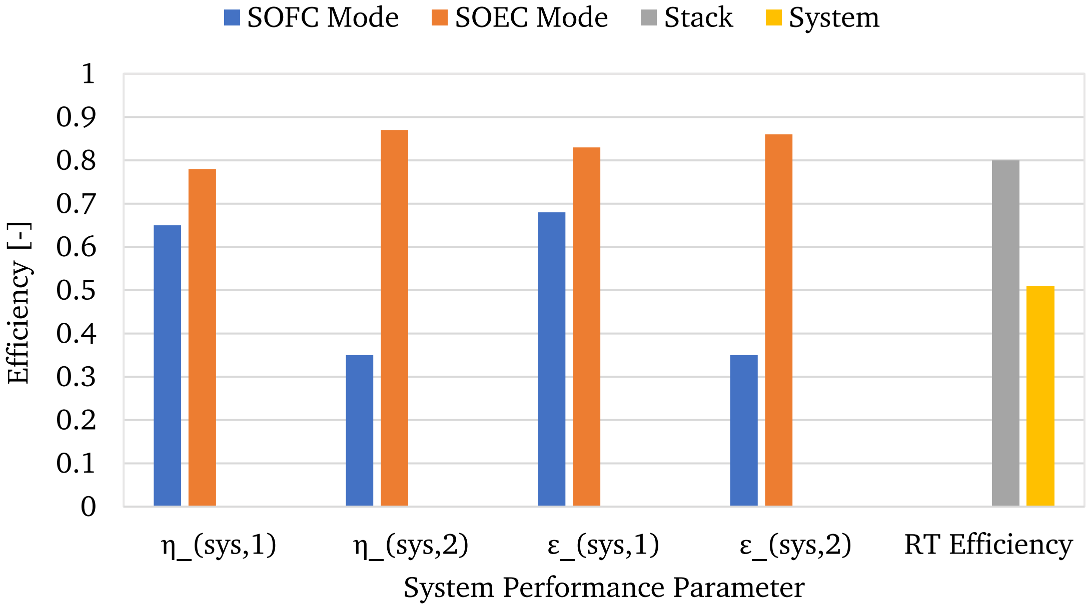

Figure 4.5 ReSOC system energy, exergy, and roundtrip efficiency at the base case operation.

The system exergetic performance coefficient of the SOEC and SOFC mode for the base case operating condition is compared in Figure 4.6. In the exergy destruction results shown in Figure 4.4, the exergy destruction ratio for the SOFC and SOEC modes of operation have close values, whereas the EPC of the SOEC mode is almost double that of the SOFC mode. This shows that the low performance of the SOFC mode of operation is not primarily caused by the exergy destruction rate. The process model in the SOFC modes needs to be improved in an overall sense if the performance needs to be improved. Since the exergetic performance coefficient is defined by the ratio of the product to the total exergy destruction rate. The higher exergetic performance in the SOEC mode means that more product is derived per unit exergy destroyed when compared to the SOFC. This higher product formation rate is what the exergy efficiency depicts while the EPC depicts the product formation rate per unit of exergy destruction rate.

The Grassmann diagram in Figure 4.7 shows the rate of exergy flow in the system and the extent of exergy destruction in the system components for both modes of operation. The Grassman diagram gives a complete overview of the system's exergetic performance and makes it easier to pinpoint points of high exergy destruction.

The distribution of the system total exergy destruction represented by the exergy destruction ratio is shown in Figure 4.8. In the SOFC mode of operation, 32% of the total exergy destruction in the system is because of exergy loss in the oxygen-deficient air exiting the system. Among the balance of plant components, the highest exergy loss is in the pressure reduction valve, ReSOC stack, and inverter, and HRC-2 summing up to 47% of system total exergy destruction. To reduce exergy destruction in the valve, a turbine can be used in its place for additional power generation in the system. In the SOEC mode, 66% of the system's total exergy destruction is from the exergy destruction in the balance of plant components as shown in Figure 4.9. 42% of the balance of plant components' exergy destruction is associated with the ReSOC stack alone. The 34% exergy destruction ratio of the exit air stream and 17% exergy destruction ratio of the pressure reduction valve in the SOEC mode shows that the system will benefit more from replacing the PRV with a turbine and adding a bottoming cycle or a heat storage device in the SOEC mode thereby, increasing overall system performance.

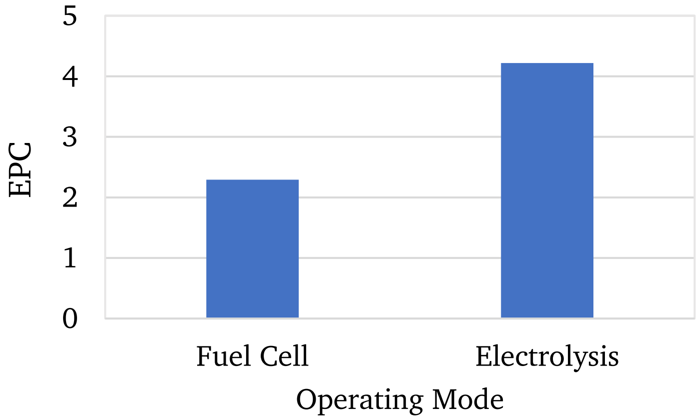

Figure 4.6 System EPC comparison for the SOFC and SOEC modes of operation

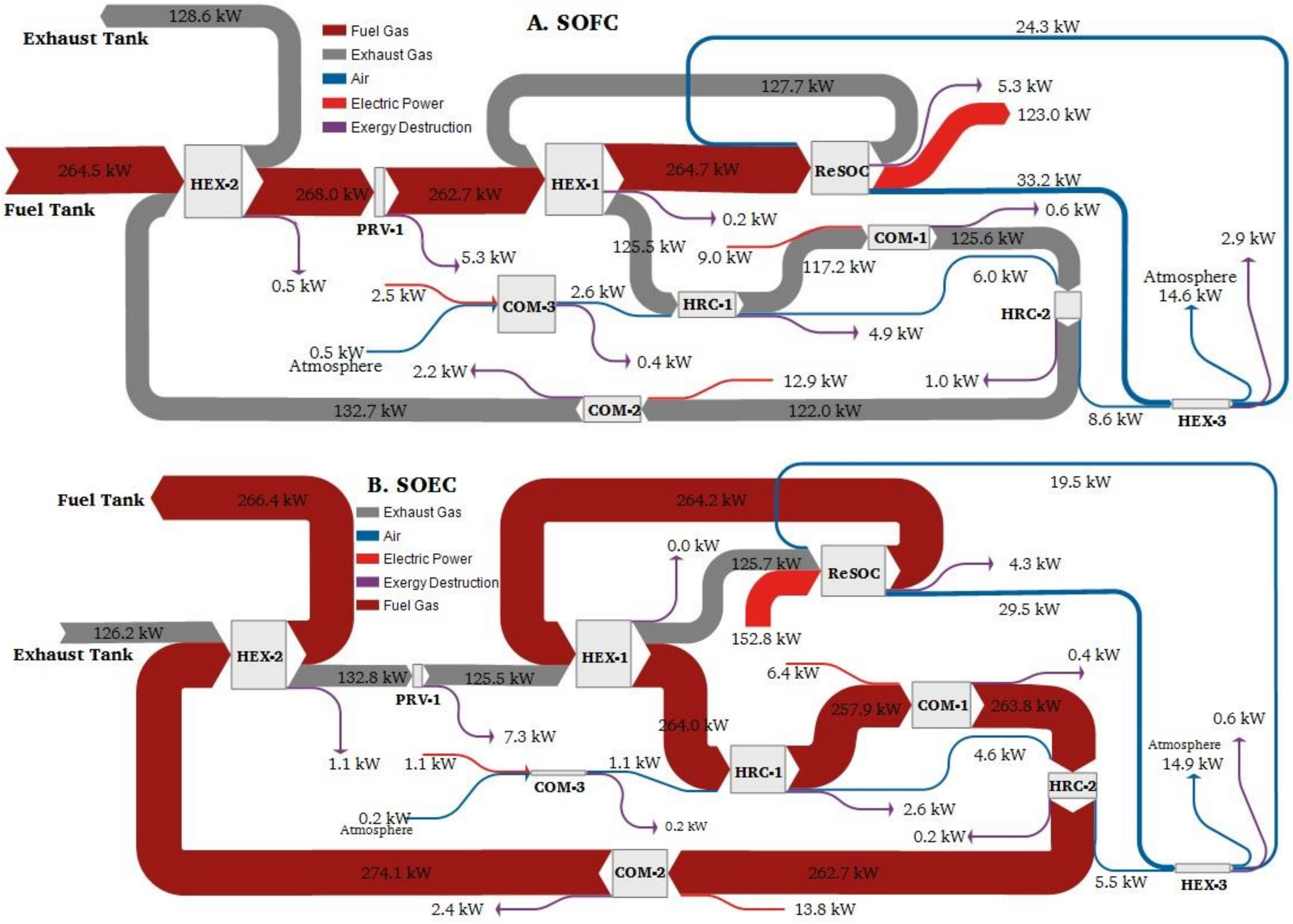

Figure 4.7 Grassmann diagram showing the rate of flow of exergy in the ReSOC system

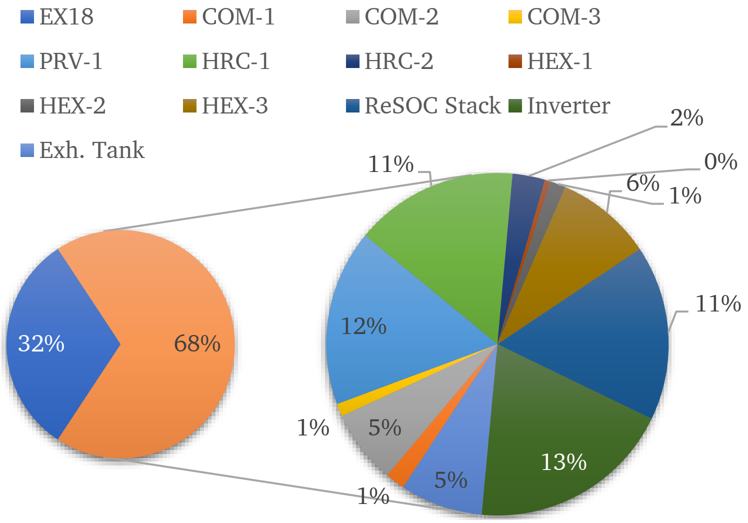

Figure 4.8 Exergy destruction ratio showing points of exergy loss and exergy destruction in the system (SOFC Mode)

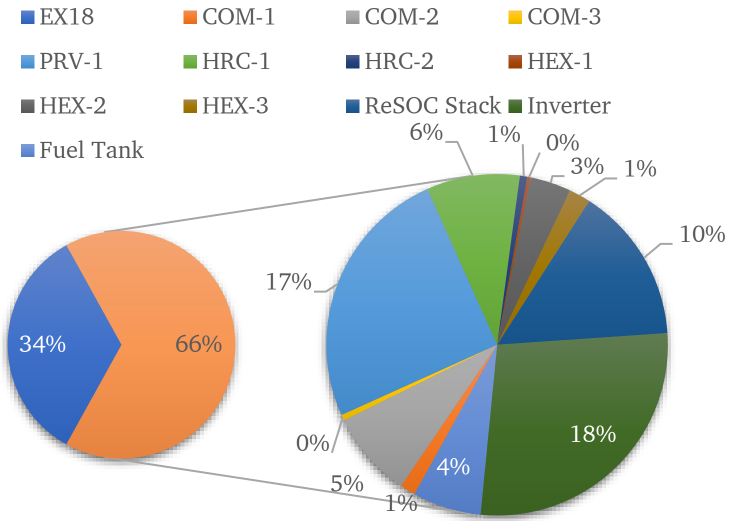

Figure 4.9 Exergy destruction ratio showing points of exergy loss and exergy destruction in the system (SOEC Mode)

4.4.1 Current density effect on performance

The effect of the ReSOC stack current Density on the overall system performance was investigated. As shown in Figure 4.10, increasing the stack operating current density affects the overall system efficiency as defined in Equations 4.33 and 4.36 for both modes of operation. This adverse performance is primarily caused by the parasitic power compression in the compressors. As the current density increased, the mass flow rate required to achieve the fuel utilization factor increases. This increased mass flow rate in turn leads to more power consumed in the compressors. The output energy viz a viz the fuel heat value for the SOEC mode and electrical power in the SOFC mode also increases with increasing operating current density as well. An indication of this is the system net power generation in the SOFC mode. Net power generation, despite the increasing parasitic power consumption and decreasing system overall efficiency, increased as the operating current density increased. From the energy equation, one would expect the system efficiency to improve as the net power generation increased since the input parameter is only the heating value of the inlet gas. In the model, however, the fuel cell inlet gas flow rate is tied to the operating current density, thus, as the operating current density increases, the inlet fuel gas heating value also increases. This increase in the inlet gas heat rate and increase in parasitic power consumption combined overshadows the corresponding increase in the stack electric power generation. This is the cause of the unavoidable adverse effect on the system's overall efficiency at high operating current density. In a model where the system mass flow rate is constant for all operating current densities, the current density will be tied to the fuel utilization parameter as seen in the stack model. An increase in efficiency will be expected as operating current density increases since more fuel will be converted at a higher current density. A similar approach is followed in the SOEC mode of operation. The SOEC mode aims to convert the exhaust gas to a fuel gas same as the initial composition of the SOFC mode. Since the SOFC outlet is the SOEC inlet, an increase in the SOFC mass flow rate will result in a corresponding increase in the SOEC mass flow rate.

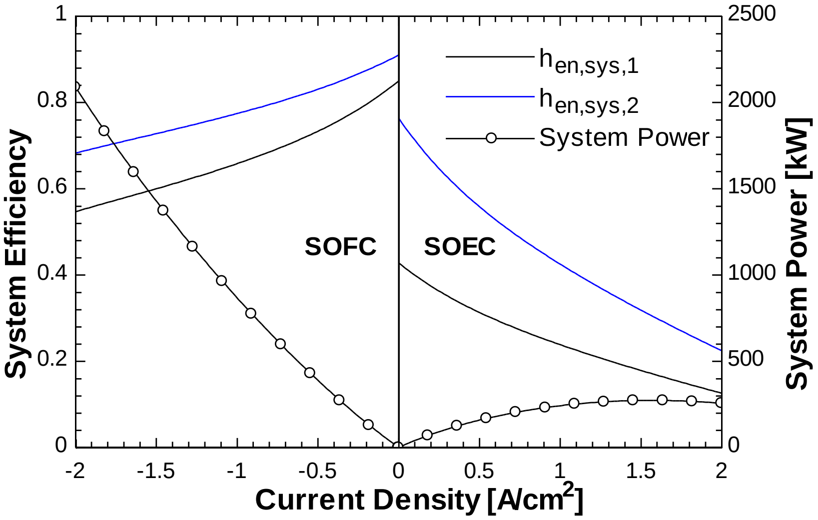

Figure 4.10 Operating current density vs system performance.

The perk of this increased mass flow rate is an increased output as the fuel heating value rate. However, this also leads to higher power consumption in the stack. The balance of plant components in the SOEC mode consumes less power compared to the SOFC mode of operation. As shown in Figure 4.10 the gross power consumed in the system in the SOEC mode increased at about 80kW per $0.1A/cm^2$ of current density while the produced fuel heat value rate increased at about 64kW. Therefore, the reduction in overall system performance at higher stack operating current density. Summarily, increasing the operating current density increased the overall system output but at a lesser system efficiency. An understanding of this efficiency problem is better highlighted in the system roundtrip efficiency. Figure 4.11 shows the ReSOC stack and overall system roundtrip efficiency as a function of operating current density. The system roundtrip efficiency is lower than the stack roundtrip efficiency. This difference is primarily a result of the power consumption in the compressors. It should be noted that the system performance is not optimized for a particular operating condition. Thus, the system performance as shown in Figure 4.10 and Figure 4.11 can be regarded as a base case scenario where components are operated to show compatibility in the system.

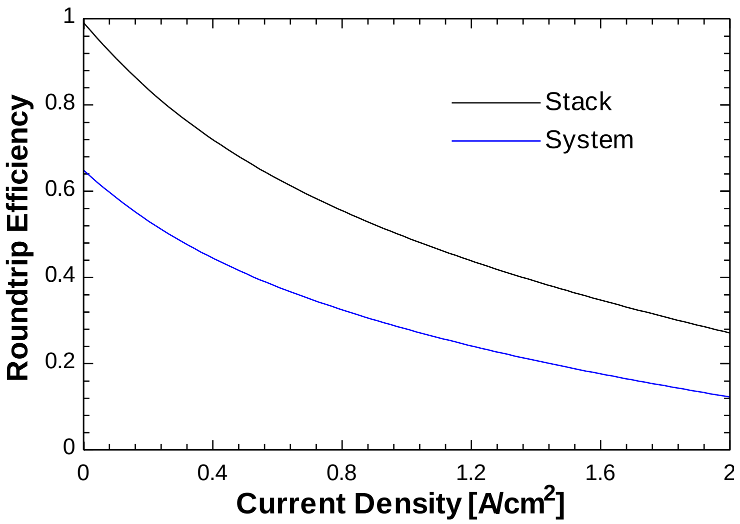

Figure 4.11 Effect of current density on roundtrip efficiency

An optimized study will seek to improve system performance for a selected design condition. Parameters such as excess air ratio, storage tank temperature, and pressure, compression ratio, etc., can be adjusted to improve system performance for a specific operating condition. Another approach that can be employed to optimizing roundtrip system performance is optimizing individual operating mode. This might lead to having more system components where some components will be idle in one operating mode and active in another.

4.4.2 Fuel utilization effect on performance

In the fuel utilization parameter study, the effect of the fuel utilization on the overall system performance was investigated for both the fuel cell and electrolysis cell mode. The system is operated at 0.2A/cm^2 current density, stack temperature of 873K, and pressure of 101.325kPa. Because of the constant operating current density, increasing the fuel utilization reduces the inlet mass flow rate, unlike when the fuel utilization is constant, and the current density varies. This decrease in mass flow rate with an increase in fuel utilization however is not directly proportional. The fuel gas used in this study contains other gas species that do not take part in the electrochemical reaction, these gas species will not be affected by the fuel utilization factor.

As far as system performance goes, Figure 4.12 shows that the performance for both modes of operation improves with increasing fuel utilization factor. Albeit a relatively very low system performance for the SOFC mode. The system performance for the SOFC mode peaked at a fuel utilization factor of about 0.7 for the SOFC mode and 0.8 for the SOEC mode. This performance reduction takes a toll on the system roundtrip efficiency as shown in Figure 4.13. While the stack roundtrip efficiency seems almost unaffected by the fuel utilization factor, a great deal is lost in the system roundtrip efficiency at very high utilization factors. From this, it can be concluded that while higher fuel utilization ratio might lead to lesser reactant gas requirement, it poses a bigger performance problem in the stack in terms of thermal requirement. Selecting a low fuel utilization factor will cause less power to be produced in the stack thus lesser net system power. But at a higher fuel utilization factor, the balance of plant components' power consumption becomes extreme, and this also poses a thermal problem on the stack. This increased power requirement and thermal stress lead to poor performance and a lesser ReSOC life span. Therefore, in determining the system design condition, the fuel utilization factor should be determined based on its effect on the system performance and the thermal requirement in the stack.

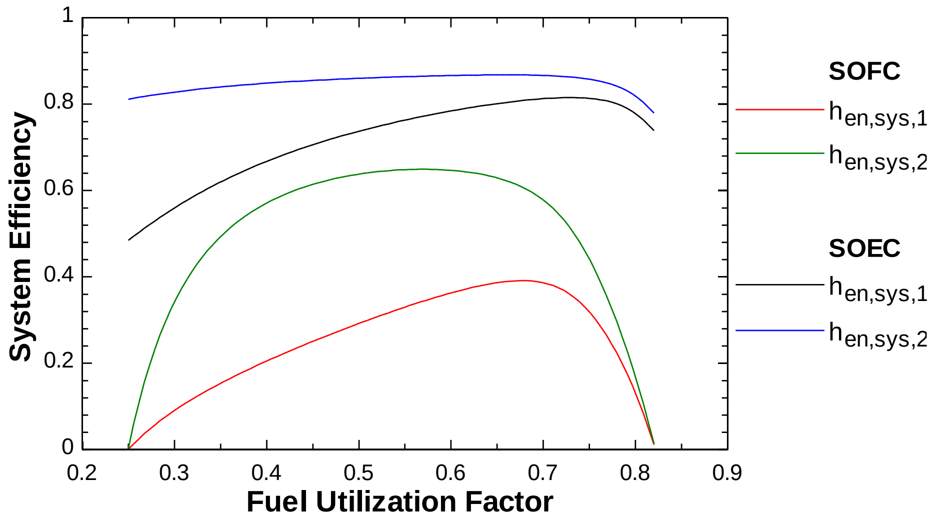

Figure 4.12 Fuel utilization effect on system efficiency

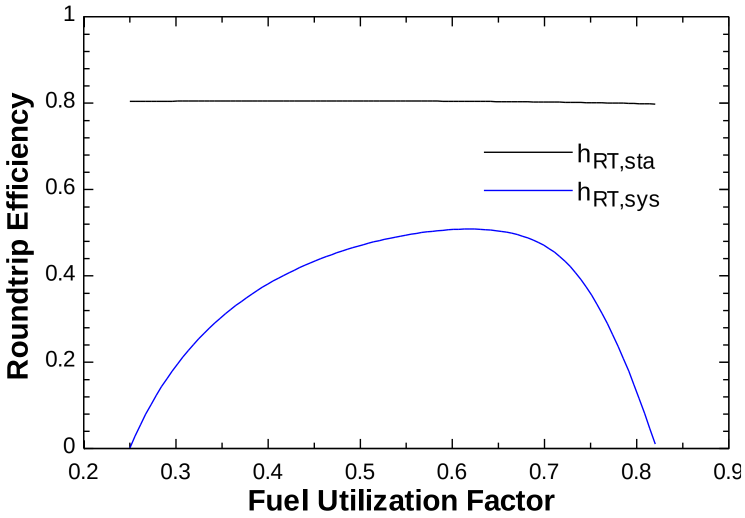

Figure 4.13 Fuel utilization effect on the overall system and stack performance

4.4.3 Stack exergy analysis

The stack exergy analysis is carried out based on the same operating conditions of the stack as analyzed in section 3.3. Figure 4.14 shows the relationship between the exergy performance metrics and operating current density for the SOFC and SOEC mode of operation at 873 K and 1.01325 bar operating temperature and pressure. The EPC parameter suggests that it is best to operate the stack at very low current densities, but the exergy destruction rate suggests the opposite. The exergy efficiency however suggests that for the SOFC mode, the stack should be operated at the lowest current density possible but in the SOEC mode at the highest possible operating current density. The difference in these performance metrics means that the performance of the stack should not be selected based on one parameter.

On comparing the EPC for the fuel cell and electrolysis mode, the fuel cell mode has a higher EPC at low current densities than the electrolysis mode and even lower EPC at higher current densities. The driving factor for this extreme behavior at the SPFC mode is the exergy destruction rate as can be seen on the graph. Because the SOFC mode of operation has a higher exergy destruction rate than the SOEC mode at high current densities, the initially excellent performance reduces drastically.

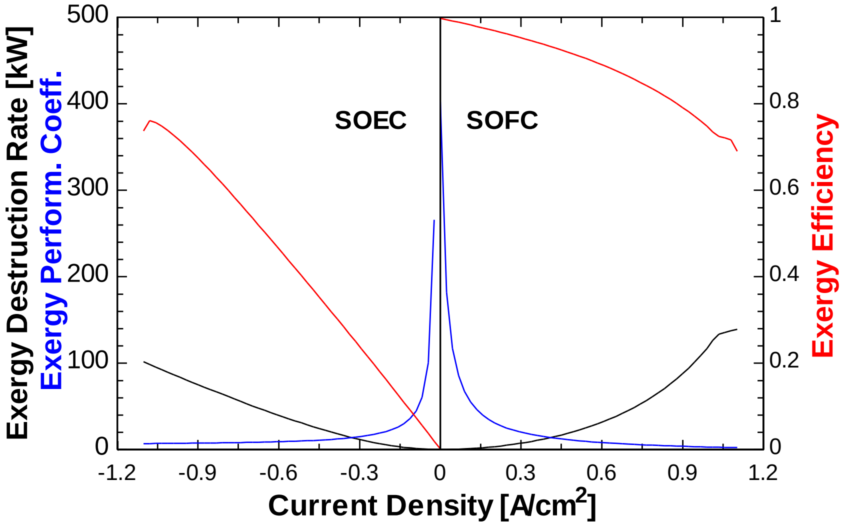

Figure 4.14 Exergetic performance of the ReSOC stack at 15g/s inlet mass flow rate

The efficiency on the other hand is highly affected by the energy performance of the ReSOC stack. In the SOFC mode, the fuel exergy rate is taken as the difference between the inlet and exit gas exergy rates. Thus, as reaction rates increase, the difference also increases but at a rate faster than the produced power due to irreversibilities in the stack. This will lead to a slowdown in stack performance as shown in the SOFC efficiency. The SOEC efficiency on the other hand measures the rate of fuel produced over the considered range of operating current density. At a current density close to the limiting value, the SOEC exergy efficiency suffered a great loss, this is caused by the extremely high electric power consumption at those current densities.

The effect of the stack inlet mass flow rate on the stack exergetic performance was investigated in Figure 4.15. For the analysis, the stack was operated at 0.25 A/cm^2 current density and an operating temperature of 973K. The exergetic efficiency of the SOFC mode of operation seems almost unbridled by the inlet mass flow rate fluctuating between 97% and 98%. The SOEC efficiency however is highly affected by the inlet mass flow rate. It may come as a surprise since the inlet mass flow rate is for the SOFC mode and the SOEC reactant is the product of the SOFC. One would naturally expect that the SOEC response should be like the SOFC. The definition of the exergy efficiency for both modes explains this difference.

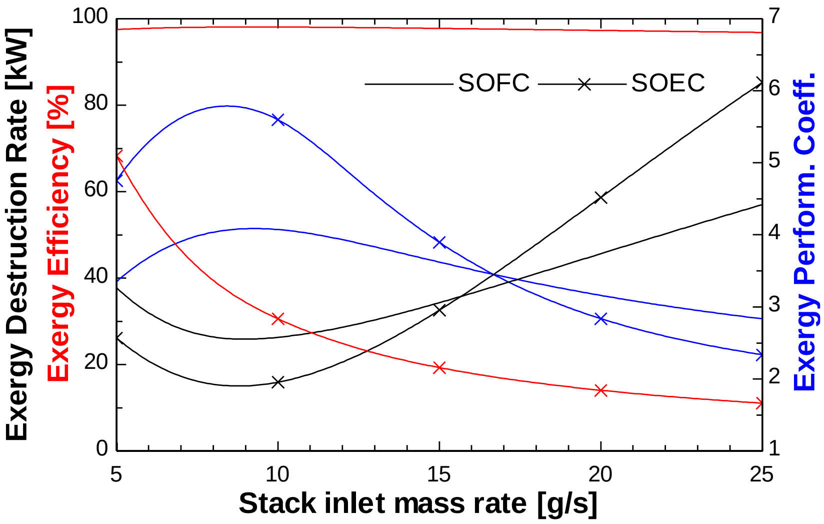

Figure 4.15 Inlet mass flow rate vs stack exergy performance for both modes of operation

In the SOFC mode, efficiency is determined by the power generated and the amount of reacting gas. In the SOEC mode, the efficiency is defined by the amount of fuel produced, the inlet fuel, and the electricity consumption. Since the amount of fuel consumed in the SOFC mode is determined by the current density. This means that for a constant current density and increasing mass flow rate, more unreacted fuel will be available at the fuel cell exit, hence, the electrolysis cell inlet. Also, in the SOEC mode, the amount of fuel produced is dependent on the current density. This means that as inlet gas increases less and less fuel will be produced, hence the reducing efficiency. The exergy destruction rate and exergy performance relationship are the same as in Figure 4.14 for both modes of operation. Other parameters affecting the exergetic performance are temperature and pressure. In Figure 4.16 and Figure 4.17, the effect of operating temperature and pressure and standard state temperature and pressure on the exergy destruction rate in the ReSOC stack for both modes of operation is investigated, respectively. In the analyses, the stack was operated at 0.25A/cm^2 current density and an inlet mass flow rate of 15 g/s.

Increasing the stack operating temperature reduces the exergy destruction for both the fuel cell mode and electrolysis mode as can be seen in Figure 4.16a. However, at stack operating temperature beyond 923K, the exergy destruction rate increases in the SOFC mode of operation. This increase in exergy destruction for the SOFC mode of operation is attributed to the higher heating demand in the stack that will have to be fulfilled by the inlet oxidant gas as defined in the model. In Figure 4.16b, increasing the operating pressure reduces the exergy destruction rate for both the fuel cell and electrolysis cell mode of operation. In the SOEC mode, the exergy destruction rate increases after an operating pressure of about 2.5 bar. This is due to increased electrical power consumption in the ReSOC stack at high operating pressure as indicated in Figure 3.15a. However, the increase in the exergy destruction rate is very minimal even at 5bar with a value of 5kW compared to over 8.4kW at 1 bar operating pressure.

The effect of the surrounding state on the stack exergy destruction rate indicates that stack performance suffers at elevated surrounding conditions for both the SOFC and SOEC modes of operation. The SOEC suffered more than the SOEC as can be seen from the gradient of the linear relationships. Evidently, the higher the surrounding state parameters, the higher the exergy destruction rate. This is because, at these elevated surrounding states, the quality (exergy) of the gases reduces. As pointed out by [70], "when energy loses its quality, exergy is destroyed", hence exergy destruction rate is expected to increase with increase surrounding state parameters such as temperature and pressure.

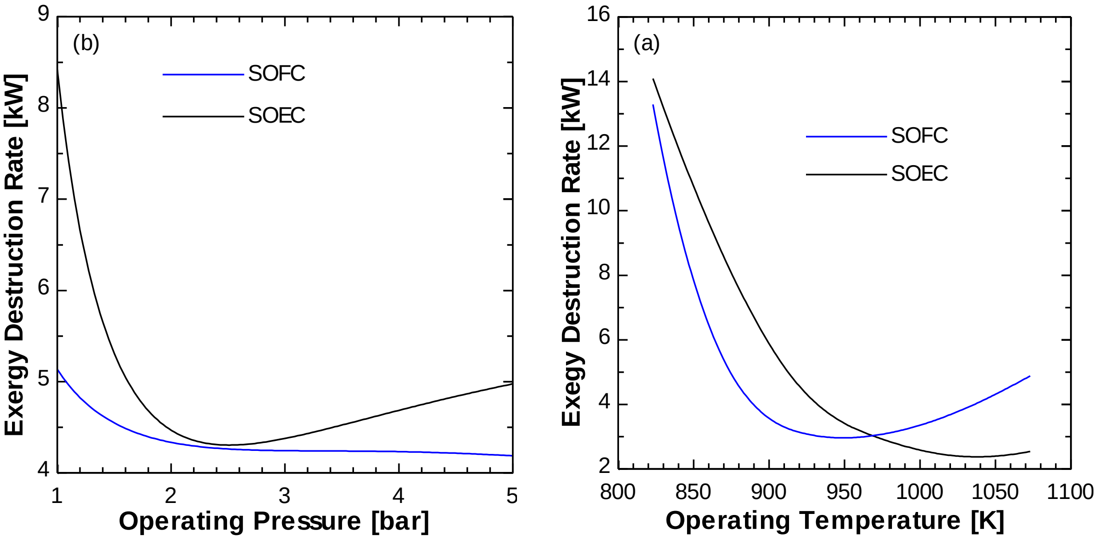

Figure 4.16 Stack operating parameters vs stack exergy a) temperature b) pressure

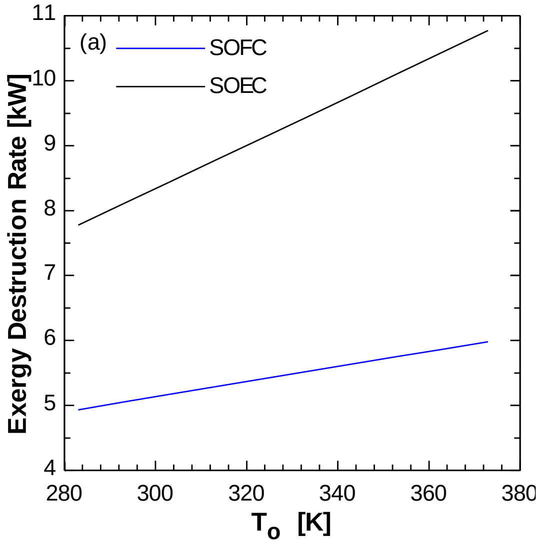

Figure 4.17 Dead state parameters vs stack exergy destruction rate a) temperature b) pressure

4.4.4 System exergy analysis

In the system exergy analysis, the system is operated as the base case with a stack nominal operating temperature of 873K, an average operating pressure of 1 bar, and fuel utilization of 0.60. The exergetic performance metrics considered are the exergy efficiency and the exergy destruction rate. Figure 4.18 shows the exergetic performance of the system as a function of operating current density. As experienced for the energetic performance analysis, higher operating current density results in lesser performance in the system. The exergy destruction rate is higher for the SOEC mode than in the SOFC mode despite the SOEC mode having a better exergetic efficiency. This is because the SOEC mode has a higher conversion efficiency than the SOFC mode, hence, the large irreversibility has little effect on the exergetic efficiency.

The exergetic efficiency for the SOEC mode at 0.2 A/cm^2 operating current density is 0.89 and 0.78 for the SOFC mode. The system has a better exergetic performance than energetic performance, especially in the SOFC mode. This shows that despite having a low energy conversion ratio, the fuel cell mode has low irreversibilities compared to conventional fuel combustion systems.

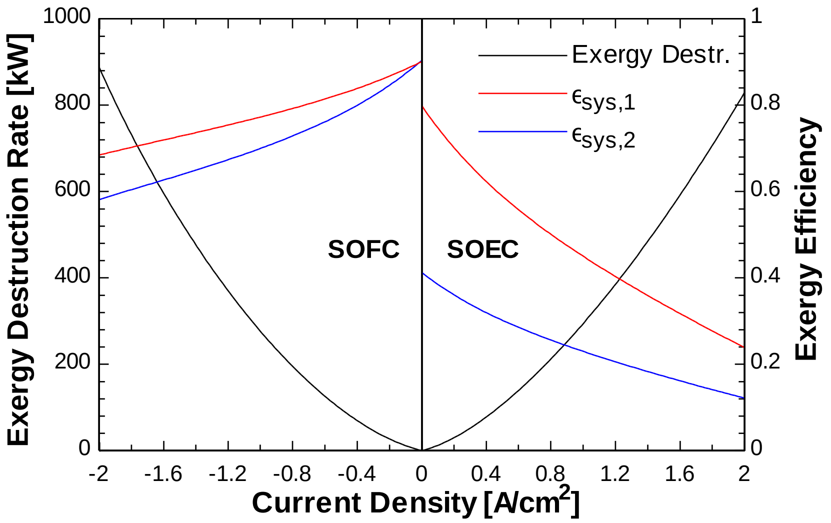

Figure 4.18 Effect of the operating current density of exergetic performance

Exergy is defined by Dinçer and Rosen [70] as the quality of energy. It is dependent on the state of the surrounding or environment, usually defined as the dead state. The dead state parameters used in this study are the dead state temperature and dead state pressure. Figure 4.19 (a to d) shows the effect of the dead state parameters on the system exergy efficiency and exergy destruction rate for both modes of operation.

In Figure 4.19a and b, the effect of the dead state temperature on the ReSOC system exergetic performance in both the SOFC and SOEC modes of operation, respectively, is shown. Operating the ReSOC system in a hotter surrounding reduces the system exergy destruction rate but also reduces system efficiency for both modes of operation. This effect of the dead state temperature is higher in the SOFC mode than in the SOEC mode. For the temperature range considered, the SOFC exergetic efficiency dropped from 0.78 at the standard room temperature of 298K to 0.7689 at 325K while the exergy destruction dropped by a mere 0.2kW from 110.6 to 110.4kW at similar temperatures. The SOEC mode on the other hand is almost unaffected by the temperature range recording changes of no more than 0.001 in the exergy efficiency. The minimal effect of the dead state temperature on the system exergetic performance is primarily associated with the extremely high operating temperature of the ReSOC stack and the high temperature of the gases in the stream. The effect of the dead state pressure is more pronounced than that of the operating temperature for the range considered. In the SOFC mode of operation (Figure 4.19c), the overall system performance improved with increasing dead state pressure. The exergy destruction rate reduced by more than 10kW between 101 kPa and 500kPa of dead state pressure while the exergy efficiency improved by approximately 0.002. In the SOEC mode, however, the exergetic efficiency and exergy destruction rate were reduced for an increasing dead state pressure. The range of change in the SOEC mode was larger than in the SOFC mode albeit that that the efficiency moved in opposite directions. In the SOEC mode, the efficiency reduced by approximately 0.1 units which is 5 times the improvement recorded in the fuel cell mode, the exergy destruction rate on the other hand reduced by more than 10kW like the SOFC mode.

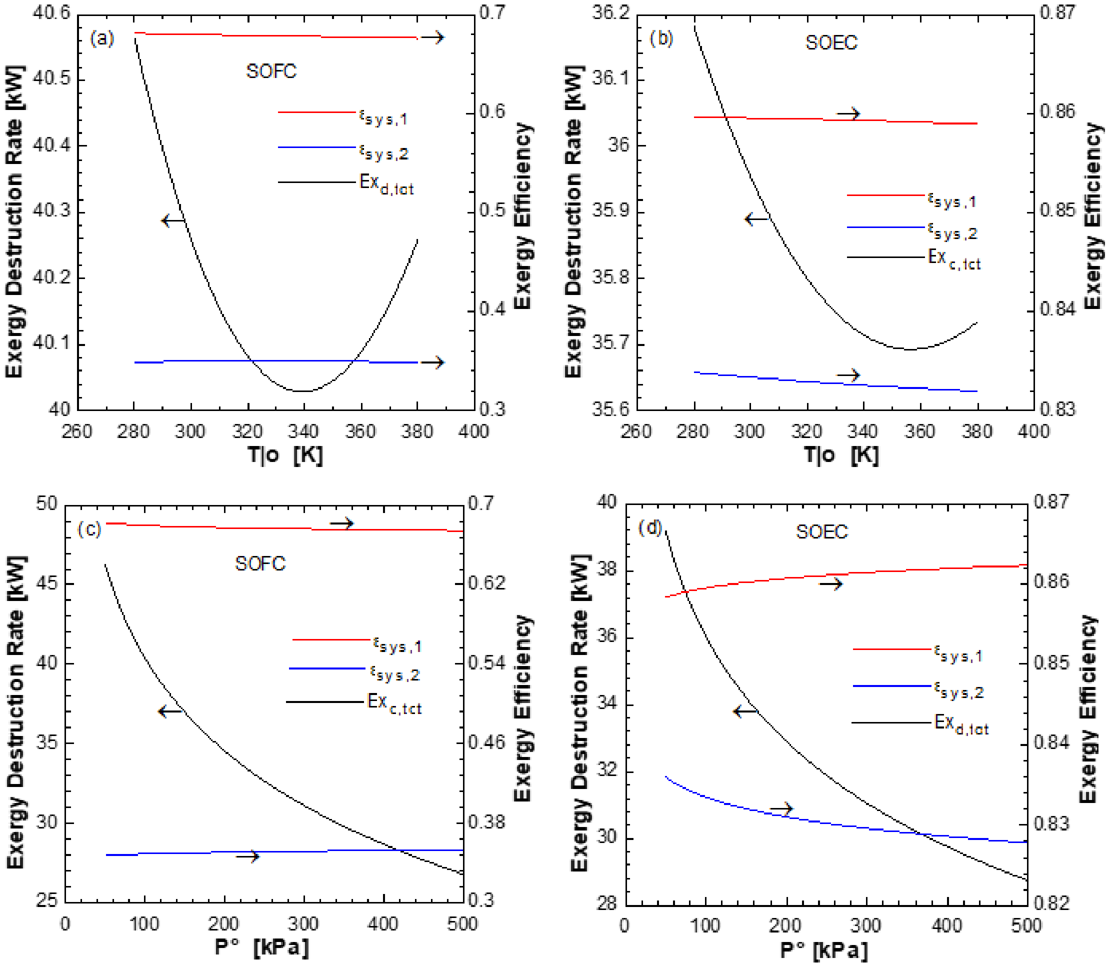

Figure 4.19 Effect of dead state parameters on the system exergetic performance

5
LEVELIZED COST OF STORAGE FOR RESOC SYSTEM

For any energy storage technology to be adopted or deployed for use, the associated cost with the technology and system must be within acceptable means. In other words, the economic feasibility of an energy storage technology or system is crucial to its adoption or commercial roll-out. In this chapter, the costs associated with the base case ReSOC system in this study will be presented and compared with the respective cost of other types of energy storage systems available in the literature. Here, a 123kW/615kWh capacity ReSOC system is considered. The system costing presented here aims to give a preliminary insight into the possibility of the ReSOC system and its economic feasibility as an electricity storage device. A 123kW system is chosen because it has a higher chance of early deployment than grid-scale systems. Also, a grid-scale system would require a more in-depth analysis beyond system economic feasibility before it can mature for deployment. The system follows the ReSOC plant described in Figure 4.1 where the fuel and exhaust gas are stored in pressurized carbon steel tanks. The system costing in this chapter describes the capital costs associated with each component and their respective operation and maintenance costs. The assumptions made are presented and the costs associated with system and system components are calculated. Finally, the calculated results are compared with costs presented in the literature for various energy storage technologies.

5.1 System Costing Methodology

As earlier stated, the ReSOC system cost is estimated from the cost of individual components. Component capital costs are determined from mathematical relations plotted from cost data as described in the literature. These costs are then scaled from the respective year to 2019 using the chemical engineers' plant cost index (CEPCI). CEPCI is a tool used by engineers to predict the present cost of process equipment and other plant-related costs using indexes that have been normalized over the years. Yearly CEPCI values for years 2000 to 2019 are presented in Table 5.1.

Table 5.1 Composite CEPCI values for 2000 to 2019 [71][72].

Year	Value
2000	394.1
2001	394.3
2002	395.6
2003	402.3
2004	444.2
2005	468.2
2006	499.6
2007	525.4
2008	575.4
2009	521.9
2010	550.8
2011	585.7
2012	584.6
2013	567.3
2014	576.1
2015	556.8
2016	541.7
2017	567.5
2018	603.1
2019	607.5

Equation 5.1 shows the relation in scaling the capital costs of any system component to 2019 prices as considered in this study.

$$Z_k^{2019} = Z_k^{ref} \cdot \left(\frac{CEPCI_k^{2019}}{CEPCI_k^{ref}} \right) \tag{5.1}$$

Where, Z_k^{2019} is the capital cost that will be considered for any component k in the system costing, Z_k^{ref} is the capital cost estimated from the mathematical relations or determined from reference literature for any component k, $CEPCI_k^{2019}$ and $CEPCI_k^{ref}$ are the respective composite CEPCI values for the reference year of the component and 2019, respectively.

The economic metrics considered in this study are the storage cost and the Levelized cost of storage (LCOS). The storage cost also described as the capital cost per cycle was employed by Yang et al. [18] in comparing various electrochemical energy storage systems. Equation 5.2 describes the storage cost as defined in the study.

$$Storage\ cost = \frac{System\ Capital\ Cost}{Energy\ Capacity \cdot Lifetime\ cyce \cdot RT\ Efficiency} \tag{5.2}$$

The system capital cost is the initial costs of all system components excluding the operation and maintenance costs, replacement costs, and handling charges. The energy capacity is the total useful amount of energy deplorable from the system in one complete discharge cycle and the roundtrip efficiency is the same as defined in earlier sections. The storage cost is in ¢/kWh per cycle output. The system's "lifetime cycle" is the total number of roundtrip cycles the system will complete over its economic lifetime. The storage cost, therefore, describes the cost per cycle associated with the system at the start of its lifetime. While this may not be a comprehensive tool in decision making, it is useful in determining the impacts of initial cost on the economic feasibility of storage technologies and comparing these technologies. Figure 5.1 shows a comparison of storage technologies using the storage costs as presented in [18].

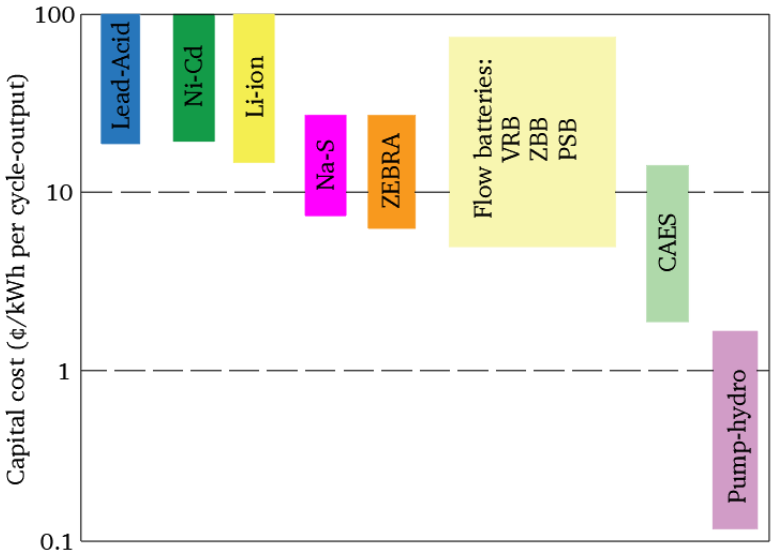

Figure 5.1 Storage cost of various energy storage technologies adapted from Ref. [18]

The LCOS like the Levelized cost of electricity (LCOE) takes all costs associated with the system lifetime into consideration to give a more reliable basis for comparing energy storage systems and technologies. It should be noted that the method of LCOS alone is not sufficient for determining the cost efficiency of a storage plant or system, cost efficiency can only be determined through the method of cash flow model considering all revenue and expenditure. The method of LCOS follows the approach for LCOE for renewable energy systems suggested by [73], [74]. The definition of the LCOS has been given in various studies [16], [75], [76]. Here we define the LCOS according to Verena Jülch [15] in equation 5.3.

$$LCOS = \frac{I_0 + \sum_{t=1}^{n} \frac{A_t}{(1+i)^t}}{\sum_{t=1}^{n} \frac{E_{out}}{(1+i)^t}} \tag{5.3}$$

I_0 is the total overnight investment cost at the start of the equipment lifetime. This is regarded in this study as the sum of the capital costs of all the components in the system. A_t is the annual recurring expenditure on the system. It consists of the operating and maintenance cost, replacement cost, and the cost of electricity supplied to the system (charging cost) as shown in equation 5.4. W_{out} is the annual energy discharge of the system. The summation term $\sum_{t=1}^{n} \frac{\blacksquare}{(1+i)^t}$ is an economic term used to determine the present value of a recurring cost over a specified period. i is the discounted rate, taken as the interest rate and n is the period which is the same as the system economic lifetime. It should be noted that the annual energy production of the system is also converted to the present worth based on the principle stated in [73], [74]. t is the respective nominal operating year and n is the total period which is the economic life of the system in years.

$$A_t = OM_t + I_{re,t} + c_{el} \cdot E_{in} \tag{5.4}$$

OM_t is the total annual operating and maintenance cost for year t, $I_{re,t}$ is the replacement cost of any component at a given year, c_{el} is the cost of electricity and E_{in} is the total electrical energy charged into the system in a year. For simplification purposes, the system is assumed to function at the same capacity over its lifetime and the charge and discharge rates are constant for every year over the system lifetime. Also, the cost of electricity is fixed at the present rate throughout the system lifetime and the replacement cost of components is equivalent to their capital cost.

5.2 Determining System Capital Cost

5.2.1 ReSOC Stack

The size of the stack has been determined from the stack modeling to be 534760 cm^2 of active cell area. The capital cost of the ReSOC stack is determined from the SOFC stack cost. The stack capital cost is defined according to Najafi et al [77] and is given in equation 5.5 as.

$$Z_{ReSOC} = A_{ReSOC}\left(2.96 \cdot T_{op} - 1907\right) \tag{5.5}$$

Where, A_{ReSOC} is the overall active stack area in m^2 and T_{op} is the stack operating temperature in K. Because the system in this study is operated at atmospheric pressure, contingency of extra costs to allow for pressurization will not be considered. The stack economic lifetime is taken to be 5 years and the replacement cost is the same as the initial capital cost. The reference year for the ReSOC stack cost is 2002 according to [78]. The composite CEPCI for 2002 is 395.6 [79].

5.2.2 Compressor

The capital cost of the compressor is determined by its electric power consumption. Calise et al [14] interpolated the compressor capital cost from literature and has been defined in terms of the power consumed in the compressor according to equation 5.6.

$$Z_{COM} = 91562 \cdot \left(\frac{\dot{W}_{COM}}{455}\right)^{0.67} \tag{5.6}$$

$\dot{W}_{COM}$ is the power consumed in the compressor in W. The reference CEPCI year for the compressors is 2003 with an index of 402.3.

5.2.3 Heat Exchanger/Recuperator

Heat exchanger capital cost is determined from the heat transfer active area. Assuming an overall heat transfer coefficient of 25 W/m-K for all heat exchangers and heat recuperators, the capital cost of the heat exchangers is determined from equation 5.7 according to Cao and Parikhani [80].

$$Z_{HEX} = 130 \cdot \left(\frac{A_{HEX}}{0.093}\right)^{0.78} \tag{5.7}$$

To account for the stainless-steel material used in the heat exchanger and recuperators on the air side, the capital cost is multiplied by a factor of 3 as stated in the chemical engineers' handbook [81]. The reference CEPCI year is 2005 with an index of 468.2.

5.2.4 Pressure Reduction Valve

According to vendor quotation on the B2B website alibaba.com, a medium pressure PRV for high-temperature application cost between \$250 to \$1250. Assuming the average price of \$750 and durability of 5 years. Also, all the valves that will be required for the system lifetime are purchased at the start of the system life cycle. Allowing for an uncertainty factor of 0.3, over the 20 years lifetime of the system lifetime, a total of 6 valves is estimated to be required. Therefore, the total capital cost for the valve is \$4500 and the lifetime is 20 years. The price for the valve is based on the current market, thus, it is not scaled using the plant index.

5.2.5 Storage Tank

The storage tank is a function of the operating duration of the system. In the base case system results, the system had a steady flow rate of 5.611g/s and 16.68g/s for the fuel and exhaust gases, respectively. For a total operating period of 2500h each and assuming 500 cycles, the system will operate at 10 hours per cycle for both modes of operation at 5 hours each. Thereby, the fuel and exhaust tank will need to have a volume of 52.28 m^3 and 65.01 m^3, respectively. Using a cost factor of 2.0 for 2000kPa of tank pressure and using carbon steel as the storage tank material according to Peters et al. [82] and the cost of the storage tank as presented in Green and Southard [81], the exhaust and fuel tank is costed at \$112000 and \$105000, respectively. The cost of the tank is measured at 2016 values, the corresponding CEPCI for 2016 is 541.7.

5.2.6 Inverter

The inverter capital cost is a function of the inverter DC power. Equation 5.8 expresses the inverter capital cost as given in Lee et al [12].

$$Z_{INV} = 100000 \cdot \left(\frac{\dot{W}_{sta,DC}}{500}\right)^{0.7} \tag{5.8}$$

$\dot{W}_{sta,DC}$ is the AC power converted in the inverter. The reference year for the inverter capital cost is 2002 as given in the literature and the CEPCI is 395.6.

5.3 System Economic Properties

From the operating duration assumed in the tank costing methodology, it is obvious that the system is suitable for both interday and intraseasonal energy storage applications. Parameters considered in the system costing and respective assumptions are presented in Table 5.2.

5.4 Results and Discussions

The parameters are used in calculating the system storage cost and the Levelized cost of storage. System components' capital costs and their respective proportion in total system capital cost are presented in Figure 5.2 and Figure 5.3, respectively. The results show that the storage tanks are the most expensive components in the system followed by the inverter and the ReSOC stack. The system had a total capital cost of 680 \$/kWh, and the cost of storage was 13 ¢/kWh. This system is competitive with the storage cost of battery storage systems as reported in [18]. The storage cost is driven primarily by the cost of storage tanks which is determinant of the energy capacity of the system. Analysis results show that increasing the size of the storage tank reduces the storage costs and can even put it at levels better than battery storage technologies for the scale of application.

Table 5.2 System economic properties

Parameter		**Value**	**Unit**
Economic Life	ReSOC Stack	5	years
	Other components	20	years
System Properties	Roundtrip efficiency	0.5071	
	Power rating	123	kW
	Energy Capacity	615	kWh
System Operation	Cycle duration in a year	5000	h
	Duration per mode	5	h
	Duration per cycle[1]	10	h
Economic Indicators	Discounted rate	0.15	
	Cost of electricity	8.8	¢/kWh
	O&M cost	6% of capital cost	

Comparing the storage cost calculated with the storage cost of other energy storage technologies presented in Figure 5.1, the system considered in this study is competitive with sodium-sulfur (NaS) battery, rechargeable molten salt battery (ZEBRA), and flow batteries. Large-scale interseason storage application of ReSOC system has shown to be competitive with conventional compressed air electricity storage (CAES) systems by Ref. [7]. Because the cost of a solid oxide cell stack is expected to reduce over time as the technology matures further, the system storage cost is also expected to reduce further over time. These preliminary results

---

[1] 1 cycle = 1 SOFC mode + 1 SOEC mode

show that the system is economically competitive and even poses a potential to get better at the considered scale of application.

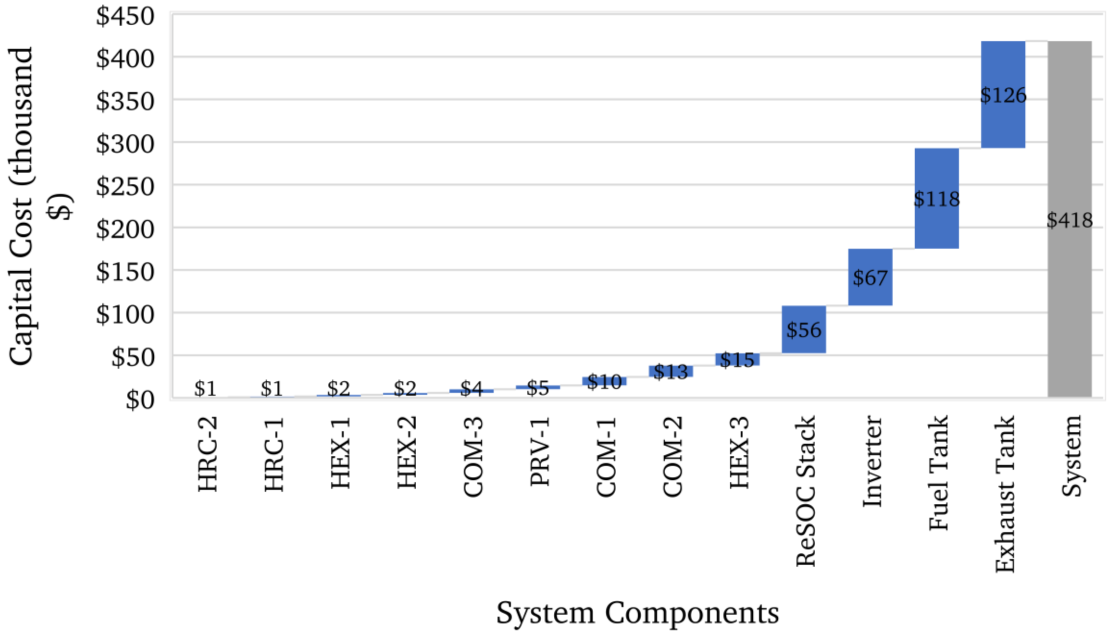

Figure 5.2 Capital costs of system components adjusted to 2019 with CEPCI.

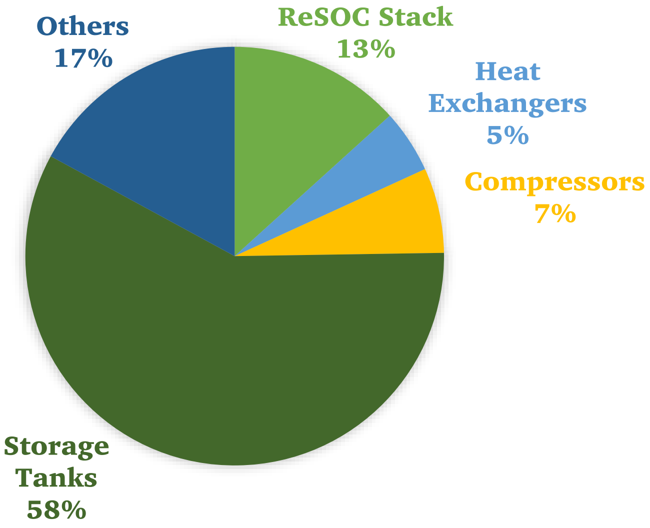

Figure 5.3 System capital cost distribution among system components

The result of the LCOS analysis is presented in Table 5.3. The table shows the flow distribution of the costs over the system lifetime and the replacement costs. The system LCOS is 50 ¢/kWh for the base case result as discussed in the earlier sections of this chapter. Other scenarios considered include:

1. Ignoring the cost of charging electricity
2. Same as scenario 1 but with no stack replacement cost
3. Not discounting the electricity produced.

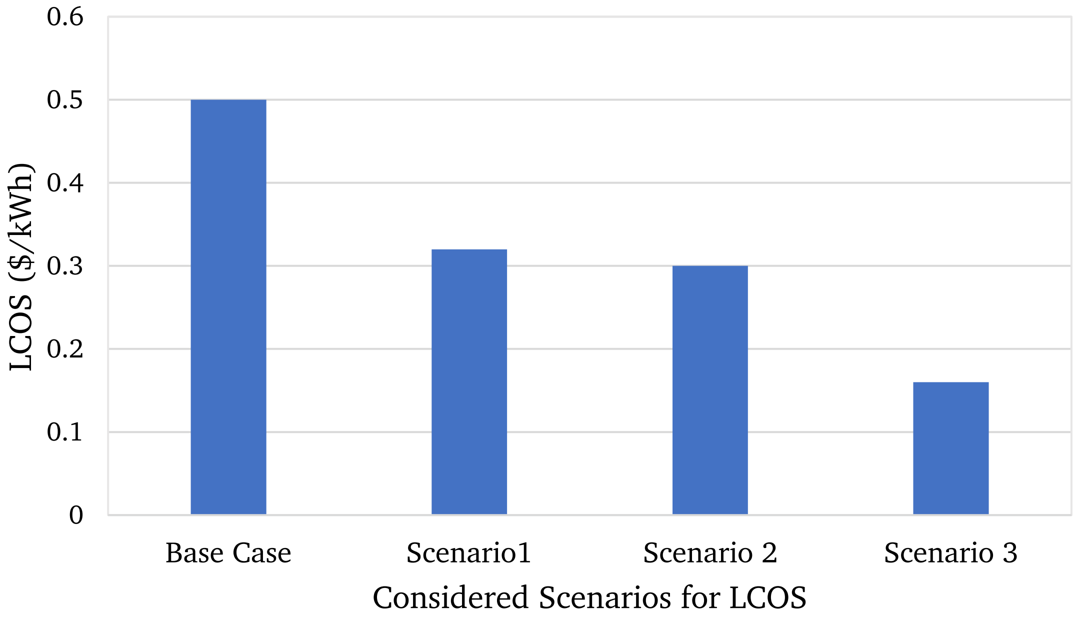

Figure 5.4 LCOS for the system base case and operating scenarios considered.

In scenario 1, the LCOS dropped by almost 40% from the base case to 32 ¢/kWh indicating that the system cost is largely dependent on the total cost of electricity stored in the system. Scenario 2 results indicate that the replacement cost of the ReSOC stack contributes a little to the system Levelized cost. The LCOS of scenario 2 was 30 ¢/kWh. In the last scenario, where the electricity production was not discounted, the least LCOS was recorded at a mere 16 ¢/kWh. The results for the LCOS of the system considered in this study were compared to results presented in [15] where the LCOS method was used to compare energy storage technologies. The results presented in the study excluded the cost of electricity. For an energy storage system with 500 yearly cycles, the LCOS for the technologies presented are shown in Figure 5.5.

Table 5.3 Cash flow over the system economic lifetime

Period	**Nominal Values**					**Discounted Values (Present Worth)**			
	Capital Cost	Replacement	O&M cost	Charging	Yearly	Replacement	O&M cost	Charging	Yearly
0	418,387.59		-	-	0		-	-	0.00
1			24,631.10	53,362.26	307500		21,418.35	46,401.96	267391.30
2			24,631.10	53,362.26	307500		18,624.65	40,349.53	232514.18
3			24,631.10	53,362.26	307500		16,195.35	35,086.55	202186.24
4			24,631.10	53,362.26	307500		14,082.91	30,510.04	175814.12
5		55,601.81	24,631.10	53,362.26	307500	27,643.92	12,246.01	26,530.47	152881.85
6			24,631.10	53,362.26	307500		10,648.70	23,069.98	132940.74
7			24,631.10	53,362.26	307500		9,259.74	20,060.85	115600.64
8			24,631.10	53,362.26	307500		8,051.95	17,444.22	100522.30
9			24,631.10	53,362.26	307500		7,001.70	15,168.88	87410.69
10		55,601.81	24,631.10	53,362.26	307500	13,743.92	6,088.43	13,190.33	76009.30
11			24,631.10	53,362.26	307500		5,294.29	11,469.86	66095.04
12			24,631.10	53,362.26	307500		4,603.73	9,973.79	57473.95
13			24,631.10	53,362.26	307500		4,003.24	8,672.86	49977.35
14			24,631.10	53,362.26	307500		3,481.08	7,541.62	43458.56
15		55,601.81	24,631.10	53,362.26	307500	6,833.16	3,027.03	6,557.93	37790.05
16			24,631.10	53,362.26	307500		2,632.20	5,702.55	32860.92
17			24,631.10	53,362.26	307500		2,288.87	4,958.73	28574.71
18			24,631.10	53,362.26	307500		1,990.32	4,311.94	24847.57
19			24,631.10	53,362.26	307500		1,730.71	3,749.52	21606.59
20			24,631.10	53,362.26	307500		1,504.97	3,260.45	18788.34
Total	**418,387.59**				**6150000**	**48,221.00**	**154,174.21**	**334,012.05**	**1924744.43**

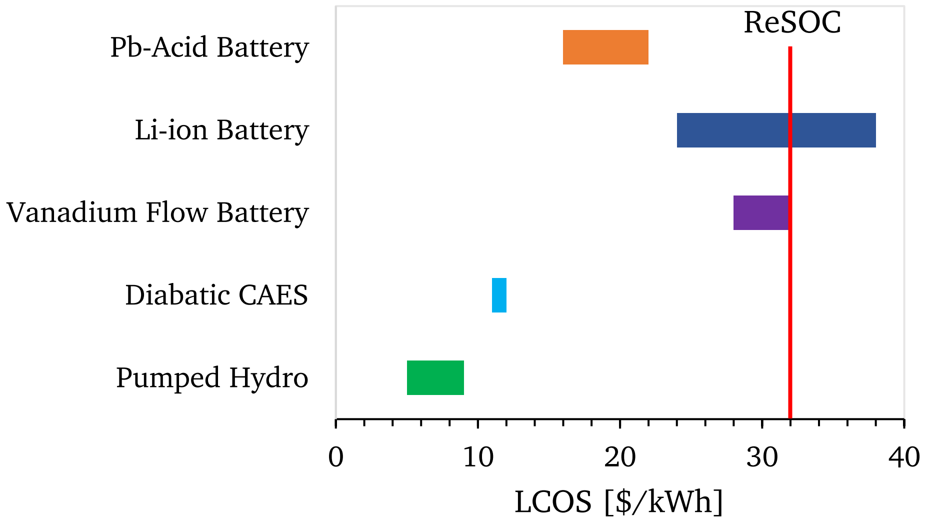

Figure 5.5 Comparison of ReSOC system LCOS with other storage technologies as presented in the literature (Jülch 2016, [15])

The results show that the system considered in this study is competitive with Vanadium redox flow battery and li-ion battery storage technologies. An advantage of this system over the presented results above is the initial system capital costs. The reference study presented systems of 100MW/400MWh rating which is approximately 1000 times larger than the system considered in this study. Also, costs associated with the system are not expected to scale linearly with the system rating/capacity. Hence, a system with a higher capacity will have a lower LCOS than calculated here.

6

EXERGOECONOMIC ANALYSIS OF RESOC SYSTEM

In this chapter, the exergoeconomic analysis of the ReSOC system presented in Chapter 4 is carried out using the base case operating parameters. The exergoeconomic method of system analysis is a method investigating the economic performance of a system using the exergy properties of this system. The implication of this is that the exergoeconomic analysis combines the exergy and economic analysis for system performance investigation and improvement. Consequently, we can say that, in an energy conversion system, an exergoeconomic analysis accounts for the monetary cost of energy conversion alongside the efficiency and limits of the energy conversion efficiency. This enables researchers to calculate the cost-exergy effectiveness of the system thereby making overall system performance improvement more effective both economically and thermodynamically. In the exergoeconomic analysis, costs such as exergy destruction costs, exergy loss costs, purchased equipment cost, the rate of these costs, exergoeconomic factor, and ratio of exergy loss rate to equipment capital cost rate are investigated. This approach is used to evaluate the cost of individual streams in the system based on their exergy rate. The stream cost rate then gives a comprehensive view of the cost rate of fuel, cost rate of the product, and the cost rate of exergy destruction in every component, giving a good outline for selecting and optimizing the design parameters on a component basis leading to an overall economic and efficiency improvement of a system. In the exergoeconomic analysis in this study, first, the system components are sized using relations found in the literature. The system size is used to determine the capital cost and operating cost of individual components. Next, the exergoeconomic relations and exergy cost balance for the individual components are determined. These relations are used to determine the exergy cost rate of individual streams in each component and the exergy cost rate of the product.

6.1 Thermoeconomic modeling approach

The thermoeconomic method of system analysis uses the exergoeconomic (exergy and economic) analysis for a cost-effective system design. Like the traditional exergy analysis, the concept of fuel and product is used in addition to the economic capital and maintenance cost of system components. The primary aim of the exergoeconomic analysis may be seen to determine the exergetic cost rate of the fuel and product streams and the capital cost rate of system components. In this thesis, the Specific Exergy Costing (SPECO) method of thermal system analysis as introduced by Lazzaretto and Tsatsaronis was used. More details on the SPECO methodology can be found in [19]. SPECO is based on three main steps.

STEP 1: Identification of the exergy streams in the system.

STEP 2: Definition of fuel (F) and product (P) in every component.

STEP 3: Determining cost equations for individual components.

STEP 1 and STEP 2 have been carried out as part of the exergy analysis of the ReSOC system. This chapter will focus more on step 3 of the SPECO analysis. For entering and exiting streams of matter or energy in any component, the exergy cost equation can be written as Equation 6.1.

$$\sum_{inlet} \left(\dot{C}_{inlet}\right)_k + \dot{Z}_k = \sum_{exit} \left(\dot{C}_{exit}\right)_k \tag{6.1}$$

Where, $\dot{C}_{inlet}$ & $\dot{C}_{exit}$ is the exergy cost rate for all inlet and exit streams of component k, respectively. These streams can be in form of fluids entering and leaving the component or heat and work generated or supplied to the component. For fluids, heat, and work, the exergy cost rate is defined as shown in Equations 6.2 to 6.4. $\dot{Z}$ is the cost associated with the capital and operation and maintenance cost of the component k. The units of $\dot{C}$ and $\dot{Z}$ is in \$/h or currency per unit time.

$$\dot{C}_{fluid} = c_{fluid} \cdot \dot{E}x_{fluid} = c_{fluid} \cdot \dot{m}_{fluid} \cdot ex_{fluid} \tag{6.2}$$

$$\dot{C}_{work} = c_{work} \cdot \dot{W} \tag{6.3}$$

$$\dot{C}_{heat} = c_{heat} \cdot \dot{Ex} = c_{heat} \cdot \dot{Q}\left(1 - \frac{T_o}{T_b}\right) \tag{6.4}$$

Here, c_i denotes the average cost per unit exergy in \$/GJ and all other parameters are the same as defined in earlier sections of this thesis. T_b is the boundary temperature at which the heat transfer occurs or surrounding temperature in the case of heat loss.

In determining the cost per unit exergy for any stream, the formulation of the auxiliary equation is essential because the number of streams per component is more than two. Determining the auxiliary equation is rooted in the P and F principles of exergy costing [83]. The P principle states that the cost per unit exergy for each exiting stream associated with the product is the same. The F principle states that the cost per unit exergy associated with the removal of exergy from a fuel stream should be treated to be the same as the average cost per exergy at which the removed exergy was supplied to the fuel stream in existing components. Combining the P and F principles produces the required auxiliary equations associated with the exergy cost balance.

The capital and operation and maintenance cost rate (total cost rate) of the kth component, $\dot{Z}_k$ is calculated considering factors such as discounted rate, capital recovery factor, maintenance factor, economic lifetime, etc. Equation 6.5 gives the total cost rate for the components used in this study as defined by Cao and Parikhani [80].

$$\dot{Z}_k = \varphi \cdot Z_k \cdot \left(\frac{CRF}{\mathrm{T}}\right) \tag{6.5}$$

φ is the operation and maintenance factor taken to be 1.06 for this study according to [84], Z_k is the present value of the component capital cost (\$) as calculated in Chapter 5, CRF is the capital recovery factor and T is the operation time of the system in a year in hours. The ReSOC system is designed to operate in the SOFC and SOEC modes for an equal amount of time, and the operating time is taken to be 2500 hours for each mode resulting in a total of 5000 operation hours per year for the system as already detailed in the system costing section (Chapter 5).

The capital recovery factor (CRF) is defined as in equation 6.6.

$$CRF = \frac{r(r+1)^n}{(r+1)^n - 1} \tag{6.6}$$

Where r is the discounted rate taken as the interest rate of 15% and n is the system economic lifetime in years taken to be 20.

6.2 Exergoeconomic Performance Indices

In this section, the SPECO method of system analysis is applied to the system in this study, and the system performance index is presented. The same system configuration will work for both the SOFC and SOEC mode, thereby, the cost equations for the components is applicable for both the SOFC and SOEC modes of operation. However, since the fuel and products in the ReSOC stack are different for both modes of operation, the difference will be paid attention to during analysis. The summary of the exergy cost balance and respective auxiliary equation for the components in the system is presented in Table 6.1. The ReSOC system aims to store electrical energy during off-peak periods and regenerate the energy during peak periods. Therefore, the primary indicator of the system exergoeconomic performance is the exergetic cost rate of the product output in the cost rate. This is defined by stream 19 in the SOFC mode. In the SOEC mode, on the other hand, the exergoeconomic performance is indicated in the exergy cost rate of the converted fuel stored in the fuel tank. This is represented by stream 11 in the result analysis and discussion. Various parameters have been presented in the literature to characterize the system's exergoeconomic performance [13], [85]–[87]. In this study, alongside streams 11 and 19 of the SOEC and SOFC mode, respectively, the exergoeconomic performance is also characterized by the exergy destruction cost and the exergoeconomic factor.

Table 6.1 Exergy cost rate balance equation and auxiliary equations for system components

Component		**Cost Balance**	**Auxiliary Equation**
ReSOC Stack	SOFC Mode	$\dot{C}_4 + \dot{C}_{16} + \dot{Z}_{ReSOC} = \dot{C}_5 + \dot{C}_{17} + \left(c_{sta,DC} \cdot \dot{W}_{sta,DC}\right)$	$\frac{\dot{C}_4^{CH} + \dot{C}_{16}^{CH}}{\dot{E}_4^{CH} + \dot{E}_{16}^{CH}} = c_5^{CH} = c_{17}^{CH};$ $c_{sta,DC} = \frac{\dot{C}_{17}^{PH} - \dot{C}_{16}^{PH}}{\dot{E}_{17}^{PH} - \dot{E}_{16}^{PH}} = \frac{\dot{C}_5^{PH} - \dot{C}_4^{PH}}{\dot{E}_5^{PH} - \dot{E}_4^{PH}};$ $c_{16}^{CH} = 0;$ $c_4^{CH} = c_4^{PH}$
	SOEC Mode	$\dot{C}_4 + \dot{C}_{16} + \left(c_{sta,DC} \cdot \dot{W}_{sta,DC}\right) + \dot{Z}_{ReSOC} = \dot{C}_5 + \dot{C}_{17}$	$\frac{\dot{C}_{16}}{\dot{E}_{16}} = \frac{\dot{C}_{17}}{\dot{E}_{17}}$
Inverter	SOFC Mode	$c_{sta,DC} \cdot \dot{W}_{sta,DC} + \dot{Z}_{INV1} = c_{sta,AC} \cdot \dot{W}_{sta,AC}$	-
	SOEC Mode	$c_e \cdot \dot{W}_{sta,AC} + \dot{Z}_{INV1} = c_{sta,DC} \cdot \dot{W}_{sta,DC}$	-
HEX-1		$\dot{E}_5 - \dot{E}_6 + \dot{Z}_{HEX1} = \dot{C}_4 - \dot{C}_3$	$c_5 = c_6$
HEX-2		$\dot{C}_{10} - \dot{C}_{11} + \dot{Z}_{HEX2} = \dot{C}_2 - \dot{C}_1$	$c_{10} = c_{11};$
HEX-3		$\dot{C}_{17} - \dot{C}_{18} + \dot{Z}_{HEX3} = \dot{C}_{16} - \dot{C}_{15}$	$c_{17} = c_{18}$
COM-1		$c_e \cdot \dot{W}_{COM1} + \dot{Z}_{COM1} = \dot{C}_8 - \dot{C}_7$	-
COM-2		$c_e \cdot \dot{W}_{COM2} + \dot{Z}_{COM2} = \dot{C}_{10} - \dot{C}_9$	-
COM-3		$c_e \cdot \dot{W}_{COM3} + \dot{Z}_{COM3} = \dot{C}_{13} - \dot{C}_{12}$	$c_{12} = 0$
HRC-1		$\dot{C}_6 - \dot{C}_7 + \dot{Z}_{HRC1} = \dot{C}_{14} - \dot{C}_{13}$	$c_6 = c_7$
HRC-2		$\dot{C}_8 - \dot{C}_9 + \dot{Z}_{HRC2} = \dot{C}_{15} - \dot{C}_{14}$	$c_8 = c_9$
PRV-1		$\dot{C}_2 + \dot{Z}_{PRV1} = \dot{C}_3$	-
Fuel Tank (SOFC)		$\dot{C}_{fuel} + \dot{Z}_{TNK1} = \dot{C}_1$	-
Exhaust Tank (SOFC)		$\dot{C}_{1'} + \dot{Z}_{TNK2} = \dot{C}_{11}$	-

Explanation for the alternative equations

1. Air is free; $c_{12} = 0$
2. No auxiliary equation means only two streams are present hence, only one unknown.
3. The specific exergy cost of the chemical exergy of air is zero; $c_{16}^{CH} = 0$
4. Heat exchangers and recuperators employ the F principle.
5. SOFC employs both the F and P principles.
6. SOEC employs the F principle.
7. c_e is the Levelized Cost of electricity; retail cost of green energy in Turkey 0.747372 TL/kWh (24.44 $/GJ) [88].
8. $\dot{C}_{fuel} = c_{fuel} \cdot \dot{E}_1$; where c_{fuel} is assumed to be readily available in the system, hence it is free; $c_{fuel} = 0$.
9. The specific exergy cost of the exhaust gas in the SOEC mode, $c_{1'}$, is the specific exergy cost of c_{11} in the SOFC mode.

6.2.1 Exergy Destruction Cost

The cost of exergy destruction is defined according to reference [67]. It is defined as the product of the exergy cost rate of the fuel and the exergy destruction rate. Here, the exergy destruction cost is defined on a component basis. Thus, the fuel will be the fuel component of exergy in the component. The exergy destruction rate for the system components is modeled according to Equation 6.7.

$$\dot{C}_{D,k} = c_{fuel,k} \cdot \dot{Ex}_{D,k} \tag{6.7}$$

Where, $\dot{C}_{D,k}$ is the cost rate of exergy destruction of component k measured in $/h, $c_{fuel,k}$ is the specific exergy cost (SPECO) of the fuel component of the exergy stream in the component measured in $/GJ and $\dot{Ex}_{D,k}$ is the exergy destruction rate in the component measured in kW.

6.2.2 Exergoeconomic factor

The exergoeconomic factor is used to determine the contribution of the capital cost and exergy destruction cost to the system or component's expenses. It gives an understanding of the cost of operating the components of a system or the system depending on the scale at which it is applied. The exergoeconomic factor also helps the designer to know how much the exergy destruction costs relative to the capital cost at the component level. This will aid decision-making in economic analysis. The higher the exergoeconomic factor the better the system thermoeconomic performance since this indicates a lower exergy loss rate or lower exergy destruction rate. The exergoeconomic factor is not only limited to system analysis but can also be defined on a per-component basis. The exergoeconomic factor for any component in the system as defined in Xi et al. [86] is given in equation 6.8.

$$\zeta_k = \frac{\dot{Z}_k}{\dot{Z}_k + \dot{C}_{D,k}} \tag{6.8}$$

Where ζ_k is the exergoeconomic factor for component k. The overall cost rate of the plant is defined as the sum of all expenditures associated with the system. This cost can be used as a basis for sizing and comparing systems employing the same technology or different systems entirely. It gives a time-based cost of plant defined in \$/h. Equation 6.9 gives a mathematical definition of the overall cost rate of the system.

$$\dot{C}_{sys} = \sum_{k=1}^{n} \left(\dot{Z}_k + \dot{C}_{D,k}\right) + \dot{C}_{L,sys} \tag{6.9}$$

$\dot{C}_{sys}$ is the overall system cost rate, $\dot{Z}_k$ and $\dot{C}_{D,k}$ is the capital and exergy destruction cost rate of component k in the system and n is the total number of components in the system. $\dot{C}_{L,sys}$ is the cost rate of the exergy loss stream. In this system, stream 17 is considered as system exergy loss in both modes of operation. The overall cost rate considers not only the investment and maintenance costs but also the cost of exergy destruction and exergy loss. Therefore, it is practically impossible for the overall cost rate to be less than the total capital cost rate of the system. The exergoeconomic thereby expresses the total capital cost rate as a proportion of the overall cost rate of the system as shown in equation 6.10. In this study, however, we are only considering the exergoeconomic factor only for the system.

$$\zeta_{sys} = \frac{\sum_{k=1}^{n} \dot{Z}_k}{\dot{C}_{sys}} \tag{6.10}$$

ζ_{sys} is the system exergoeconomic factor and it is a dimensionless quantity.

6.3 Analysis Results and discussion

The result for the base case performance of the system exergoeconomic analysis is presented. The base case operating condition is the same as employed in the system exergy analysis. The cost balance equations and capital cost derivation for system balance of plant components presented in the earlier sections of this thesis are used to determine the cost of the gas streams in each mode of operation. The gas flow rates, specific exergies, specific exergy costs, and stream cost rates are shown in Table 6.2 and Table 6.3 for the SOFC and SOEC modes of operation, respectively.

Table 6.2 Base case system exergoeconomic performance in SOFC mode.

Stream	$\dot{m}_i[g/s]$	$\dot{n}_i[mol/s]$	$ex_i^{PH}[J/g]$	$ex_i^{CH}[J/mol]$	$c_i[\$/GJ]$	$\dot{C}_i[\$/h]$
1	5.611	0.7687	1234	334350	2.62	2.49
2	5.611	0.7687	1964	334350	2.75	2.65
3	5.611	0.7687	1020	334350	2.91	2.75
4	5.611	0.7687	1376	334350	2.95	2.81
5	16.68	1.057	708.4	109584	3.09	1.42
6	16.68	1.057	578.9	109584	3.09	1.40
7	16.68	1.057	80.04	109584	3.09	1.31
8	16.68	1.057	582.2	109584	5.10	2.31
9	16.68	0.057	367.8	109584	5.10	2.24
10	16.68	1.057	1009	109584	7.63	3.65
11	16.68	1.057	765.3	109584	7.63	3.53
12	106.7	3.699	0.00	128.4	0.00	0.00
13	106.7	3.699	20.03	128.4	33.17	0.31
14	106.7	3.699	51.94	128.4	19.29	0.42
15	106.7	3.699	76.29	128.4	16.02	0.50
16	106.7	3.699	223.1	128.4	24.48	2.14
17	95.65	3.353	340.3	186.9	19.96	2.38
18	95.65	3.353	146.1	186.9	19.96	1.05
19	-	-	-	-	10.85	4.56

Table 6.3 Base case system exergoeconomic performance in SOEC mode.

Stream	$\dot{m}_i[g/s]$	$\dot{n}_i[mol/s]$	$ex_i^{PH}[J/g]$	$ex_i^{CH}[J/mol]$	$c_i[\$/GJ]$	$\dot{C}_i[\$/h]$
1	16.68	1.057	616.4	109584	13.64	6.19
2	16.68	1.057	1016	109584	14.57	6.97
3	16.68	1.057	578.9	109584	15.63	7.06
4	16.68	1.057	591.2	109584	15.74	7.13
5	5.611	0.7687	1286	334359	25.86	24.60
6	5.611	0.7687	1233	334359	25.86	24.57
7	5.611	0.7687	152	334359	25.86	24.01
8	5.611	0.7687	1215	334359	26.04	24.74
9	5.611	0.7687	1010	334359	26.04	24.63
10	5.611	0.7687	3048	334359	26.48	26.13
11	5.611	0.7687	1661	334359	26.48	25.39
12	44.4	1.539	0.00	128.4	0.00	0
13	44.4	1.539	20.03	128.4	36.36	0.14
14	44.4	1.539	98.84	128.4	44.08	0.73
15	44.4	1.539	120.1	128.4	42.75	0.85
16	44.4	1.539	434.8	128.4	34.92	2.45
17	55.47	1.885	522.8	261.3	25.86	2.75
18	55.47	1.885	260.1	261.3	25.86	1.39
19	-	-	-	-	24.44	14.16

While the specific exergy cost gives the cost per unit exergy, the exergy cost rate gives the cost per unit time. Therefore, streams with low exergy will have a lower exergy cost rate compared to high exergy streams. In understanding the exergoeconomic performance of the system (or the streams), both the specific exergy cost and exergy cost rate are of equal importance. In the system considered in this study, the air side of the system has the highest specific exergy cost in both modes of operation but also the least exergy cost rate. The reactant gas side however has relatively lower specific exergy costs but higher exergy cost rates. To improve and understand the exergoeconomic performance of a system, however, focused will be placed on the specific exergy cost because it relates the actual performance of the system to the costs associated with it. The cost of the SOFC mode's system inlet stream (stream 1) is the cost of the fuel gas and the fuel storage tank cost. Likewise, in the SOEC mode, stream 1 includes both the cost of the exhaust stream (stream 11) of the SOFC mode of operation and the exhaust tank. The system product of the SOFC mode of operation is the AC electricity produced in stream 19 and the SOEC mode, it is the produced fuel gas in stream 11. The specific exergy cost of the electricity (stream 19) and system inlet and exit streams (stream 1 & 11) is highly influenced by the capital cost of the inverter and storage tanks. The higher specific exergy cost of the reactant gas stream in the SOEC mode (streams 1 to 11) is because of the high-cost system inlet stream that was used.

Table 6.4 shows the capital cost rate and exergy destruction cost rates of the ReSOC in both modes of operation. Contrary to the exergy performance results, the SOFC mode of operation has a better exergoeconomic performance than the SOEC mode of operation. The SOFC mode of operation has a higher system capital cost rate but a lower exergy destruction and exergy loss cost rate for the system than the SOEC mode. The exergoeconomic factor used as the performance metric for this study also shows that the SOFC performs better than the SOEC mode of operation with an absolute difference of 0.09. This better performance shown in the SOFC mode of operation is associated with the cost of the fuel gases consumed by the system in the SOFC mode of operation which was taken as zero. The system inlet gas in the SOEC mode of operation on the other hand had a cost associated with it. Therefore, to improve the exergoeconomic performance of the system, attention needs to be paid to the specific costs of the exergy destruction in the system components and the extent of exergy loss in the system. The exergoeconomic performance of the system components as shown in Figure 6.1 and Figure 6.2 buttress that the lesser performance recorded in the SOEC mode of operation is because of the increased cost rate of exergy destruction in the system components. The components with the highest capital cost rates are the storage tank, inverter, and ReSOC stack. Reducing these capital costs especially for the tank will reduce the cost of the overall system. For both modes of operation, the inverter and COM-2 were among the components that had the highest exergy destruction cost rate. This shows the importance of not just improving inverter efficiency but also reducing inverter cost to reducing overall system cost. Also, using DC electric power in the system can eliminate the need for an inverter thereby reducing system cost. Another approach that can be employed to reduce overall system cost is reducing storage tank volume, storage tank pressure, or the number of tanks. The use of a variable volume (floating piston) tank or connecting the system to an existing gas pipeline for injection purposes has been suggested as a good way of reducing storage tank requirements [25], [41].

Table 6.4 Base case exergoeconomic performance of the ReSOC system

Operating Mode	$\zeta_{sys}[-]$	$\dot{\boldsymbol{Z}}_{sys}$ $[\$/\boldsymbol{h}]$	$\dot{\boldsymbol{C}}_{L,sys}[\$/\boldsymbol{h}]$	$\dot{\boldsymbol{C}}_{D,tot}[\$/\boldsymbol{h}]$	$\dot{\boldsymbol{C}}_{sys}$ $[\$/\boldsymbol{h}]$
SOFC	0.74	9.79	3.39	1.16	14.34
SOEC	0.65	9.71	2.75	2.48	14.94

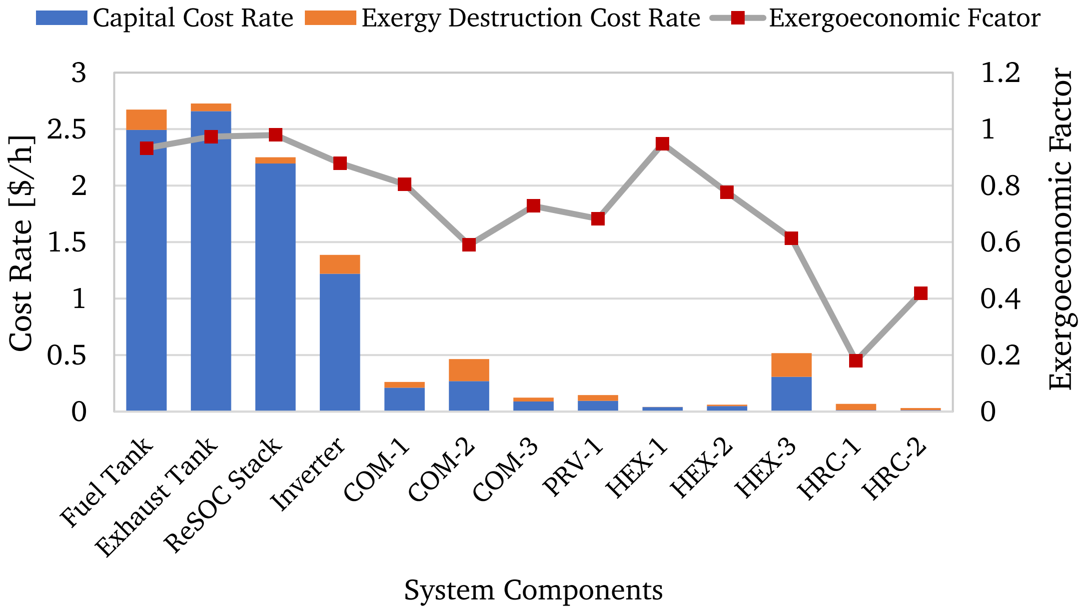

Figure 6.1 ReSOC system exergoeconomic performance in the power generation mode of operation (SOFC)

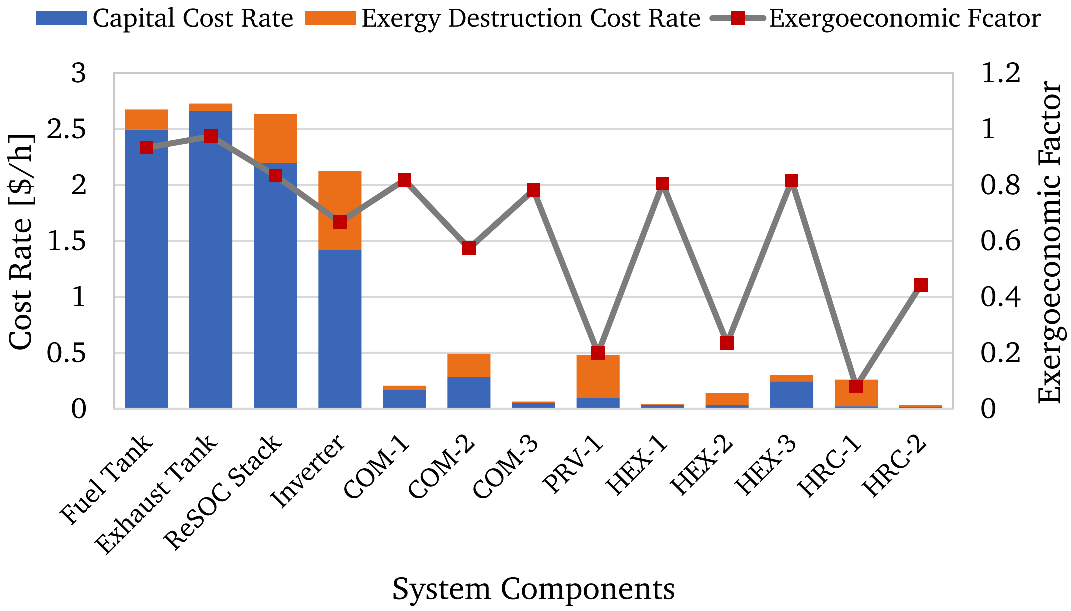

Figure 6.2 ReSOC system exergoeconomic performance in the power generation mode of operation (SOEC)

Components with a higher capital cost rate had a higher exergoeconomic factor than the components with lower capital costs. Comparing the exergoeconomic and exergy performance of the system components showed that the exergoeconomic analysis goes a step further in characterizing the performance and not just a duplicate of the exergy performance. A high exergy performance does not automatically correspond to a high exergoeconomic performance and the same is noticed for the exergy destruction rate and the cost of exergy destruction rate. The exergoeconomic analysis, therefore, takes the exergy performance analysis further and indicates how this performance is interpreted in the system cost and product cost.

6.3.1 Sensitivity analysis of system exergoeconomic performance

The system operating conditions also affect the system's exergoeconomic performance. In the SOFC mode, the product-specific exergy cost is the specific exergy cost of stream 19 and in the SOEC mode of operation, it is stream 11. Figure 6.3 and Figure 6.4 show the effect of the operating current density and the fuel utilization factor on the product-specific exergy cost, respectively. The specific exergy cost drops rapidly with increasing current density for both modes of operation. However, at current densities beyond ±0.5A/cm^2 in the respective operating mode, the change in the cost becomes almost unnoticeable. This implies that it is economically beneficial to operate the system only up to certain current densities. The specific exergy cost of the product screen in both modes of operation responded to the fuel utilization factor differently in comparison to the operating current density. For both modes of operation, the cost increased with increasing fuel utilization factor.

The cost increased almost linearly between the fuel utilization factor of 0.3 and 0.7, beyond the 0.7 utilization factor, the cost increased exponentially for both modes of operation. Therefore, the system performs better economically at moderately high operating current density and low fuel utilization factor. The exergoeconomic factor on the other hand reduced with increasing operating current density. The exergoeconomic factor performance concerning the stack fuel utilization factor is more interesting than the current density. In the SOFC mode, the system exergoeconomic performance peaked at a fuel utilization factor of approximately 0.36 with an exergoeconomic factor of 0.79 while for the SOEC mode, it peaked at about 0.7 fuel utilization factor with an exergoeconomic factor of 0.66. At the point of maximum exergoeconomic factor in the SOEC mode, the SOFC mode despite its decline in performance still had a factor of 0.72 which is higher than the SOEC mode. These conflicting trends imply that even at the economic analysis level, there is the need for a trade-off between cost and performance when selecting optimal and cost-effective system operating conditions. While the specific exergy cost of products might be low or increasing, it does not directly translate to a better exergoeconomic performance.

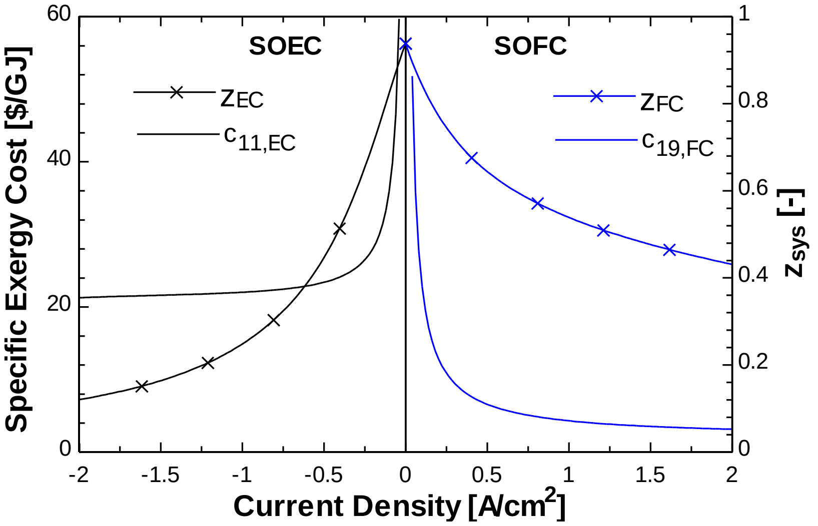

Figure 6.3 Operating Current Density vs system exergoeconomic performance.

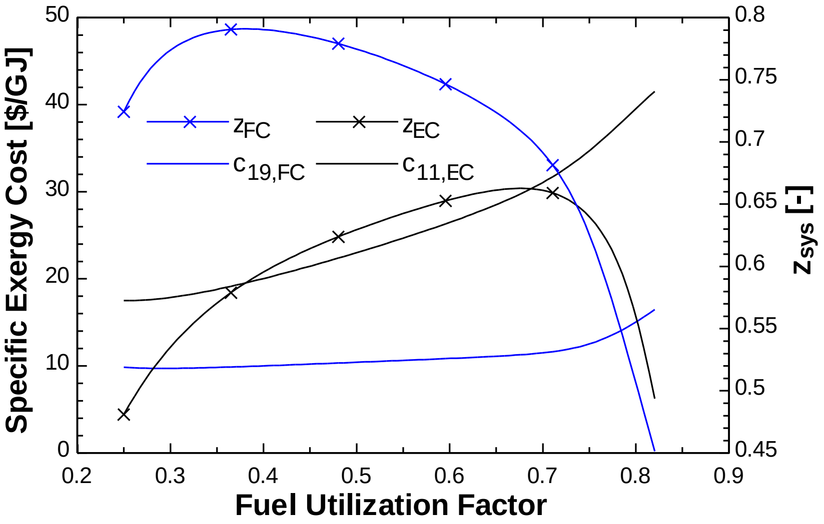

Figure 6.4 Fuel Utilization factor vs system exergoeconomic performance

In Figure 6.5, the effect of the exergy dead state parameters on the specific exergy cost of the system products in both modes of operation is investigated. An increase in the dead state temperature (Figure 6.5a) leads to a respective increase in both stream 11 and stream 19 specific exergy cost of the SOEC and SOFC modes, respectively. The dead state pressure however only influences the product exergy stream of the SOEC mode of operation. The exergoeconomic factor analysis shows that what may be beneficial in the SOEC mode is not necessarily beneficial for the SOFC mode. Also, the dead state conditions highly influence the exergy destruction cost rate in the system for both modes of operation even if it has a relatively low effect on the specific exergy cost especially in the SOFC mode of operation.

In the economic analysis of thermodynamic systems, the cost performance of the system is not only influenced by the system's thermodynamic performance. The economic condition under which the system operates is also of high importance. Figure 6.6 and Figure 6.7 show the effect of the economic parameters on the system's exergoeconomic performance. In Figure 6.6, the specific exergy cost of both product streams increased linearly with an increasing discounted rate. This is because of the increased capital recovery factor associated with the increased discounted rate. This will in turn cause an increase in the capital cost rate hence the cost of the overall system.

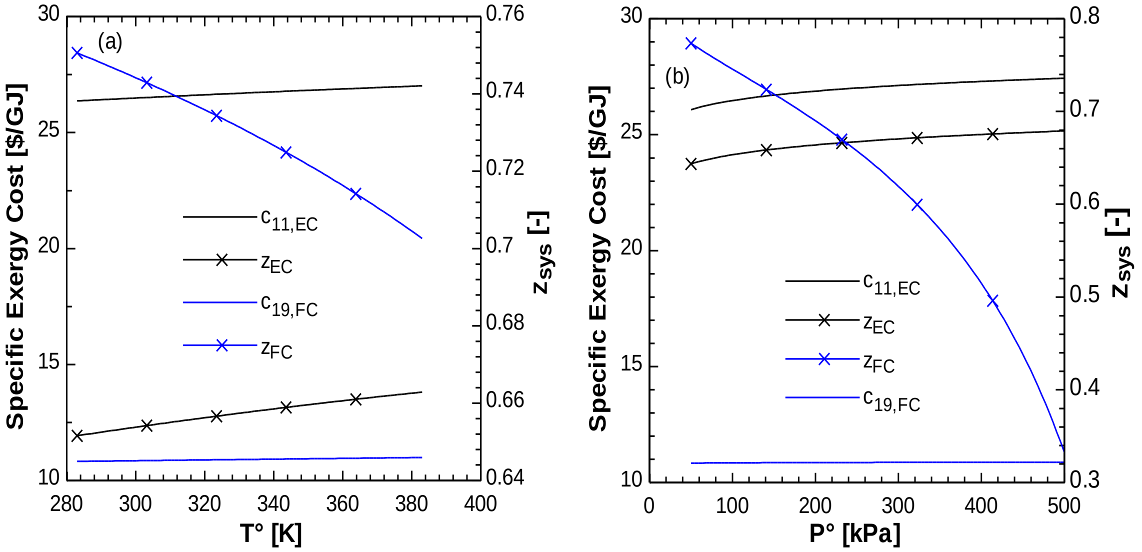

Figure 6.5 Dead State Parameters vs system exergoeconomic performance

The exergoeconomic factor’s response showed that the system performance improved with an increased discounting rate. This response is a function of the extremely large capital cost rate compared to the exergy destruction cost rate. Therefore, it is not a performance improvement, rather it is a lesser exergy destruction cost to system capital cost ratio. Apart from the annual discounted rate, another economic factor considered is the cost of “fuel” consumed by the system. In the SOFC mode, the “fuel” cost is the cost of natural gas and for the SOEC mode, it is the cost of electricity. In Figure 6.7, the sensitivity of the

Levelized Cost of electricity on system product cost is investigated for both operating modes. The specific exergy cost of the electricity produced in the SOFC mode of operation is insensitive to the Levelized cost of electricity because of the low power consumption of the air blower (COM-3). The SOEC mode product stream on the other hand is highly sensitive to the Levelized cost of electricity primarily because the "fuel" consumed in the SOEC mode is electricity and the additional electric power consumption by the compressors before storing the produced gas in the storage tanks. The Levelized Cost of electricity does not affect the capital cost rate but highly influences the exergy destruction and exergy loss cost rate. The system exergoeconomic factor reduces with the increasing cost of electricity. Thereby, we can conclude that a high cost of electricity is not good for either mode but affects the SOEC mode more than the SOFC mode. In summary, the sensitivity analysis has shown that both the thermodynamic and economic parameters influence the exergoeconomic performance of the system. While economic parameters such as discounted rate, and cost of electricity cannot be influenced by the system designer, including these parameters in system analysis helps to select system optimum performance condition, determine how these cost change system dynamics, and the feasibility of the system for commissioning.

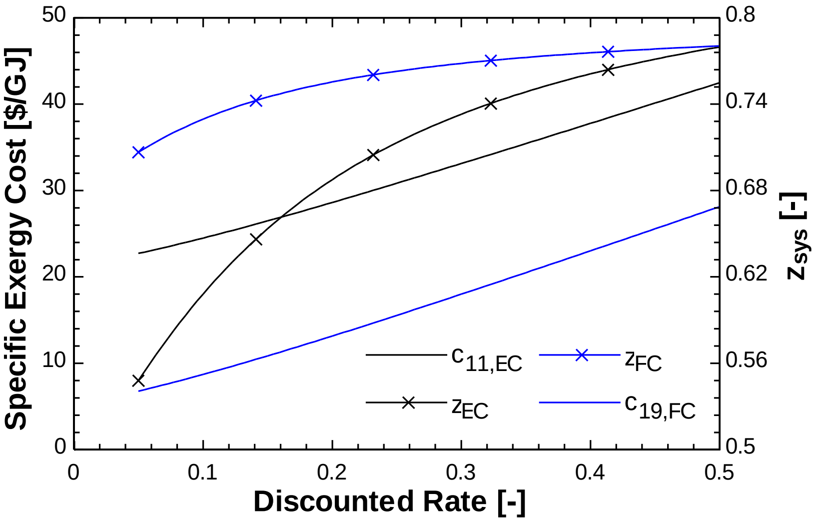

Figure 6.6 Discounted rate vs system exergoeconomic performance

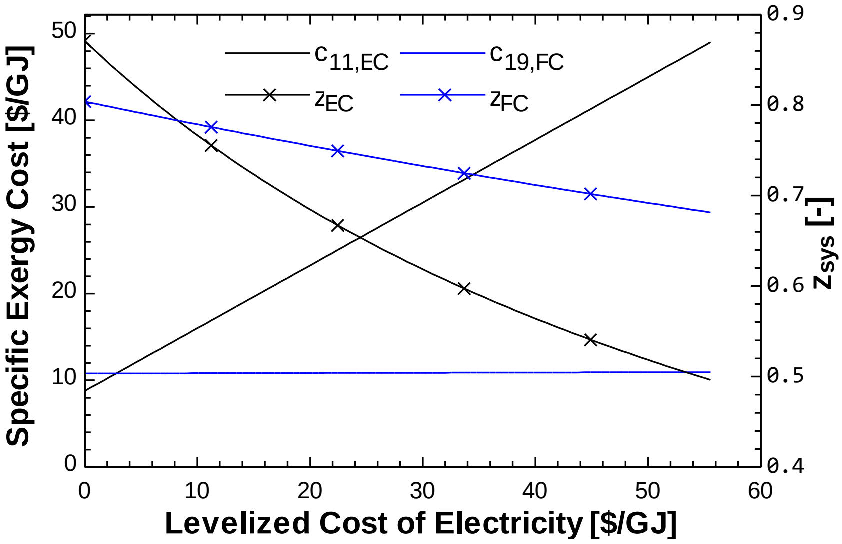

Figure 6.7 Cost of Electricity vs system exergoeconomic performance

7

CONCLUSION AND FUTURE WORKS

This thesis has presented a computational model for a reversible solid oxide cell system based on a reversible solid oxide cell stack with pressurized gas storage. A detailed model of the ReSOC stack operating in the fuel cell and electrolysis mode of operation was also presented. The model is based on a zero-dimensional model of system components to allow a first-look understanding of the system operation and how the operating condition of the system affects the system performance. The electrochemical, energy, exergy, economic, and exergoeconomic approaches have been employed for the analysis of the system presented in this study.

In the electrochemical cell and stack modeling and performance analysis, cell performance is the basis of stack performance. Asides from the cell materials and characteristics, fuel composition, and operating temperature, and pressure, the fuel utilization factor and operating current density are also factors affecting the cell performance. For the stack, however, the electrochemical performance is greatly dependent on the method of stack operation. This operation method is defined either by a constant inlet mass flow rate or constant fuel utilization. The energy analysis result shows the system suffers further performance losses compared to the stack primarily because of the parasitic power consumption by the balance of plant components. The roundtrip efficiency of the stack was 0.8 and 0.51 for the ReSOC system. Operating the system at high operating current density is not beneficial to system efficiency for both modes of operation and roundtrip efficiency. However, for higher energy output, the system must be operated at a high current density since the stack size limits the system output. While the current density reduces the system efficiency as it increases, the fuel utilization factor improves the system performance to a maximum of about 70% before the system performance begins to deteriorate. The thermal analysis result shows increasing air flow rate is enough as a thermal management approach for cooling ReSOC stacks. The result of the exergy analysis shows that the major points of exergy destruction in the system are the ReSOC stack, inverter, pressure reducing valve, and storage tanks. Other points of exergy destruction are the heat exchangers and recuperators, but they are not as consistent as the aforementioned. The SOEC mode has a higher exergy performance than the SOFC mode, more importantly, the overall rate of useful product per unit exergy destruction otherwise known as the EPC for the SOEC mode of operation is almost double that of the SOFC mode. This agrees with the exergetic efficiency and reflects that despite having almost equal exergy destruction rates, the useful exergy product in the SOEC mode is more than the SOFC mode of operation.

System economics and costing showed that the considered system is competitive with flow batteries and Li-ion batteries but still has a long way to go to be competitive with large-scale storage systems such as CAES and pumped hydro. Also, system capital cost is largely driven by the storage tank cost, taking more than half of the total system cost, reducing storage cost, or using alternative storage methods to reduce the system capital cost might put the ReSOC system in a competitive position with other storage technologies. In the exergoeconomic analysis results, system performance showed that the high capital cost of the tank, stack and inverter is a major driver in the economic feasibility of the system. Furthermore, the specific exergy cost of the products for both modes of operation is affected by the stack operating parameters. The exergoeconomic factor analysis also showed a similar capital cost rate in both modes of operation which means that the SOFC mode of operation had a higher exergoeconomic factor because of the lesser exergy destruction cost rate. The exergoeconomic analysis also showed that the SPECO method of analysis helps find points of high costs in the system which can be used to reduce overall system cost. The result shows that it is economically favorable to operate the stack at moderate current density and low fuel utilization factor. For the system to be economically feasible, economic players such as discounted rate and cost of electricity are of high importance.

Finally, because the system performance relies much on the stack performance, improving call and stack performance by reducing the overpotentials is a good approach for improving overall system performance. Also, eliminating or reducing the cost of storage in ReSOC systems will improve the economic performance of the ReSOC systems. Therefore, integration with existing gas handling systems or utilization as a hybrid system or an intermediary gas producer or electricity producer will reduce the Levelized system cost.

The study presented in this thesis has successfully given an overview of the basics of the design and operation of a ReSOC under steady-state conditions. Based on the system and methodology presented in this study, the possibility of adding a bottoming cycle to the exit air stream to maximize the exergy of that stream should be explored. The performance of the system under transient and dynamic operation should be studied because, under practical conditions, a steady-state operation might not be always feasible. Also, studies should be carried out focusing primarily on strategies for reducing storage costs and stack costs.

Further studies on ReSOC systems should focus on designing optimum reactant gas for performance improvement under specific applications and operating conditions. Also, due to the large number of parameters operating parameters in the ReSOC stack and system, optimization studies need to be carried out. A general algorithm for optimizing the thermodynamic and economic performance of ReSOC systems should be developed.

REFERENCES

[1] M. B. Mogensen *et al.*, “Reversible solid-oxide cells for clean and sustainable energy,” *Clean Energy*, vol. 3, no. 3, pp. 175–201, 2019, doi: 10.1093/ce/zkz023.

[2] P. Song *et al.*, “The Study on the Role of Reversible Solid Oxide Cell (rSOC) in Sector-coupling of Energy Systems,” *2018 International Conference on Power System Technology, POWERCON 2018 - Proceedings*, no. 201806140000004, pp. 2210–2215, 2019, doi: 10.1109/POWERCON.2018.8602346.

[3] P. Kazempoor and R. J. Braun, “Model validation and performance analysis of regenerative solid oxide cells for energy storage applications: Reversible operation,” *International Journal of Hydrogen Energy*, vol. 39, no. 11, pp. 5955–5971, 2014, doi: 10.1016/j.ijhydene.2014.01.186.

[4] B. Königshofer *et al.*, “Performance assessment and evaluation of SOC stacks designed for application in a reversible operated 150 kW rSOC power plant,” *Applied Energy*, vol. 283, no. November 2020, 2021, doi: 10.1016/j.apenergy.2020.116372.

[5] M. Navasa, X. Y. Miao, and H. L. Frandsen, “A fully-homogenized multiphysics model for a reversible solid oxide cell stack,” *International Journal of Hydrogen Energy*, vol. 44, no. 41, pp. 23330–23347, 2019, doi: 10.1016/j.ijhydene.2019.06.077.

[6] Y. Wang, A. Banerjee, L. Wehrle, Y. Shi, N. Brandon, and O. Deutschmann, “Performance analysis of a reversible solid oxide cell system based on multi-scale hierarchical solid oxide cell modelling,” *Energy Conversion and Management*, vol. 196, no. May, pp. 484–496, 2019, doi: 10.1016/j.enconman.2019.05.099.

[7] C. H. Wendel, “Design and Analysis of Reversible Solid Oxide Cell Systems for Electrical Energy Storage,” Colorado School of Mines, Golden, Colorado, 2015.

[8] V. T. Giap, Y. D. Lee, Y. S. Kim, and K. Y. Ahn, “A novel electrical energy storage system based on a reversible solid oxide fuel cell coupled with metal hydrides and waste steam,” *Applied Energy*, vol. 262, no. September 2019, p. 114522, 2020, doi: 10.1016/j.apenergy.2020.114522.

[9] V. T. Giap, S. Kang, and K. Y. Ahn, “HIGH-EFFICIENT reversible solid oxide fuel cell coupled with waste steam for distributed electrical energy storage system,” *Renewable Energy*, vol. 144, pp. 129–138, 2019, doi: 10.1016/j.renene.2018.10.112.

[10] N. C. Ullvius and M. Rokni, “A study on a polygeneration plant based on solar power and solid oxide cells,” *International Journal of Hydrogen Energy*, vol. 44, no. 35, pp. 19206–19223, 2019, doi: 10.1016/j.ijhydene.2018.04.085.

[11] B. Chen, Y. S. Hajimolana, V. Venkataraman, M. Ni, and P. V. Aravind, “Integration of reversible solid oxide cells with methane synthesis (ReSOC-MS) in grid stabilization: A dynamic investigation,” *Applied Energy*, vol. 250, no. April, pp. 558–567, 2019, doi: https://doi.org/10.1016/j.apenergy.2019.04.162.

[12] Y. D. Lee, K. Y. Ahn, T. Morosuk, and G. Tsatsaronis, “Exergetic and exergoeconomic evaluation of a solid-oxide fuel-cell-based combined heat and power generation system,” *Energy Conversion and Management*, vol. 85, pp. 154–164, 2014, doi: 10.1016/j.enconman.2014.05.066.

[13] A. A. AlZahrani and I. Dincer, “Exergoeconomic analysis of hydrogen production using a standalone high-temperature electrolyzer,” *International Journal of Hydrogen Energy*, vol. 46, no. 27, pp. 13899–13907, 2021, doi: 10.1016/j.ijhydene.2020.04.055.

[14] F. Calise, M. Dentice d’ Accadia, L. Vanoli, and M. R. von Spakovsky, “Single-level optimization of a hybrid SOFC-GT power plant,” *Journal of Power Sources*, vol. 159, no. 2, pp. 1169–1185, 2006, doi: 10.1016/j.jpowsour.2005.11.108.

[15] V. Jülch, “Comparison of electricity storage options using levelized cost of storage (LCOS) method,” *Applied Energy*, vol. 183, pp. 1594–1606, 2016, doi: 10.1016/j.apenergy.2016.08.165.

[16] V. Jülch *et al.*, “A holistic comparative analysis of different storage systems using levelized cost of storage and life cycle indicators,” *Energy Procedia*, vol. 73, pp. 18–28, 2015, doi: 10.1016/j.egypro.2015.07.553.

[17] A. Baldinelli, L. Barelli, G. Bidini, and G. Discepoli, “Economics of innovative high capacity-to-power energy storage technologies pointing at 100% renewable micro-grids,” *Journal of Energy Storage*, vol. 28, no. December 2019, p. 101198, 2020, doi: 10.1016/j.est.2020.101198.

[18] Z. Yang, J. Zhang, M. C. W. Kintner-meyer, X. Lu, D. Choi, and J. P. Lemmon, “Electrochemical Energy Storage for Green Grid: Status and Challenges,” *ECS Meeting Abstracts*, pp. 3577–3613, 2011, doi: 10.1149/ma2011-02/4/155.

[19] A. Lazzaretto and G. Tsatsaronis, “SPECO: A systematic and general methodology for calculating efficiencies and costs in thermal systems,”

Energy, vol. 31, no. 8–9, pp. 1257–1289, 2006, doi: 10.1016/j.energy.2005.03.011.

[20] K. Motylinski, J. Kupecki, B. Numan, Y. S. Hajimolana, and V. Venkataraman, “Dynamic modelling of reversible solid oxide cells for grid stabilization applications,” *Energy Conversion and Management*, vol. 228, no. November 2020, p. 113674, 2021, doi: 10.1016/j.enconman.2020.113674.

[21] E. P. Reznicek and R. J. Braun, “Reversible solid oxide cell systems for integration with natural gas pipeline and carbon capture infrastructure for grid energy management,” *Applied Energy*, vol. 259, p. 114118, Feb. 2020, doi: 10.1016/j.apenergy.2019.114118.

[22] R. Braun and E. Reznicek, “Reversible Solid Oxide Cells for Energy Storage,” 2017, [Online]. Available: http://aes.mines.edu

[23] E. Reznicek, “Design and Simulation of Reversible Solid Oxide Cell Systems for Distributed Scale Energy Storage,” 2016.

[24] E. Reznicek and R. J. Braun, “Techno-economic and off-design analysis of stand-alone, distributed-scale reversible solid oxide cell energy storage systems,” *Energy Conversion and Management*, vol. 175, pp. 263–277, 2018, doi: 10.1016/j.enconman.2018.08.087.

[25] E. Reznicek and R. J. Braun, “Renewable Energy-Driven Reversible Solid Oxide Cell Systems for Grid-Energy Storage and Power-to-Gas Applications,” *ECS Transactions*, vol. 78, no. 1, pp. 2913–2923, May 2017, doi: 10.1149/07801.2913ecst.

[26] United Nations, *PARIS AGREEMENT*. Paris, 2015.

[27] IEA, “Historical CO2 emissions and projected emissions from operating energy infrastructure as it was used historically, 1900-2100,” 2020.

[28] Hannah Ritchie and M. Roser, “Emissions by sector (Sector by sector: where do global greenhouse gas emissions come from?),” 2021. https://ourworldindata.org/emissions-by-sector (accessed Apr. 20, 2021).

[29] E. Shafirovich and A. Varma, “Metal-CO2 propulsion for Mars missions: Current status and opportunities,” *Journal of Propulsion and Power*, vol. 24, no. 3, pp. 385–394, 2008, doi: 10.2514/1.32635.

[30] E. Dlugokencky, P. Tans, and NOAA/GML, “Global Monthly Mean CO2,” *NOAA/GML*, 2021. https://www.esrl.noaa.gov/gmd/ccgg/trends/global.html (accessed Apr. 11, 2021).

[31] D. Yergin, *The New Map: Energy, Climate and the Clash of Nations*, vol. 241, no. 11. New York: Penguin Press, 2020.

[32] IEA, "World Energy Outlook 2019," 2019.

[33] IRENA, "Synergies Between Renewable Energy and Energy Efficiency, A Working Paper Based on Remap 2030," *International Renewable Energy Agency (IRENA)*, vol. 1, no. 1, pp. 1–52, 2015.

[34] T. M. Letcher, *Storing Energy: With Special Reference to Renewable Energy Sources*. 2016. doi: 10.1515/ci-2016-0627.

[35] S. Kalaiselvam and R. Parameshwaran, "Chapter 2 - Energy Storage," in *Thermal Energy Storage Technologies for Sustainability*, S. Kalaiselvam and R. Parameshwaran, Eds. Boston: Academic Press, 2014, pp. 21–56. doi: https://doi.org/10.1016/B978-0-12-417291-3.00002-5.

[36] T. F. Fuller and J. N. Harb, *Electrochemical engineering*. John Wiley & Sons Ltd, 2018.

[37] M. Ni and T. S. Zhao, *Solid Oxide Fuel Cells: From materials to system modeling*. 2013.

[38] R. M. Dell and D. A. J. Rand, "Energy storage - A key technology for global energy sustainability," *Journal of Power Sources*, vol. 100, no. 1–2, pp. 2–17, 2001, doi: 10.1016/S0378-7753(01)00894-1.

[39] J. Eyer and G. Corey, "Energy storage for the electricity grid: Benefits and market potential assessment guide," *Lightning in a Bottle: Electrical Energy Storage*, no. February, pp. 1–191, 2011.

[40] G. Butera, S. H. Jensen, and L. R. Clausen, "A novel system for large-scale storage of electricity as synthetic natural gas using reversible pressurized solid oxide cells," *Energy*, vol. 166, pp. 738–754, 2019, doi: 10.1016/j.energy.2018.10.079.

[41] E. P. Reznicek and R. J. Braun, "Reversible solid oxide cell systems for integration with natural gas pipeline and carbon capture infrastructure for grid energy management," *Applied Energy*, vol. 259. 2020. doi: 10.1016/j.apenergy.2019.114118.

[42] L. Barelli, G. Bidini, G. Cinti, and A. Ottaviano, "Study of SOFC-SOE transition on a RSOFC stack," *International Journal of Hydrogen Energy*, vol. 42, no. 41, pp. 26037–26047, 2017, doi: 10.1016/j.ijhydene.2017.08.159.

[43] A. V. Akkaya, "Electrochemical model for performance analysis of a tubular SOFC," *International Journal of Energy Research*, vol. 31, no. 1, pp. 79–98, Jan. 2007, doi: 10.1002/er.1238.

[44] C. C. Wu and T. L. Chen, “Design and dynamics simulations of small scale solid oxide fuel cell tri-generation system,” *Energy Conversion and Management: X*, vol. 1, Jan. 2019, doi: 10.1016/j.ecmx.2018.100001.

[45] C. Holzinger, T. Pelletier, T. Grejtak, and C. Robinson, “Global Energy Storage Market Forecast 2019,” *Lux Research*, p. Lux Research, 2019.

[46] C. H. Wendel and R. J. Braun, “Design and techno-economic analysis of high efficiency reversible solid oxide cell systems for distributed energy storage,” *Applied Energy*, vol. 172, pp. 118–131, 2016, doi: 10.1016/j.apenergy.2016.03.054.

[47] S. H. Jensen *et al.*, “Large-scale electricity storage utilizing reversible solid oxide cells combined with underground storage of CO2 and CH4,” *Energy and Environmental Science*, vol. 8, no. 8, pp. 2471–2479, 2015, doi: 10.1039/c5ee01485a.

[48] R. J. Braun, E. P. Reznicek, and C. H. Wendel, “Reversible Solid Oxide Cells as Flexible, Dispatchable Resource for Grid-Energy Storage and Natural Gas Production Using CO2 and CH4,” in *CO2 SUMMIT III: PATHWAYS TO CARBON CAPTURE, UTILIZATION, AND STORAGE DEPLOYMENT*, 2017, vol. 6, no. 1. [Online]. Available: http://repositorio.unan.edu.ni/2986/1/5624.pdf%0Ahttp://fiskal.kemenkeu.go.id/ejournal%0Ahttp://dx.doi.org/10.1016/j.cirp.2016.06.001%0Ahttp://dx.doi.org/10.1016/j.powtec.2016.12.055%0Ahttps://doi.org/10.1016/j.ijfatigue.2019.02.006%0Ahttps://doi.org/10.1

[49] E. P. Reznicek and R. J. Braun, “Reversible solid oxide cell systems for integration with natural gas pipeline and carbon capture infrastructure for grid energy management,” *Applied Energy*, vol. 259, p. 114118, 2020, doi: 10.1016/j.apenergy.2019.114118.

[50] S. Y. Gómez and D. Hotza, “Current developments in reversible solid oxide fuel cells,” *Renewable and Sustainable Energy Reviews*, vol. 61, pp. 155–174, 2016, doi: 10.1016/j.rser.2016.03.005.

[51] G. Botta, R. Mor, H. Patel, and P. V. Aravind, “Thermodynamic evaluation of bi-directional solid oxide cell systems including year-round cumulative exergy analysis,” *Applied Energy*, vol. 226, no. May, pp. 1100–1118, 2018, doi: 10.1016/j.apenergy.2018.05.061.

[52] A. V. Akkaya, B. Sahin, and H. Huseyin Erdem, “Exergetic performance coefficient analysis of a simple fuel cell system,” *International Journal of Hydrogen Energy*, vol. 32, no. 17, pp. 4600–4609, 2007, doi: 10.1016/j.ijhydene.2007.03.038.

[53] C. H. Wendel, Z. Gao, S. A. Barnett, and R. J. Braun, "Modeling and experimental performance of an intermediate temperature reversible solid oxide cell for high-efficiency, distributed-scale electrical energy storage," *Journal of Power Sources*, vol. 283, pp. 329–342, 2015, doi: https://doi.org/10.1016/j.jpowsour.2015.02.113.

[54] K. Sasaki and Y. Teraoka, "Equilibria in Fuel Cell Gases," *Journal of The Electrochemical Society*, vol. 150, no. 7, p. A885, 2003, doi: 10.1149/1.1577338.

[55] K. Sasaki and Y. Teraoka, "Equilibria in Fuel Cell Gases," *Journal of The Electrochemical Society*, vol. 150, no. 7, p. A878, 2003, doi: 10.1149/1.1577337.

[56] G. H. J. Broers and B. W. Treijtel, "Carbon Deposition Boundaries and other Constant Parameter Curves, in the Triangular Representation of C-H-O Equilibria, with Applications to Fuel Cells," *Advanced Energy Conversion*, vol. 5, pp. 365–382, 1965.

[57] S. D. Ebbesen and M. Mogensen, "Electrolysis of carbon dioxide in Solid Oxide Electrolysis Cells," *Journal of Power Sources*, vol. 193, no. 1, pp. 349–358, Aug. 2009, doi: 10.1016/J.JPOWSOUR.2009.02.093.

[58] G. Hoogers *et al.*, *Fuel Cell Technology Handbook*. CRC Press LLC, 2003.

[59] B. P. O. Ryan, S. Cha, W. G Colella, and Fritz, *Fuel Cell Fundamentals*, Third Ed. Wiley, 2016.

[60] P. Kazempoor and R. J. Braun, "Model validation and performance analysis of regenerative solid oxide cells for energy storage applications: Reversible operation," *International Journal of Hydrogen Energy*, vol. 39, no. 11, pp. 5955–5971, 2014, doi: 10.1016/j.ijhydene.2014.01.186.

[61] A. Perna, M. Minutillo, and E. Jannelli, "Designing and analyzing an electric energy storage system based on reversible solid oxide cells," *Energy Conversion and Management*, vol. 159, no. November 2017, pp. 381–395, 2018, doi: 10.1016/j.enconman.2017.12.082.

[62] M. Reytier *et al.*, "Stack performances in high temperature steam electrolysis and co-electrolysis," in *International Journal of Hydrogen Energy*, Sep. 2015, vol. 40, no. 35, pp. 11370–11377. doi: 10.1016/j.ijhydene.2015.04.085.

[63] M. Chen, J. V. T. Høgh, J. U. Nielsen, J. J. Bentzen, S. D. Ebbesen, and P. V. Hendriksen, "High temperature co-electrolysis of steam and CO2 in an SOC stack: Performance and durability," *Fuel Cells*, vol. 13, no. 4, pp. 638–645, 2013, doi: 10.1002/fuce.201200169.

[64] S. D. Ebbesen, J. Høgh, K. A. Nielsen, J. U. Nielsen, and M. Mogensen, "Durable SOC stacks for production of hydrogen and synthesis gas by high temperature electrolysis," *International Journal of Hydrogen Energy*, vol. 36, no. 13, pp. 7363–7373, 2011, doi: 10.1016/j.ijhydene.2011.03.130.

[65] R. C. Reid, T. K. Sherwood, J. M. Prausnitz, and B. E. Poling, *The Properties of Gases and Liquids*. McGraw Hill, 1987.

[66] C. H. Wendel and R. J. Braun, "Design and techno-economic analysis of high efficiency reversible solid oxide cell systems for distributed energy storage," *Applied Energy*, vol. 172, pp. 118–131, 2016, doi: https://doi.org/10.1016/j.apenergy.2016.03.054.

[67] A. Bejan, G. Tsatsaronis, and M. Moran, *Thermal Design and Optimization*. New York: John Wiley & Sons, Ltd, 1995.

[68] T. L. Bergman, AdrienneS. Lavine, F. P. Incropera, and D. P. Dewitt, *Fundamentals of Heat and Mass Transfer*, Seventh Ed. New Jersey: John Wiley & Sons, Ltd, 2017.

[69] G. Towler and R. Sinnott, *Chemical Engineering Design: Principles, Practice and Economics of Plant and Process Design*, Second. Elsevier, 2013.

[70] I. Dincer and M. A. Rosen, *Exergy: Energy, Environment And Sustainable Development*, Second Edi. Oxford: Elsevier Ltd., 2013.

[71] R. Turton, J. A. Shaeiwitz, D. Bhattacharyya, and W. B. Whiting, *Analysis, Synthesis, and Design of Chemical Processes*, Fifth Edit. Pearson Education, 2018.

[72] "THE CHEMICAL ENGINEERING PLANT COST INDEX." https://www.chemengonline.com/pci-home

[73] C. Kost *et al.*, "Fraunhofer ISE: Levelized Cost of Electricity - Renewable Energy Technologies, March 2018," *Fraunhofer ISE: Levelized Cost of Electricity - Renewable Energy Technologies*, no. March, 2018.

[74] C. Kost, J. N. Mayer, and S. Philipps, "Levelized Cost of Electricity Renewable Energy Technologies Edition : November 2013," no. November, pp. 1–50, 2013.

[75] B. Zakeri and S. Syri, "Electrical energy storage systems: A comparative life cycle cost analysis," *Renewable and Sustainable Energy Reviews*, vol. 42, pp. 569–596, 2015, doi: 10.1016/j.rser.2014.10.011.

[76] B. Battke, T. S. Schmidt, D. Grosspietsch, and V. H. Hoffmann, "A review and probabilistic model of lifecycle costs of stationary batteries in multiple applications," *Renewable and Sustainable Energy Reviews*, vol. 25, pp. 240–250, 2013, doi: 10.1016/j.rser.2013.04.023.

[77] B. Najafi, A. Shirazi, M. Aminyavari, F. Rinaldi, and R. A. Taylor, "Exergetic, economic and environmental analyses and multi-objective optimization of an SOFC-gas turbine hybrid cycle coupled with an MSF desalination system," *Desalination*, vol. 334, no. 1, pp. 46–59, 2014, doi: 10.1016/j.desal.2013.11.039.

[78] M. Sadeghi, A. Chitsaz, S. M. S. Mahmoudi, and M. A. Rosen, "Thermoeconomic optimization using an evolutionary algorithm of a trigeneration system driven by a solid oxide fuel cell," *Energy*, vol. 89, pp. 191–204, 2015, doi: 10.1016/j.energy.2015.07.067.

[79] W. M. Vatavuk, "Updating the Cost Index," *Chemical Engineering*, no. January, pp. 62–70, 2002.

[80] Y. Cao and T. parikhani, "A solar-driven lumped SOFC/SOEC system for electricity and hydrogen production: 3E analyses and a comparison of different multi-objective optimization algorithms," *Journal of Cleaner Production*, vol. 271, p. 122457, 2020, doi: 10.1016/j.jclepro.2020.122457.

[81] A. E. De Paepe *et al.*, *Perry's Chemical Engineers' Handbook*, 9th Editio., vol. 53, no. 9. McGrawHill Education, 2019. doi: 10.1017/CBO9781107415324.004.

[82] M. S. Peters, K. D. Timmerhaus, and R. E. West, *Plant Design and Economics for Chemical Engineers*, Fifth Edit. International: McGraw Hill, 2003.

[83] F. Razi, I. Dincer, and K. Gabriel, "A specific exergy costing assessment of the integrated copper-chlorine cycle for hydrogen production," *International Journal of Hydrogen Energy*, vol. 45, no. 56, pp. 31425–31439, 2020, doi: 10.1016/j.ijhydene.2020.08.269.

[84] H. Y. Kwak, D. J. Kim, and J. S. Jeon, "Exergetic and thermoeconomic analyses of power plants," *Energy*, vol. 28, no. 4, pp. 343–360, 2003, doi: 10.1016/S0360-5442(02)00138-X.

[85] H. Atalay and E. Cankurtaran, "Energy, exergy, exergoeconomic and exergo-environmental analyses of a large scale solar dryer with PCM energy storage medium," *Energy*, vol. 216, p. 119221, 2021, doi: 10.1016/j.energy.2020.119221.

[86] Z. Xi, S. Eshaghi, and F. Sardari, "Energy, exergy, and exergoeconomic analysis of a polygeneration system driven by solar energy with a thermal energy storage tank for power, heating, and freshwater production," *Journal of Energy Storage*, vol. 36, no. September 2020, p. 102429, 2021, doi: 10.1016/j.est.2021.102429.

[87] S. M. Alirahmi, S. Bashiri Mousavi, A. R. Razmi, and P. Ahmadi, "A comprehensive techno-economic analysis and multi-criteria optimization of

a compressed air energy storage (CAES) hybridized with solar and desalination units," *Energy Conversion and Management*, vol. 236, no. December 2020, p. 114053, 2021, doi: 10.1016/j.enconman.2021.114053.

[88] T.C. EPDK, "Elektrik Faturalarina Esas Tarife," 2021. https://www.epdk.gov.tr/Detay/Icerik/3-1327/elektrik-faturalarina-esas-tarife-tablolari (accessed May 15, 2021).

PUBLICATIONS FROM THE THESIS

Contact information: muizadekunle@yahoo.com

Conference papers

1. **M. A. Agbaje** and A. V. Akkaya, "Electrochemical, Energy and Exergy-Based Performance Assessment of a Reversible Solid Oxide Cell (ReSOC) Stack" in Proceedings of the International Congress on Engineering and Technology Management, Online, 2021, pp. 647.
2. **M. A. Agbaje** and A. V. Akkaya, "Zero-Dimensional Modelling and Analysis of a Reversible Solid Oxide Cell System for Electrical Energy Storage" in Proceedings of the International Conference on Energy, Environment and Storage of Energy (ICEESEN), Erciyes University (Online), 2020, pp. 1–12.

Project

1. Topic: Modeling and Analysis of a Reversible Solid Oxide Cell System
   Project award number: FYL-2021-3884
   Sponsor: Office of the Rector, Yildiz Technical University (Scientific Research Projects Coordination Unit)
   Project Supervisor: Dr. Ali Volkan AKKAYA
   Researcher: **Muiz Adekunle AGBAJE** (Student)
   Period: 6 months
   Budget: 3000TL